TÉCNICO LISBOA

UNIVERSIDADE DE LISBOA

INSTITUTO SUPERIOR TÉCNICO

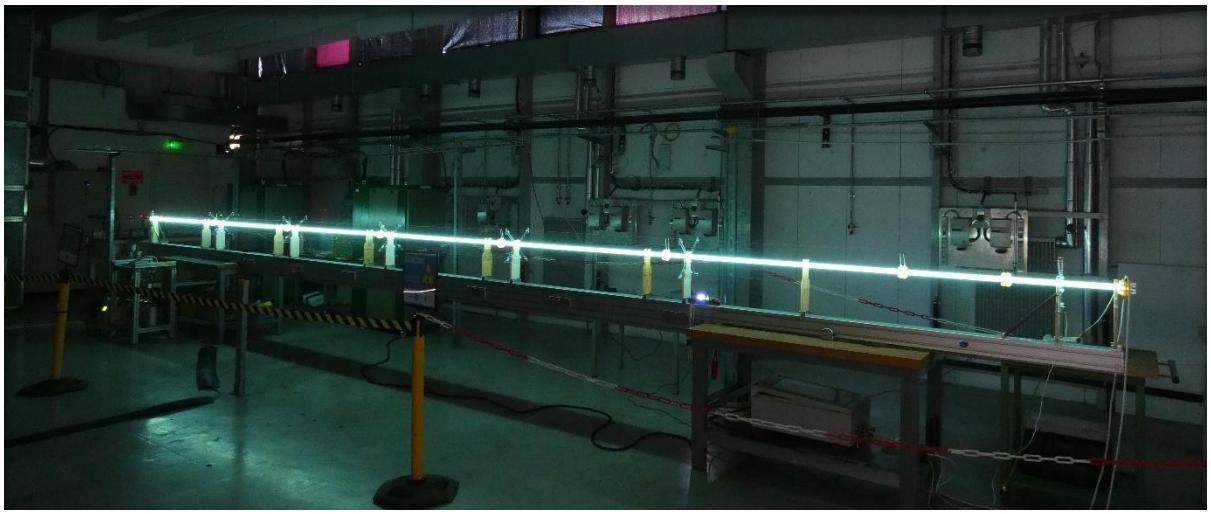

Pulse generator for a scalable discharge plasma source for the AWAKE experiment

Nuno Espanha Torrado da Silva

Supervisor: Doctor José Fernando Alves da Silva

Co-Supervisor: Doctor Nelson Manuel Carreira Lopes

Thesis approved in public session to obtain the PhD Degree in

Electrical and Computer Engineering

Jury final classification:

Pass with Distinction

2025

UNIVERSIDADE DE LISBOA

INSTITUTO SUPERIOR TÉCNICO

Pulse generator for a scalable discharge plasma source for the AWAKE experiment

Nuno Espanha Torrado da Silva

Supervisor: Doctor José Fernando Alves da Silva

Co-Supervisor: Doctor Nelson Manuel Carreira Lopes

Thesis approved in public session to obtain the PhD Degree in

Electrical and Computer Engineering

Jury final classification:

Pass with Distinction

Jury:

Chairperson:

Doctor Paulo José da Costa Branco, Instituto Superior Técnico, Universidade de Lisboa

Members of the committee:

Doctor José Fernando Alves da Silva, Instituto Superior Técnico, Universidade de Lisboa

Doctor Ricardo Parreira de Azambuja Fonseca, Escola de Tecnologias e Arquitectura, ISCTE-Instituto Universitário de Lisboa

Doctor Maria do Rosário Alves Calado, Faculdade de Engenharia, Universidade da Beira Interior

Doctor Horácio João Matos Fernandes, Instituto Superior Técnico, Universidade de Lisboa

Doctor Rui Manuel Esteves Araújo, Faculdade de Engenharia, Universidade do Porto

Doctor Sónia Maria Nunes dos Santos Paulo Ferreira Pinto, Instituto Superior Técnico, Universidade de Lisboa

Funding institution: Fundação para a Ciência e a Tecnologia (FCT)

2025

Acknowledgments

First and foremost, I could not have undertaken this journey without the trust and guidance of my supervisor, Nelson Lopes. Nelson introduced me to the AWAKE - Discharge Plasma Source project in 2019 when its double pulse generator existed only as a few drawings and "PowerPoint engineering." It was a tremendous honour to be part of the development of such a technology. The support Nelson gave me and the dedication he showed to his projects, as well as to his students, were nothing short of tireless and serve as an example I will always aspire to.

I would also like to express my deepest appreciation to Professor Fernando Silva, whose knowledge, guidance, and presence were essential in achieving the many objectives of this PhD.

I have been part of IST and GoLP since my master's, and I am extremely grateful to the people who assisted in this project and for the resources I was granted to complete it. Thank you as well to FCT and CERN doctoral programme for funding my PhD studies.

I am deeply grateful to Alban Sublet, who guided me through my year at CERN and provided endless encouragement, advice, and valuable feedback.

I also extend my gratitude to the many people at CERN who contributed to this project and, by doing so, made this thesis possible. To name but a few: Mauro Taborelli, Paul Garritty, Matthew Watkins, Pedro Costa Pinto, Wilhelm Vollenburg, Spyridon Fiotakis, Miguel Santos, Olivier Barriere, Emmanuel Said, and Benjamin Ninet. Many thanks as well to the AWAKE members who supported the DPS run: Patric Muggli, Edda Gschwendtner, Marlene Turner, Livio Verra, Michele Bergamaschi, Arthur Clairembaud, Jan Mezger, Eloise Guran, Jan Pucek, Fern Pannell, Nikita van Gils, and Giovanni Zevi Della Porta. I would be remiss not to mention John Farmer, Stewart Leith, Ricardo Barrué and Carlota Pereira for their friendship and support.

I want to express my deepest gratitude to my family: my father, for sharing his enthusiasm for learning and discovery in every aspect of life; my mother, for demonstrating every day the strongest of wills; and Gonçalo, Pedro, and Sofia, for being my fellowship and the greatest gift I have ever received — you bow to no one! I am also thankful to Avó Gigi, Avó São, Pi, and Mimi, for their love and support.

Last but not least, thank you to Carolina—my PhD partner, my desk partner, my partner in crime, and my life partner. This thesis is as much yours as it is mine. I am forever grateful for your unwavering support and love.

Resumo

Descargas eléctricas pulsadas podem gerar plasmas adequados para aceleração baseada em plasma. Esta tese descreve o desenvolvimento e dimensionamento de um gerador de impulsos de alta tensão e de alta corrente para alimentar uma fonte de plasma para a experiência AWAKE, no CERN.

Uma fonte de plasma adequada ao AWAKE requer parâmetros únicos de comprimentos (tipicamente 10 m), densidade de plasma electrónica ($\sim 7\times10^{14}\,\mathrm{cm}^{-3}$), reprodutibilidade, escalabilidade e uniformidade de densidade ($< 0.25\%$). Descargas em plasma por sua vez apresentam desafios a sistemas de electrónica de potência devido ao comportamento dinâmico e não linear do plasma.

Para operar perante os requerimentos de comprimento, reprodutibilidade e densidade, o gerador de impulsos utiliza dois impulsos de tensão, o foco do primeiro impulso é a ignição do plasma e utiliza um impulso de tensão de crescimento rápido para gerar o plasma com o mínimo de variação temporal; o segundo é um impulso de aquecimento que, aproveitando a redução na impedância, vai aumentar a corrente aplicada e a densidade de plasma, de forma altamente reprodutível. Adicionalmente, para estabelecer escalabilidade em comprimento, múltiplos plasmas em sequência e sincronismo podem ser produzidos utilizando bobinas acopladas de resposta em alta-frequência, de modo a equalizar a amplitude de corrente de cada plasma.

Esta tese inclui o dimensionamento do gerador de duplo-impulso e das bobines acopladas para balanceamento de correntes, simulações em PSpice do gerador de impulsos utilizando um modelo de plasma, e resultados experimentais da fonte de plasmas baseada no gerador de duplo-impulso. Esta tese inclui adicionalmente uma descrição da operação da fonte de plasma na sua primeira utilização na experiência AWAKE, a aplicação para o qual foi concebida.

Palavras-chave: fonte de plasma, gerador de duplo impulso, balanceamento de correntes pulsadas, AWAKE, acelerador baseado em plasma

Abstract

Pulsed electrical discharges can generate plasmas suitable for wakefield particle acceleration experiments. This thesis describes the development and design of a semiconductor-based high-voltage and high current pulse generator topology for a plasma source for the Advanced WAKEfield Experiment (AWAKE).

A plasma source for AWAKE depends upon unique parameters regarding the length (typically $10\,\mathrm{m}$), plasma electron density ($\sim 7 \times 10^{14}\,\mathrm{cm}^{-3}$), reproducibility, scalability, and density uniformity ($< 0.25\%$ over $10\,\mathrm{m}$). Plasma discharges present unique challenges for power electronic systems due to the highly non-linear plasma dynamic behaviour.

To operate under the required length, reproducibility and density values, the pulse generator uses two voltage pulses, the first for the processes of ignition, using a fast-rising high-voltage pulse to generate the plasma with minimum jitter; and the second for heating, taking advantage of the lower impedance to boost the current and consequently the plasma density with high reproducibility. Furthermore, to meet the scalability objectives multiple neighbouring synchronised plasma discharges can be produced using high-frequency coupled inductors to equalise the current amplitudes.

This thesis describes the double pulse generator design, component selection, the development of the coupled inductors balancing modules, PSpice simulations of the pulse generator using a suitable plasma model, and the experimental results of the discharge plasma source double pulse generator. Additionally, this thesis provides an account of the plasma source operation in the AWAKE experiment, reporting its first use in its intended application.

Keyords: plasma source, double pulse generator, pulsed current balancing, AWAKE, plasma wakefield accelerator

Contents

List of Tables

List of Figures

CHAPTER 1

Introduction

Plasma wakefield acceleration (PWFA) is a method for accelerating particle beams using electric fields that can be up to three orders of magnitude stronger than those found in conventional radio-frequency (RF) cavities. One of the main components of a plasma wakefield accelerator is its plasma. This thesis focuses on the development of an AWAKE (Advanced WAKefield Experiment - Figure 1.1) suitable plasma source, driven by double pulse generators, with length scalability potential.

In this chapter, we present the motivation for the development of this plasma source and provide an overview of PWFA and the AWAKE experiment. We also introduce the plasma source requirements, the thesis objectives, and the structure of the thesis.

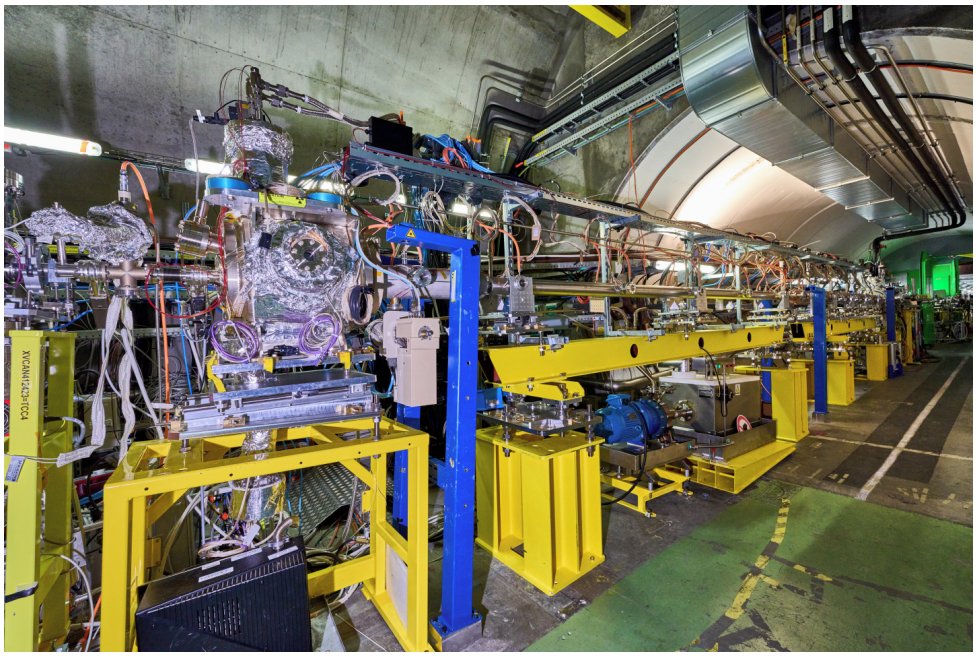

Figure 1.1: AWAKE Experiment at CERN

1.1 Motivation

1.1.1 Particle Accelerators

Particle accelerators use electromagnetic fields to increase the energy of charged particle beams. To investigate the interactions between elementary particles, the accelerated charged particle beams are directed towards fixed solid targets or against each other. The resulting interaction products are analysed using sophisticated detectors. To achieve fundamental particle scientific breakthroughs, producing ever higher beam energies remains a central goal in accelerator physics research.

Conventional accelerators rely on RF cavities to generate the longitudinal electric fields responsible for particle acceleration. However, RF particle accelerating cavities face one main limitation: their maximum acceleration gradients are limited to around $100\,\mathrm{MV/m}$ [1]. Consequently, linear colliders using RF technology always need to increase in length to reach the required energies for high-energy physics. Circular colliders, on the other hand, will be forced to go to higher diameters to overcome the energy loss by synchrotron radiation and beam rigidity.

To reduce the footprint and the cost of future accelerators it is necessary to develop alternative technologies with higher accelerating gradients. Therefore, alternatives like muon colliders, energy recovery linacs (linear particle accelerators), and plasma wakefield acceleration are being considered [2–9].

1.1.2 Plasma wakefield acceleration

The groundwork for plasma acceleration was laid in 1979 by Toshiki Tajima and John Dawson [6]. Using an intense laser pulse or a relativistic charged particle bunch [7] as the *driver*, travelling through the plasma, the electromagnetic field created will displace the plasma electrons but the plasma ions, much more massive than the electrons, will remain almost immobile at the relevant timescale. The ions will provide charge-neutrality restoring force that induces an oscillation of the plasma electrons in the wake of the driver. The local charge non-neutrality will sustain electrostatic waves called wakefields [6, 7]. A following particle or bunch (the *witness*) will be accelerated to high energies when travelling in the focusing and accelerating phase of the wakefields [7].

Typically, plasma wakefield experiments use plasma electron densities in the $[10^{14} - 10^{18}]\,\mathrm{cm^{-3}}$ range, with maximum accelerating fields of up to $100\,\mathrm{GV/m}$, a thousand times higher than those achievable in conventional RF cavities [10, 11]. For this reason, plasma wakefield accelerators have the potential to reduce the size and cost of future accelerators.

Different experiments are showing groundbreaking results in plasma acceleration: FACET, at SLAC was able to demonstrate $42\,\mathrm{GeV}$ energy gain in a 1-meter long accelerator in 2007 [12], the highest energy gain achieved in PWFA; BELLA, Berkeley Lab, US, accelerated electrons to $7.8\,\mathrm{GeV}$ in $20\,\mathrm{cm}$, reaching the highest energy gain with laser-based wakefield accelerators (LWFA) [13]; FLASHForward, DESY recorded energy-transfer efficiencies of over 40% [14].

Following these results, organisations like the EuroNNAc in Europe, the US Department of Energy (DOE), and the international ALEGRO collaboration defined the R&D needs for future plasma-based accelerators and colliders [2]. One of the objectives defined by the *European Strategy for Particle Physics* is length-scalable plasma accelerators to allow electron acceleration up to the TeV level. This challenge is being addressed by the AWAKE

experiment.

1.1.3 AWAKE experiment and plasma sources

The AWAKE experiment at CERN (Figure 1.1) studies proton-driven plasma wakefield acceleration [15, 16]. AWAKE uses $400\,\mathrm{GeV}$ proton bunches delivered by CERN's Super Proton Synchrotron (SPS), which are injected through plasma creating a wakefield for electron acceleration [17, 18].

In its initial run, AWAKE relied on a short, intense laser pulse to generate the plasma in a rubidium vapour source [19]. This laser pulse co-propagates with the proton bunch, creating a relativistic ionisation front that reproducibly seeds the self-modulation of the trailing section of the $1\,\mathrm{ns}$ long proton bunch that, after this process, can reproducibly drive the wakefield structure [20, 21]. However, AWAKE's laser field ionisation plasma source is not scalable to lengths significantly higher than $10\,\mathrm{m}$. To achieve the targeted TeV-range energies, plasma sources able to exceed the current 10 m limitation are crucial. This limitation led to R&D in scalable plasma sources [22].

AWAKE plasma sources must operate under strict requirements. The desired plasma must reach a precise density in the range of $[1\times10^{14}-1\times10^{15}]\,\mathrm{cm}^{-3}$ with 0.25% longitudinal uniformity [18]. It must also exhibit high shot-to-shot reproducibility across multiple discharges in both density (to achieve stable acceleration) and timing (time synchronisation deviations - jitter - must be minimised relative to the incoming proton beam). Furthermore, a valid alternative source must be able to reach unprecedented plasma lengths from the current $10\,\mathrm{m}$ to beyond $100\,\mathrm{m}$.

Two technologies to produce length scalable plasmas are being considered, a helicon plasma source [23] and a Discharge Plasma Source (DPS) [24] (Figures 1.2 and 1.3 respectively). Helicon plasmas are a type of plasma heated by radio-frequency waves in the presence of a magnetic field, using a dielectric vacuum vessel, filled with a low pressure gas, and an external wave excitation antenna [25]. Such sources are intrinsically scalable in length and avoid the necessity for staging.

The discharge plasma source produces plasma with direct current microsecond pulsed discharges in low-pressure gases. Its scalability may be achieved by stacking together multiple plasma sections using common electrodes.

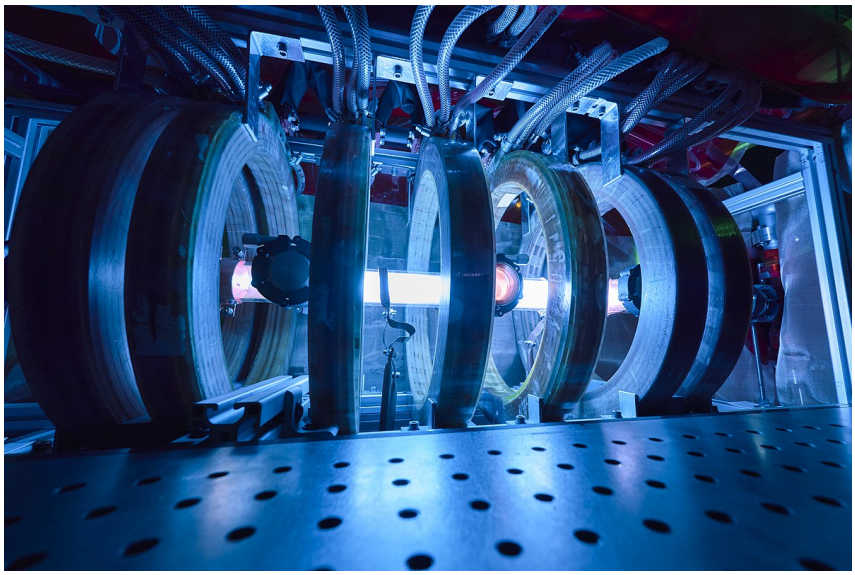

Figure 1.2: CERN Helicon Plasma Source

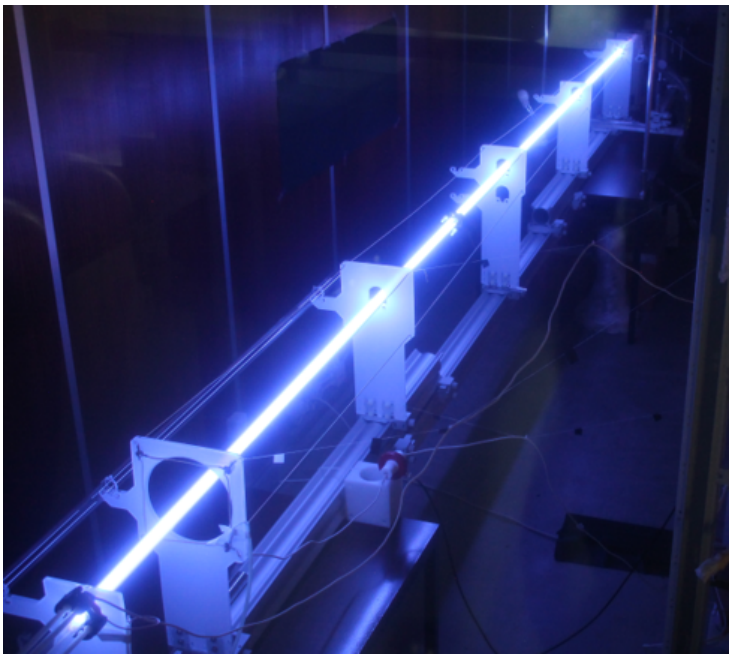

Figure 1.3: IST Discharge Plasma Source

The development of a scalable discharge plasma source suitable for AWAKE is the main objective of this thesis.

1.2 Discharge plasma sources

Plasma discharges refer to the application of electric voltage and current suitable to ionise gas mediums, releasing electrically charged particles, typically in the form of ions or electrons, developing the gas into a plasma. This phenomenon occurs when a high voltage is applied in a gap across electrodes, causing the gas to ionise and become conductive [26]. There are several applications for this phenomenon including lighting, lasers, surge protection devices, and materials processing [27–31]. Plasma sources based on plasma discharges are used in industrial, environmental, and medical applications [32–34], but have also been commonly used in PWFA [35–37].

The voltage threshold needed to initiate the gas electrical breakdown is called ignition potential or breakdown voltage. This value depends on the gas, the pressure, the gap width of the electrodes, and their material and shape. Equation (1.1) describes this relation, where A and B are experimentally determined constants that will depend on the gas and the electrodes, p corresponds to the pressure and d is the length between the electrodes [26]. From (1.1), under a certain experimental setup, V_t will depend only on the product of pressure and electrode distance (pd). The experimental curves $V_t(pd)$ are called Paschen curves [38] - Figure 1.4.

$$V_t = \frac{A(pd)}{B + ln\,(pd)}, \tag{1.1}$$

The minimum of the Paschen curves will be at the pressure-length conditions where the ionisation is easier. Before the minimum, for low pressure-length values, the breakdown voltage is higher because the distance between electrodes, combined with reduced pressure, is shorter than the mean free path of the electrons (the average distance an electron travels before colliding with a gas molecule) which decreases the probability of impact for the electrons and reduces the probability of ionisation and charge multiplication.

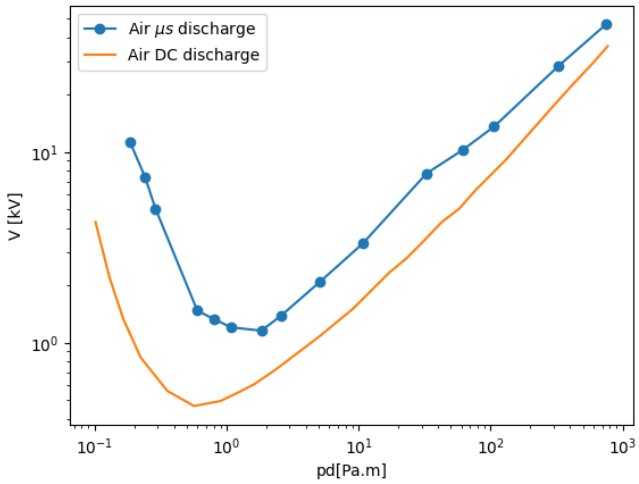

Figure 1.4: Paschen curves example for air with DC and μs pulses - produced using data from [39]

After the Paschen curve minimum, as pressure-length rises the breakdown voltage increases almost proportionally. This is attributed to the shorter mean free path at higher pressures and to the decrease of the electric field value with the length (for the same applied voltage).

When the applied voltage surpasses the breakdown threshold of the gas, an electron can trigger an avalanche through impact ionisation. To improve the reproducibility in time, a steep-rise voltage is required to initiate a rapid plasma ignition, thereby creating faster breakdown mechanisms that are less dependent on probabilistic events [40]. Typically, Paschen curves refer to DC-applied voltage (or very long pulses). To generate an arc in microseconds comparatively higher voltages are required (Figure 1.4) [39, 41].

Furthermore, the typical V-I characteristic curve of plasma discharges (Figure 1.5) contains two reduced impedance regimes: glow and arc discharges. Glow discharges can occur when the threshold voltage is reached and are characterised by low density currents (typically $\mu\mathrm{A/cm^2} - \mathrm{mA/cm^2}$) spread over a larger area, resulting in a diffuse appearance. Arc discharges operate at a higher current density (typically over $1\ \mathrm{A/cm^2}$), and the current emanates from small areas of the cathode (hotspots), producing intense localised heating and brightness [26]. The arc regime is the only condition that induces a high ionisation fraction, crucial for achieving the AWAKE required plasma electron density and uniformity.

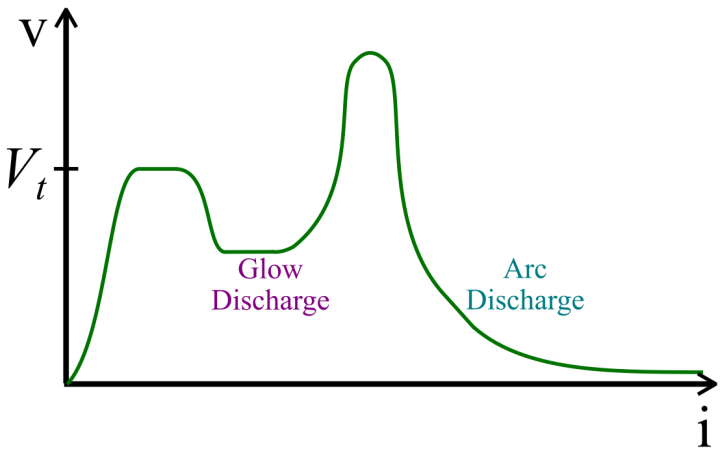

Figure 1.5: Typical V-I characteristic curve of gas discharges - adapted from [26]

1.3 Double pulse generator and current balancing solutions

Reproducible timing is achieved using a voltage pulse with a rapid rise time to ignite the plasma quickly ($\sim 20\,\mathrm{kV}$). Additionally, attaining the nominal density for AWAKE requires a high-current pulse ($\sim 500\,\mathrm{A}$) [42]. Combining these voltage and current requirements in a single, high-power pulse (over $10\,\mathrm{MW}$) is impractical due to the power limitations of the existing fast-switching semiconductors and concerns regarding compactness, efficiency, and cost.

This thesis details the development of a double pulse generator that addresses these challenges, taking advantage of the gas incremental negative impedance to break the challenge using two pulse generator topologies for the processes of plasma ignition and heating.

The first topology delivers a fast-rising voltage pulse for rapid ignition, while the second one delivers a lower voltage but a much higher current pulse for efficient heating. Taking advantage of the plasma's low-impedance created by the ignition pulse, the heating pulse, generated by the second topology, can achieve a highly reproducible (low time jitter and low current amplitude variation), high-current plasma lasting tens of microseconds [24]. This double pulse approach offers a cost-effective and compact solution that meets the demanding requirements of the AWAKE experiment [43].

Generally, pulsed power systems are composed of a power supply unit, an energy storage component, a primary switch, and a load [44]. The energy storage can be either capacitive or inductive and its charging time depends largely on the specifications of the power source, varying from microseconds to minutes. The simplest pulse generator topologies are the basic capacitive discharge topology and the basic inductive discharge topology (Figure 1.6) [45].

In the basic capacitive discharge topology of Figure 1.6-A, the pulse will be applied to the load once the switch turns-ON. For resistive loads, the pulse fall time depends solely on the time-constant (determined by the resistance and capacitance values - RC constant). While theoretically, the rise time could be instantaneous, the non-ideal components introduce unwanted parasitics, slowing down the voltage and current rise.

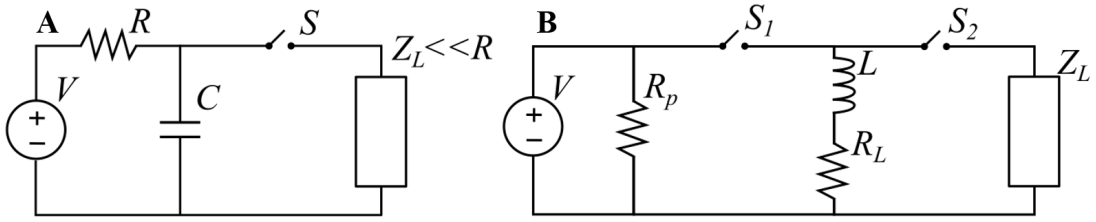

Figure 1.6: A: Basic capacitive discharge topology; B: Basic inductive discharge topology

In the basic inductive discharge topology of Figure 1.6-B, the operation starts with a direct current through the inductor. When the switch S_1 turns OFF, this current rapidly drops, generating a negative voltage across the inductor, turning ON switch S_2 (a diode), delivering the resulting pulse to the load [44]. Inductive storage pulse generator topologies can also take advantage of the step-up in voltage caused by the opening of charged inductor circuits [45, 46].

An example (boost converter-based pulse generator) is shown in Figure 1.7. During the S switch-ON time the energy is stored in the inductor L. By opening the switch S (turn-OFF), the energy stored in L is transferred to the load Z_L, resulting in load voltages that can be significantly higher than the supply voltage V. The magnitude of

this voltage depends on the values of Z_L and I, and is limited by the maximum blocking voltage of the switch S. Diode D can be omitted if the Z_L voltage drops to zero before the turn-ON of switch S.

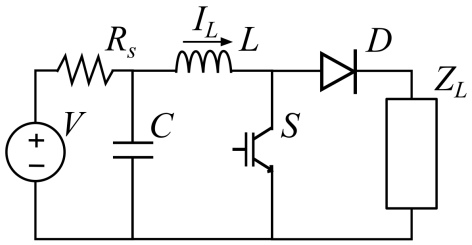

Figure 1.7: Boost converter-based pulse generator topology

Another voltage step-up strategy in pulse generators is using a pulse transformer [47, 48]. This has the advantage of allowing the use of lower voltage rating devices on the primary side while providing galvanic isolation to the load. Examples of these are pulse generator topologies derived from forward and flyback power converters [49]. The forward-type pulse generator (Figure 1.8-A) uses a capacitive storage that discharges through the transformer and to the load when the switch is turned ON. The flyback-type pulse generator topology (Figure 1.8-B) combines the step-up properties of both the pulse transformer and the inductor switch-open, by taking advantage of the transformer magnetising inductance.

The main difference between the two topologies is the polarity of the diode *D*, which leads to a completely different operation. While the switch *S* is ON, the capacitive stored energy is not delivered to the load but remains in the primary loop, storing the energy as core flux in the transformer magnetising inductance. The switch turn-OFF will activate the diode generating a pulse in the load Z_L [49]. The inductance switch-OFF combined with the transformer ratio, steps up the voltage to the target values.

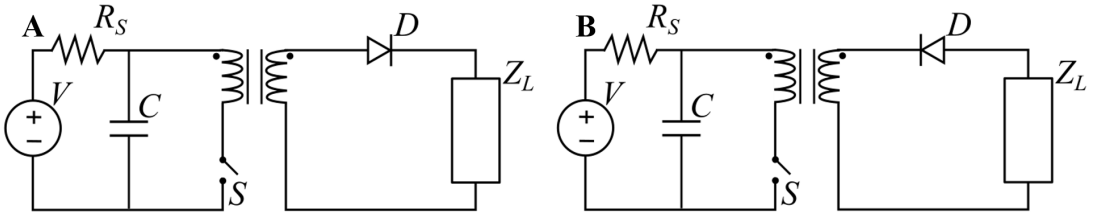

Figure 1.8: A: Forward-type pulse generator topology; B: Flyback-type pulse generator topology

The flyback-type pulse generator presented in Figure 1.8-B can deliver a fast-rising voltage, limited by the power of the pulse generator and the parasitics of the load, and is tolerant to shorted loads considering that the switch is OFF during the output pulse. After the plasma breakdown, the remaining stored energy will discharge through the plasma, sustaining it for hundreds of microseconds. This topology introduces the practical advantage of confining the peak voltage to just a portion of the topology (transformer secondary, flyback diode, and output); however, a snubber is still required on the primary side to sustain the turn-OFF overvoltage, especially in this application, as the plasma does not form instantaneously. These characteristics make the flyback-type pulse generator topology a suitable candidate for the double pulse generator ignition module.

The heater module of the pulse generator is a modified capacitive discharge topology. It will operate after the ignition, when the plasma acts closer to a relatively small valued ohmic load with a parasitic series inductor. The relatively low impedance of the plasma puts off the need for a voltage step-up, and, since the plasma impedance

variation is much smaller during the heater pulse, having the pulse during the switch turn-ON has minimal risk. The low jitter requirements of both pulses, combined with the need for compactness and long lifetime of the system, are obtained using solid-state switches in the ignition and the heater modules.

Furthermore, scalability to achieve longer plasma lengths can be obtained by connecting multiple plasma tubes in a sequence using alternating common cathodes and anodes (Figure 1.9). Current balancing techniques are essential to ensure uniform plasma properties across the extended length.

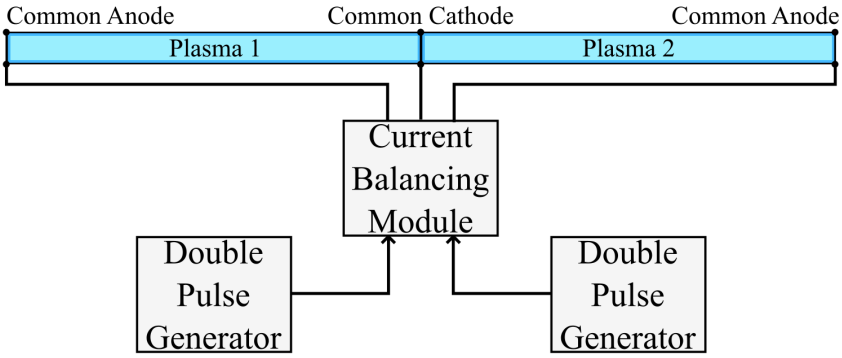

Figure 1.9: Schematic of a two-plasma configuration

1.4 Objectives

This PhD aims to develop a novel pulsed electric discharge plasma source specifically tailored for the AWAKE experiment. In this thesis we will explore how to develop such a plasma source and how it fits the application. Therefore, the main objectives are:

- To design the pulse generators required to produce separate high-voltage ignition and high-current heating pulses.
- To develop a *PSpice* model of the system for electrical simulations.
- To test the plasma source with a 10 m tube length.
- To analyse the electrical tests to optimise and improve the design for AWAKE compliance.
- To install and operate the DPS in the AWAKE experiment with the propagation of high-energy proton beams.
- To investigate the scalability of the source by connecting two plasma tubes in sequence.
- To publish comprehensive documentation and insights to guide future development of pulse generators and plasma sources.

Three main methodologies will be employed:

1. Theoretical Design: Sizing and design of the entire pulsed generator and its components, as well as the current balancing module for multiple plasmas.
2. Electrical Simulation: Using PSpice software to simulate the behaviour of the pulse generators and to study its behaviour.
3. Experimental Validation: The designed pulse generators will be built and tested as a discharge plasma source.

1.5 Outline

Chapter 2 provides an overview of the current state of the art, focusing on pulsed power systems, current balancing techniques, and the electrical modelling of plasmas. Chapter 3 describes the development and operation of the double pulse generator. Chapter 4 outlines the design of the different components of the plasma set-up, the ignition and heater modules, and the current balancing module. Chapter 5 presents the preliminary simulation and experimental results obtained in the DPS laboratory at CERN. Chapter 6 details the experimental results acquired at the AWAKE. The closing Chapter 7 summarises the findings of this thesis, offering a critical analysis of the outcomes and outlining possible future developments.

CHAPTER 2

State of the art on pulse generators and current balancing

This chapter will provide a comprehensive review of the state-of-the-art on pulse generator technology, current balancing techniques, and plasma impedance models for electrical simulations. It will serve as the basis for the design choices and developments presented in Chapter 3.

2.1 Pulsed power

Pulsed power technology research typically develops in two main branches [45]. The first one focuses on technology to push the limits on the power of the pulses and building facilities capable of producing pulsed currents and voltages with the highest possible magnitude. These facilities contribute to research programs on subjects such as

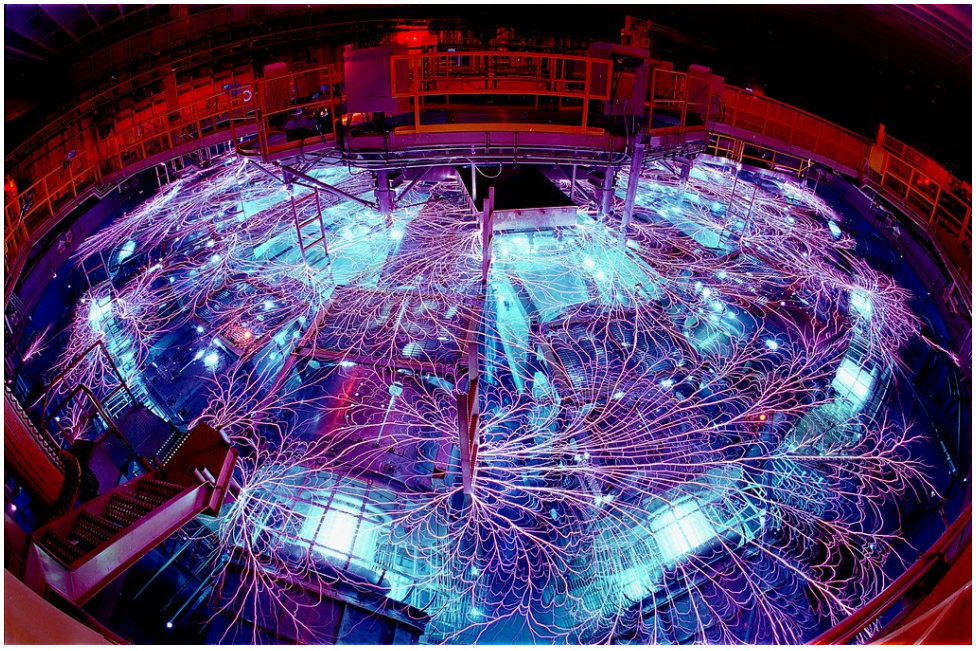

Figure 2.1: Z-Machine in Sandia National Laboratories, Albuquerque, N.M. *source:* sandia.gov/z-machine/

inertial thermonuclear fusion, the production of high-power lasers, X-rays, neutron pulses, etc. [50–52]. The example with the highest power capability is the *Z machine* in Figure 2.1 [53], on Sandia National Laboratories, capable of generating pulse powers over 100 TW on the nanosecond scale [54].

The pulse generators of the second branch are based on power electronics, with a higher focus on performance, particularly in power density and compactness, pulse repetition rate and lifetime. Power electronics-based pulse generators provide a wide range of technological applications such as radiation, plasma, particle beam, laser technologies, communication, purification of wastes, water treatment, and sterilisation of tools and products [55–61].

Both branches are based on high-power voltage and current pulse generators, which typically operate around energy storage (low-power, long-time input) and conversion during the final power amplification phase (high-power, short-time output) [52]. As mentioned in section 1.3, pulse generators typically consist of a power supply unit, an energy storage device, power switch modules, and a load. The fundamental principle of pulse generators is taking electrical energy with lower power delivered (by the power supply unit) over a relatively long duration (into the energy storage) and converting it (using one or more switch modules) into very short but much higher peak power electrical pulses, a single one or a programmed repetitive sequence [44].

2.1.1 Pulse generator topologies

Pulse generators typically pursue design requirements such as voltage and current rating, pulse repetition rate, rise and/or fall time, power density, reproducibility, reliability, and high flexibility and controllability [62–71]. These requirements, along with the characteristics of the load, determine the best-suiting pulsed power generator topology for an application.

Classic pulse generator topologies like Marx Generators [72], Pulse Forming Line and Blumlein lines [73, 74], Tesla Transformers [75], and Magnetic Pulse Compression [76, 77], are typically more common in the aforementioned first branch, with applications prioritising the voltage and current ratings. High-voltage pulse generators of the second branch, based on power electronics, have attracted more research attention recently due to their advantages on compactness, reproducibility, repetition rate, and lifetime [78].

Examples of power-electronics-based pulse generators include:

- High-voltage pulse generators derived from switched mode power topologies. The most used are DC/DC modified isolated converters for their step-up capabilities. The forward and flyback-type pulse generator topologies analysed in Chapter 1, belong in this category. Other examples include boost and buck-boost-derived topologies as in [46, 79–81]. However, neither presents the advantages of the flyback-type pulse generator selected: peak voltage confined only to the output and switch in OFF-state during the pulse protecting the semiconductors from load faults [49].

- Solid-state Marx Generators, which follow the same principle as the classical Marx generator but instead of mechanical switches use power semiconductor devices [82, 83]. This topology performs a voltage step-up without a transformer and is relatively easy to scale (increasing the number of capacitor and switch modules); however, has the disadvantage of requiring multiple switches that require good synchronisation. Developments on this topology include self-triggering configurations that require only one integrated driver (Figure 2.2) [84] but still need a high number of components (diodes, switches, and capacitors) and a more complex operation than the pulse generator topologies selected for the ignition and heater modules.

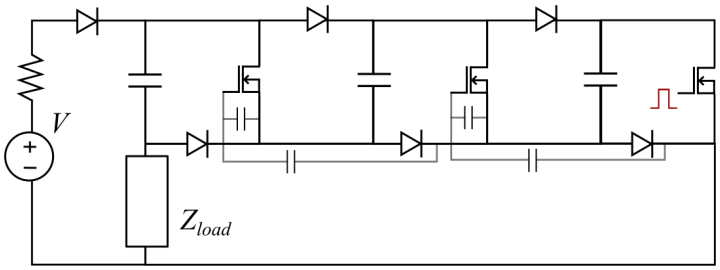

Figure 2.2: Self-triggering Marx generator [84]

- Semiconductor Opening Switch-Based Circuits use semiconductor devices with high current density, high voltage rating and short current cut-off time [85–88] and operate through carrier accumulation by the forward current followed by extraction through the reverse current. This is possible with devices such as drift step recovery diodes (DSRD) [89] and diode opening switches (DOS) [45] and allows for nanosecond jitters, high response speed, and high power capacity (Figure 2.3). However, SOS diodes are not available off-the-shelf, and the lack of manufacturers limits the use of this technology [90]. Furthermore, the absence of a transformer limits the gain of this topology.

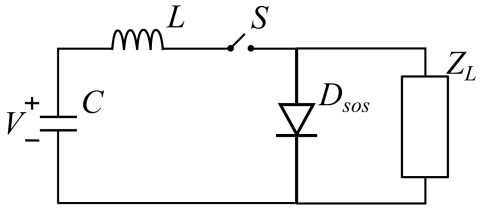

Figure 2.3: Semiconductor opening switch inductive discharge topology

Beyond these conventional designs, other topologies are being developed to address specific challenges. A common approach involves combining different topologies making use of their strengths to meet the application requirements [91–93]. As technology advances, the development of these topologies and entirely new configurations will continue. This ongoing evolution is driven largely by advancements in pulse generator switch technology.

2.1.2 Semiconductor power switches for pulsed power

Pulse generator switches are usually based on either reed switches, spark gaps or semiconductor switches. Reed switches (Figure 2.4-A) consist of two ferromagnetic metal contacts enclosed in a glass tube filled with inert gas, that operate based on the presence or absence of a magnetic field - when a magnetic field is applied, the contacts are drawn together, closing the circuit [94]; spark gaps (Figure 2.4-B) comprise two electrodes separated by a small gap, often filled with air or another insulating medium, which switch-ON by ionising the gap between electrodes when a voltage above a certain threshold is applied; solid-state switches are made of semiconductor devices such as transistors or thyristors, which can be turned ON or OFF electronically [95, 96].

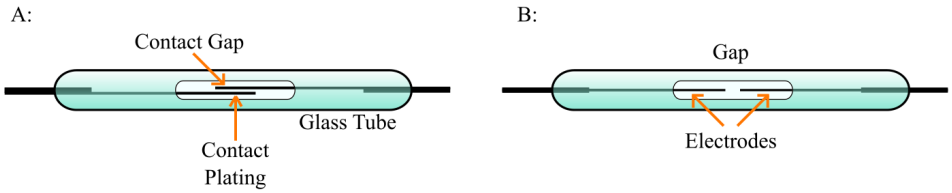

Figure 2.4: A: Reed switch example; B: Spark gap example

Solid-state switches offer advantages such as fast switching speeds, high efficiency, precise control, long lifetime, and ability to operate at high frequency, making them suitable for a wide range of pulsed power applications [97], while reed switches (relatively slow switching speed, limited power handling capability, and mechanical wear over time) and spark gaps (can handle high voltages and currents, with fast switching speeds, but may require high triggering voltages and exhibit arcing) are preferred for specific applications based on their unique characteristics and requirements.

The performance of pulse generators based on power electronics is linked to the capabilities of the power semiconductors. There is a wide range of semiconductor devices that boast varying voltage, current, switching speed, and lifespan parameters. High-voltage diodes, thyristors, injection-enhanced gate transistors (IEGTs), metal-oxide-semiconductor field-effect transistors (MOSFETs), power junction field-effect transistors (JFETs), and insulated-gate bipolar transistors (IGBTs), are some of the power semiconductors used in pulsed power applications. Each has particular operating principles, and different ranges of volt-ampere ratings and switching speeds [83, 98–103].

Due to their high-voltage capabilities, semiconductors based on silicon carbide (SiC) structures are under tremendous attention [65, 101, 104, 105], reaching now the $15\,\mathrm{kV}$ range with SiC-IGBTs and SiC-MOSFETs [106, 107]. Gallium nitride (GaN) is another promising alternative to SiC and Si for pulsed power and is being explored for high-speed GaN-JFETs. These offer relatively fast switching ($100\,\mathrm{MHz}$, $10\,\mathrm{ns}$) compared to existing options, with cascode configurations reaching $10\,\mathrm{kV}$ blocking voltages [108, 109].

IGBTs are one of the most used semiconductor devices in pulsed-power technology. They can be viewed as high-voltage PNP bipolar transistors controlled by a MOSFET; hence similar gate drivers can be used: IGBT is switched ON if v_{GE} exceeds the threshold value V_{GEth}. However, high-voltage IGBTs boast a reduced ON-state voltage drop, compared to MOSFETs. This is achieved thanks to an extra P+ layer (either placed in the drain side or replacing the N+ layer), introducing holes that enhance conductivity. IGBTs experience a relatively slow turn-OFF and exhibit tail currents, causing higher switching losses than in MOSFETs [110]. However, IGBTs exhibit superior hold-off voltage and current characteristics compared to Si MOSFETs, making them the preferred choice in several high-voltage applications [111–113].

Stacking semiconductor devices in series enhances voltage rating, while parallel connections increase current capability, allowing tailored switch design for specific control of high-power applications [96, 110]. For series assemblies, maintaining the voltage balance both in steady-state and transient conditions across the semiconductor devices is crucial. These devices cannot sustain voltages beyond their specified ratings, and the reverse currents and recovered charges vary among devices, even those of the same type and manufacturer. Consequently, the device with the smallest reverse leakage current will be exposed to a higher voltage. Voltage balance techniques include resistors and Zener diodes for steady-state balancing, and resistor-capacitor and Transient-voltage-suppression

(TVS) diodes for transient balancing [114].

For parallel assemblies, semiconductors with a positive temperature coefficient, like MOSFETs and IGBTs, typically do not require current balancing devices. It is important though to ensure symmetry to reduce stray inductances and capacitances, and to maintain a balanced temperature across the junctions. Semiconductors with a negative temperature coefficient (diodes, thyristors, bipolar transistors, etc), must resort to techniques like series resistors, current-sharing coupled inductors, and current feedback control techniques [96, 115, 116].

Carefully designing the current paths for the stacked devices as well as pre-selecting and matching similar devices are also techniques that reduce imbalances in series and parallel assemblies of semiconductors [117, 118].

2.2 Current balancing techniques

Some power electronics systems require current to be distributed equally across parallel paths, current balancing techniques can be used to improve the robustness and efficiency of these systems. These techniques span diverse applications, from multiphase converters minimising ripple in DC-DC conversion to battery management systems safeguarding cell life further extending to photovoltaic systems maximising energy harvest and electric vehicle chargers guaranteeing efficient grid integration [119–121].

Current balancing techniques typically split into passive, active, and hybrid methods. Passive strategies, such as the use of resistors or inductors, offer simplicity but potentially lower performance [122]. Active approaches, employing feedback-based control methods, achieve superior accuracy at the cost of increased complexity [114]. Hybrid methods aim to strike a balance between these two extremes [123]. Recent advancements in low-frequency applications include wireless communication (enables decentralised balancing in intricate systems) [124] and machine learning (adaptive and optimised balancing strategies) [125].

Passive current balancing methods using coupled inductors, offer the advantages of simplicity and increased power ratings and are therefore still adopted by many modern power electronic systems (Figure 2.5) [122, 126, 127].

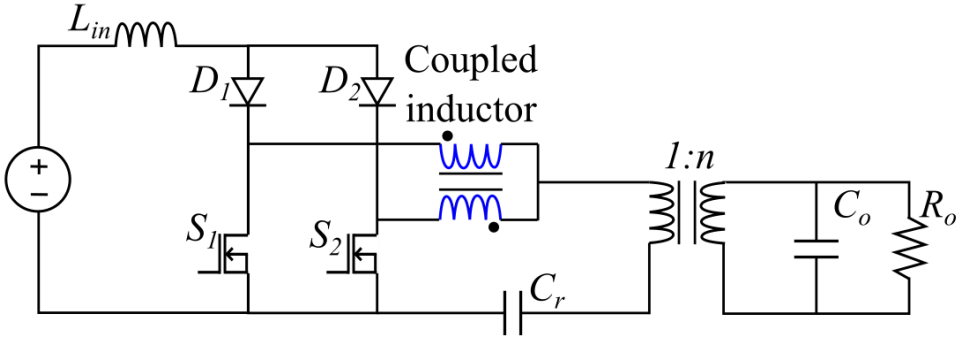

Figure 2.5: Example of passive current balancing method - coupled inductor for semiconductor current balancing in a pulsed power application [122]

Chapter 4 explores how coupled inductors were used to balance the pulsed current of two neighbouring synchronised plasmas in the DPS [43].

2.3 Plasma models for electrical simulations

The ability to understand and predict the behaviour of plasmas under various conditions is relevant to different research subjects. Distinct plasma models [128–130] have been developed to analyse diverse plasma characteristics that focus on parameters relevant to each application.

Particle-in-cell (PIC) simulations directly model the motion of charged particles under the influence of electromagnetic fields [128, 131]. PIC methods can handle a wide range of plasma conditions, including collisionless plasmas, relativistic regimes, and multi-species systems. However, the fine resolution required for accurate particle tracking and field calculations leads to high computational demands, particularly for large systems or long simulation times. PIC simulations are extensively used in plasma physics particularly in the study of plasma instabilities and wave-particle interactions [132], modelling of laser-plasma interactions in inertial confinement fusion, beam-plasma interactions in particle accelerators, and analysis of space plasmas and magnetospheric dynamics [133].

Plasma models for electrical applications typically use macromodels for the plasma electrical impedance dynamic behaviour, as seen from the electrical circuits that interact with the plasma. As gas tube inductance and capacitance are distributed parasitics, the main parameter to be modelled is the plasma resistance. The models developed show that the arc resistance is generally inversely proportional to some function of the arc current: inverse integral equation forms [134–136], and inverse exponential equation forms [137–139]. These resistance models consider (and neglect) particular physical effects of the plasma and were developed for very distinct test conditions and applications [129].

Alternatively, black box models (that disregard the physical processes and focus solely on the electrical properties), employ differential equations to represent the arc impedance. The Cassie and Mayr arc models are examples of plasma/arc black box models [140, 141] and are suitable for several applications from the development of spark gaps to fault arc study [130].

Mayr's model assumes constant arc cross-section and thermal conduction as the sole energy loss mechanism [142] and describes the arc conductance (g) over time based on the power balance between the input energy and the arc's cooling. It can be described by the equation (2.1), where τ is the arc time constant, P is the power applied to the arc (the product of the arc current with its applied voltage), and P_0 is the power loss constant (cooling constant).

$$\frac{1}{g}\frac{dg}{dt} = \frac{d(ln\, g)}{dt}\frac{1}{\tau}\left(\frac{P}{P_0} - 1\right) \tag{2.1}$$

Cassie's model assumes constant arc temperature, current density, and electric field, while the arc cross-section varies with current and time, and energy losses through thermal convection. Its focus is on the arc voltage v rather than conductance, and it considers the arc as governed by a relationship between arc current and voltage. The model is described by the differential equation (2.2), where V_0 is a constant representing the arc voltage in steady-state [130].

$$\frac{1}{g}\frac{dg}{dt} = \frac{1}{\tau}\left(\frac{v^2}{V_0^2} - 1\right) \tag{2.2}$$

Mayr's model uses the logarithmic relationship of conductance and is more sensitive to energy dissipation.

Cassie's model uses a quadratic relationship for voltage, emphasising stability around a steady-state voltage. The Cassie Arc Model was chosen for the plasma modelling and simulations of this thesis due to its suitability for high-intensity currents and relatively steady behaviour. From (2.2) we obtain the (2.3):

$$r\frac{d}{dt}\left(\frac{1}{r}\right) = \frac{1}{\theta}\left(\left(\frac{v}{V_0}\right)^2 - 1\right) \Rightarrow r = \int\left(1 - \left(\frac{v}{V_0}\right)^2\right)\frac{r}{\theta}dt. \tag{2.3}$$

Figure 2.6 represents the Cassie-arc equation using the PSpice library. The initial value of R is $120\,\mathrm{k}\Omega$ representing the tube impedance before the plasma breakdown. The time-varying resistance is included in the model using a voltage-controlled current source.

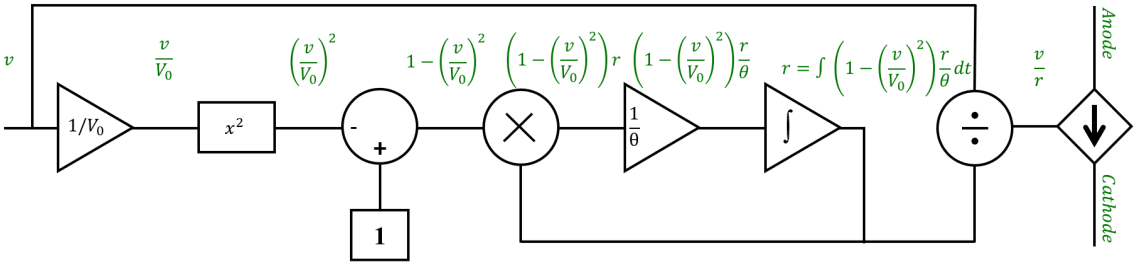

Figure 2.6: Cassie Arc Model in PSpice

Simulations using the model of Figure 2.6 were used for the design and development of the plasma source pulse generator topologies and are explored throughout the thesis, particularly in the chapters 3 and 5.

CHAPTER 3

Plasma source electrical design and operation analysis

Based on the requirements established in Chapter 1 and the state-of-the-art designs explored in Chapter 2, the design and operation of the semiconductor-based pulse generator for the AWAKE plasma source are explored in this chapter.

3.1 AWAKE plasma source requirements

To analyse the requirements and challenges of the pulse generator, it is necessary to study the characteristics of gas discharges and the behaviour of the plasma, considering the particular parameters of length, diameter, gas, pressure, etc.

A discharge plasma source for AWAKE requires a pulse jitter of a few nanoseconds (to ensure synchronisation with the incoming proton beam), a $10\,\mathrm{m}$ length, and pressures between $1 - 50\,\mathrm{Pa}$ to reach the target plasma densities [18, 22]. Analysing the Paschen curves for microsecond pulses [41], a low-jitter ignition requires a pulse rise-time (to $\sim 20\,\mathrm{kV}$) under $1\,\mu\mathrm{s}$. Furthermore, to reach the plasma density target of 7×10^{14} the discharge must have a current density $\sim 100\,\mathrm{A/cm^2}$ which, for a $25\,\mathrm{mm}$ diameter tube, results in a current of $\sim 500\,\mathrm{A}$ [42, 43]. Combining the necessary voltage for low-jitter ignition and current for plasma heating requires one high-power pulse of over $10\,\mathrm{MW}$. The power limitations of the existent fast-switching semiconductors combined with considerations related to compactness, efficiency, safety, and cost, prompt the adoption of two distinct pulses for the plasma ignition (high-voltage) and heating (high-current) processes. The heating pulse can take advantage of the low-impedance plasma created by the ignition pulse to obtain a highly reproducible high-current plasma, lasting tens of microseconds.

Preliminary experiments revealed that ignition discharge jitters under $10\,\mathrm{ns}$ can be obtained with $20\,\mathrm{kV}$ peak voltage pulses, with a rise time of $\sim 1\,\mu\mathrm{s}$ [24]. After the breakdown, this voltage will fall sharply again due to the low impedance established in the plasma. It is important that the ignition pulse source stores enough energy to maintain a stable plasma ($I > 10\,\mathrm{A}$) until the activation of the heater pulse.

The heater pulse must be able to supply the target current of $500\,\mathrm{A}$ but will require a lower voltage pulse. Preliminary results indicate that a $5 - 8\,\mathrm{kV}$ heater pulse can reach the target current for a $10\,\mathrm{m}$ plasma.

3.2 Double pulse generator development

The ignition and the heater pulses will be delivered by two pulse generators with different topologies, the ignition and the heater [24]. Each has specific parameters considering the distinct objectives of each pulse, as explored in section 1.3. The ignition module is based on the flyback-type pulse generator presented in the simplified schematic of Figure 1.8-B. The heater module is a negative pulse capacitive discharge (Figure 3.1) adapted from the more basic topology in Figure 1.6-A.

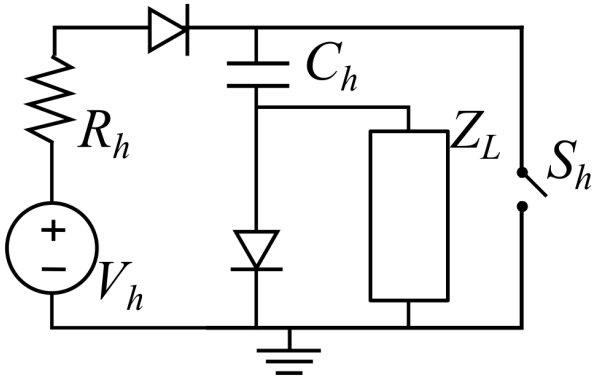

Figure 3.1: Capacitor discharge negative-pulse generator

Through the simplified schematic of Figure 3.2, it is possible to understand the fundamental concept of the double pulse generator. The two modules are familiar pulse generator topologies that will produce the ignition and the heater pulse following the requirements explained in section 1.3. The merger of both topologies (ignition on the right-hand side and heater on the left-hand side) is possible with the inclusion of a coupling diode allowing a seamless operation of the double pulse generator.

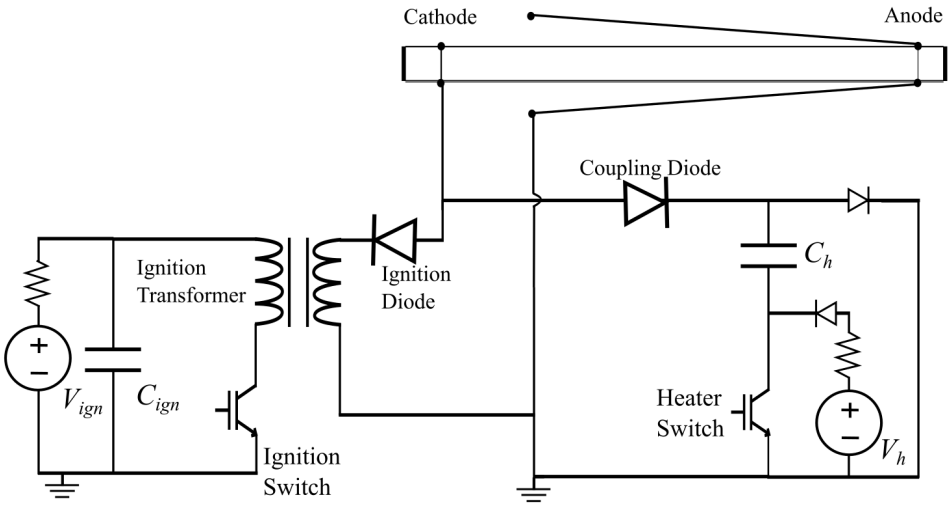

Figure 3.2: Merger of flyback-type pulse generator and negative-pulse capacitive discharge with the discharge plasma as load

To analyse the double pulse generator operation a more complete schematic (Figure 3.3) that includes the protection elements is required. The ignition switch and the heater switch will turn-OFF charged inductances (magnetising inductance of the ignition transformer L_μ and the parasitic inductance of the heater loop respectively), to avoid an overvoltage spike a snubber is paramount. A resistor-diode (RD - R_{isn} and D_{isn}) snubber is used for the ignition pulse generator and a resistor-capacitor-diode (RCD - R_{hdis}, C_{hsn} and D_{hsn}) for the heater pulse generator. We forgo the inclusion of a capacitor in the ignition snubber to reduce the output voltage rise time.

After ignition the plasma acts like an incremental negative impedance (dropping further with the current rise), to avoid overcurrent during the heater pulse a series resistor R_c is included to limit the current value. The inductor L_h prevents an overcurrent in the heater charging loop after the heater switch turn-OFF. The return path of the plasma load contains an *anode cage* to establish field distribution uniformity - maintaining the plasma density uniform in length and cylindrically symmetric [24].

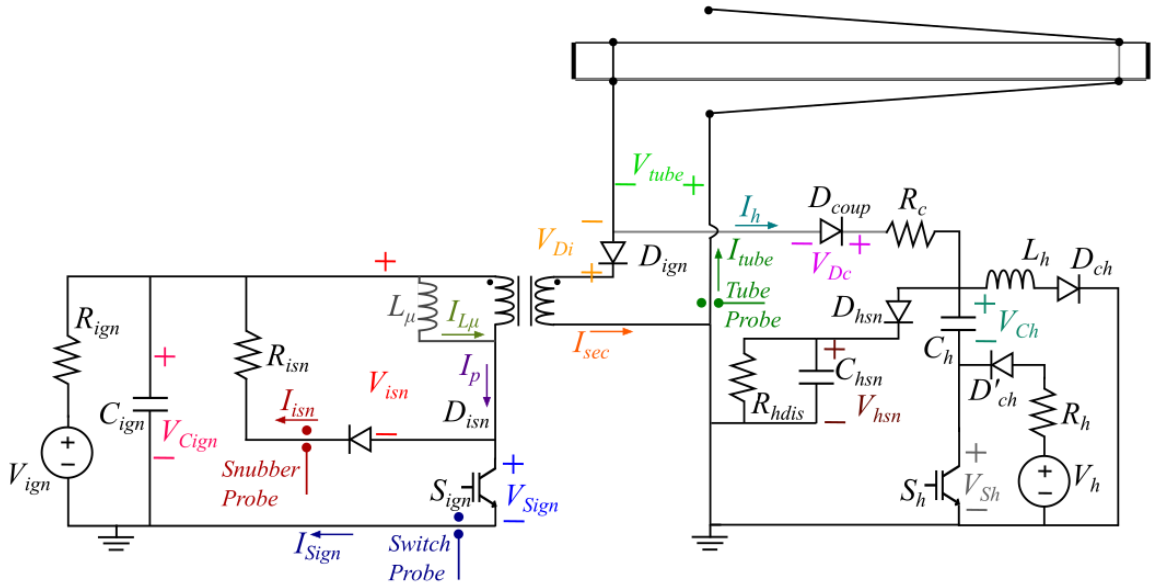

Figure 3.3: Main schematic of the double pulse generator and the plasma, with the relevant elements, voltages and currents, as well as the three current probes used experimentally

3.3 Double pulse generator operation

The operation of the double pulse generator may be analysed considering six steps, corresponding to different switch and gas/plasma states.

First step

The first step happens when the switches of both modules (S_{ign} and S_h) are OFF, and both capacitors charge to the voltage set in the correspondent source (V_{ign} and V_h), as represented with solid lines in Figure 3.4.

Second step

The second step is initiated by the turn-ON of the ignition switch S_{ign} (lasting t_{SignON}). Due to the reverse bias position of the ignition diode (D_{ign}) on the secondary side, the charge in C_{ign} will flow through the primary winding of the transformer, storing magnetic energy in the transformer's magnetising inductance L_μ (solid lines in Figure 3.5).

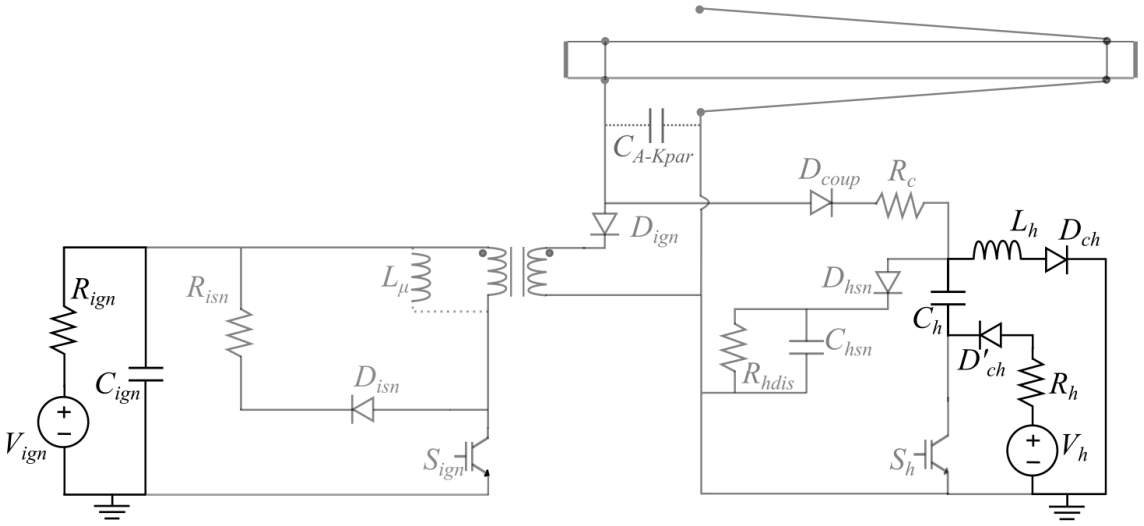

Figure 3.4: First step of double pulse generator operation

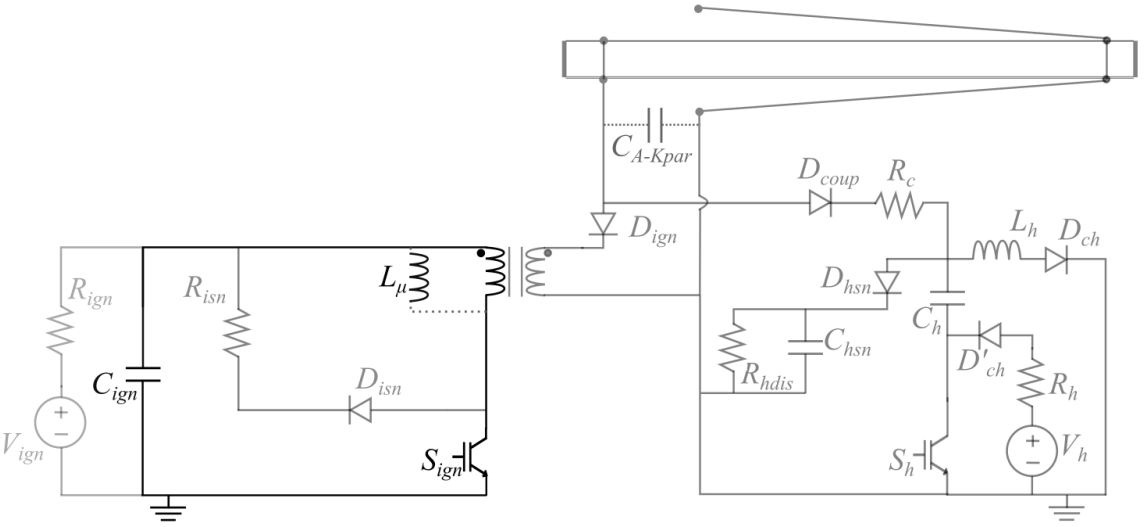

Figure 3.5: Second step of double pulse generator operation - schematic

The power supply V_{ign} high-value series resistance scarcely contributes to the inductor charging current $i_{L\mu}$, with most of the needed energy being supplied from capacitor C_{ign}. The ideal primary circuit, disregarding the ignition switch ON-resistance, switching time, leakage inductances and parasitic capacitances, can therefore be considered an undamped resonant circuit, with impedance $Z_\mu = \sqrt{L_\mu/C_{ign}}$ and resonance frequency $\omega_r = 1/\sqrt{L_\mu C_{ign}}$. Since $\omega_r t_{SignON} << 1$, the current $i_{L\mu}$ (Figure 3.6) and the voltage V_{Cign} (Figure 3.7) can be approximated as

$$i_{L\mu} = \frac{V_{ign}}{Z_\mu} sin(\omega_r t) \rightarrow I_{L_\mu(t=t_0+t_{SignON})} \approx \frac{V_{ign}}{L_\mu} t_{SignON}, \tag{3.1}$$

$$V_{Cign} = V_{ign} cos(\omega_r t) \rightarrow V_{Cign(t=t_0+t_{SignON})} \approx V_{ign}\left(1 - \frac{(\omega_r t_{SignON})^2}{2}\right). \tag{3.2}$$

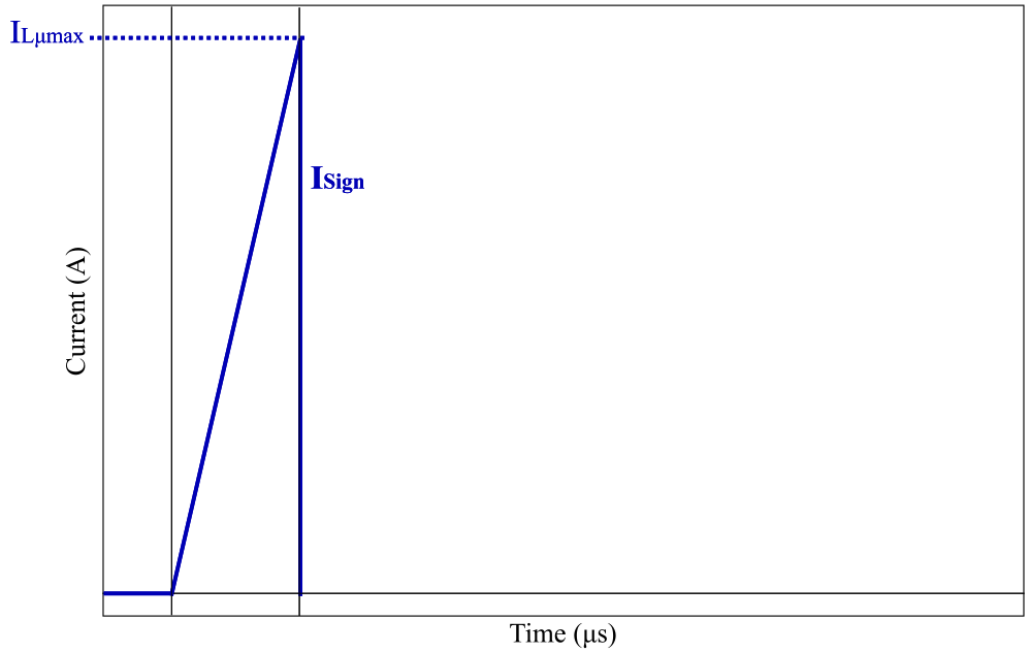

Figure 3.6: Second step of double pulse generator operation - current waveforms

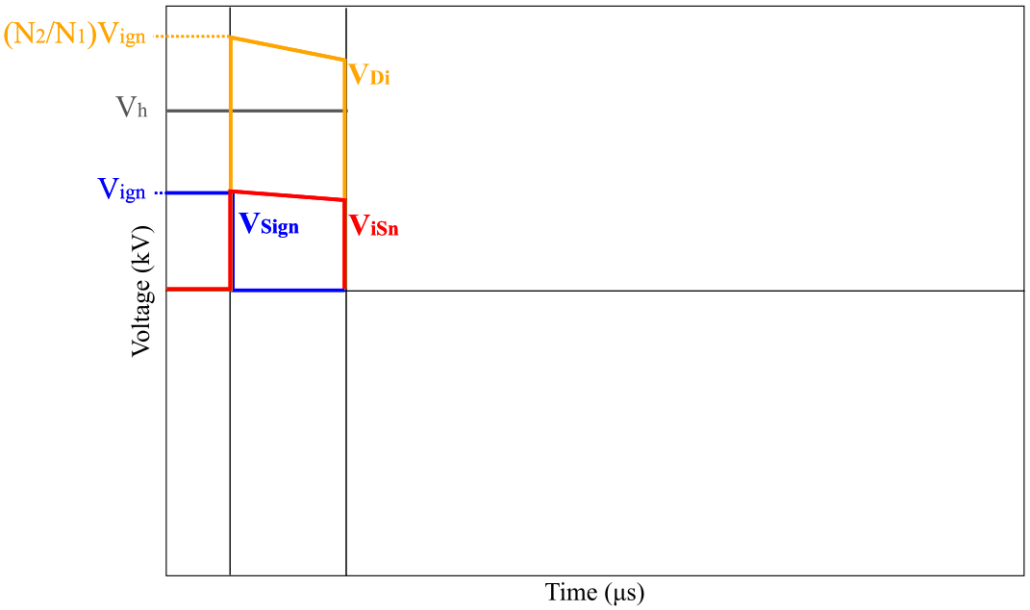

Figure 3.7: Second step of double pulse generator operation - voltage waveforms

Third step

In the third step, by turning OFF the ignition switch (S_{ign}), the snubber D_{isn} and the ignition diodes (D_{ign}) become forward-biased (solid lines in Figure 3.8). This means the voltage spike generated from the switch turn-OFF is applied to both the snubber and the load on the secondary (the latter multiplied by the transformer ratio N_2/N_1). Nevertheless, plasma generation does not occur instantly. The increase in current on the secondary side is constrained by the transformer's leakage and circuit stray inductances, as well as the charging of the tube parasitic capacitance before gas ignition (C_{A-Kpar}). Therefore, in this step, the ignition snubber on the primary side absorbs some of the stored energy that cannot be transmitted to the secondary, thus setting the voltage spike as

$$V_{isnMax} = -I_{L_\mu} R_{isn}, \tag{3.3}$$

and, consequently, the switch hold-OFF voltage as

$$V_{SignMax} = V_{ign} - V_{isnMax}. \tag{3.4}$$

The peak voltage applied to the secondary side of the transformer will be approximately

$$V_{plasma} \approx V_{isnMax} N_2/N_1, \tag{3.5}$$

This step lasts between S_{ign} turn-OFF and plasma ignition. This period (called ignition lag - t_{lag}) ranges from 1 μs to 2 μs and depends on the plasma tube/gas parameters (length, gas type, pressure value) and the V_{ign} voltage setpoint.

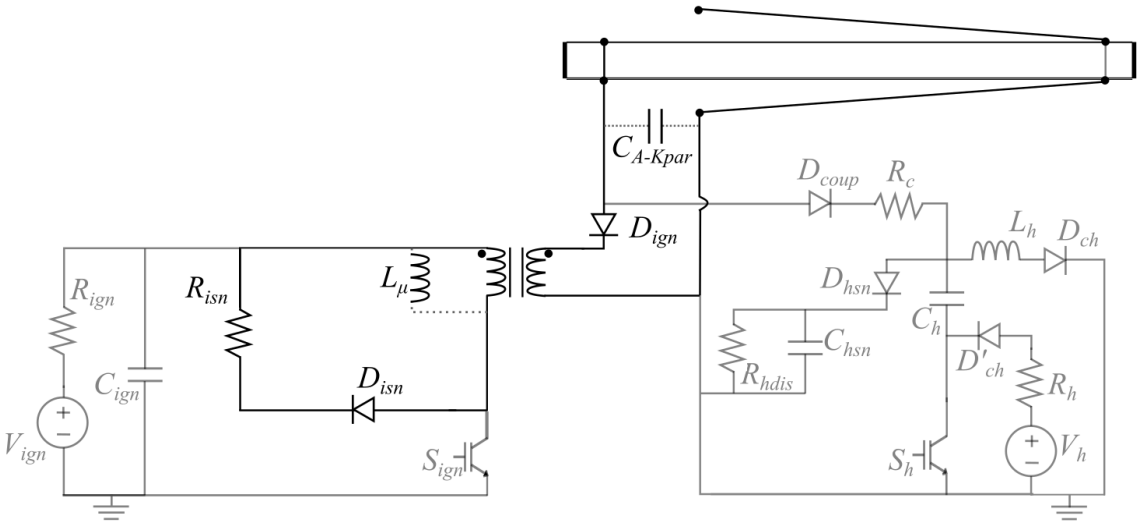

Figure 3.8: Third step of double pulse generator operation - schematic

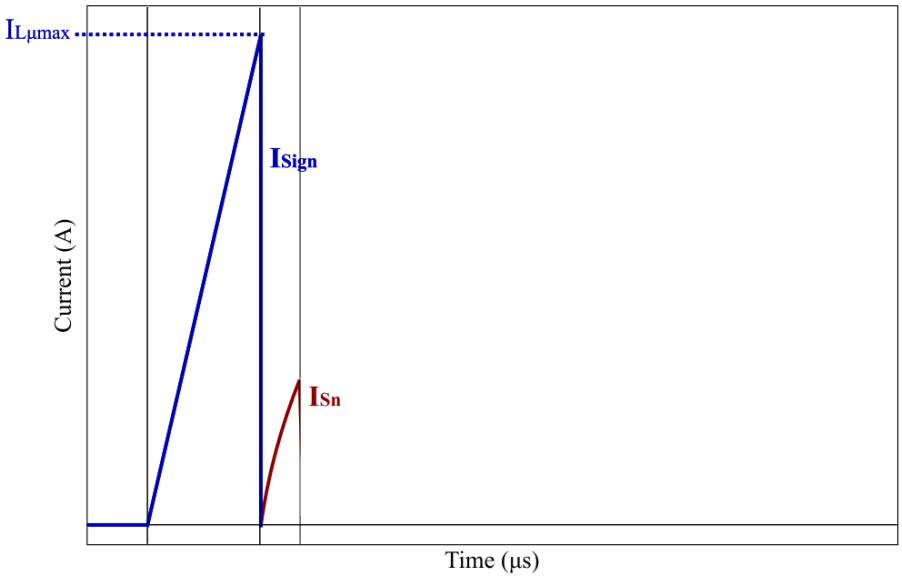

Figure 3.9: Third step of double pulse generator operation - current waveforms

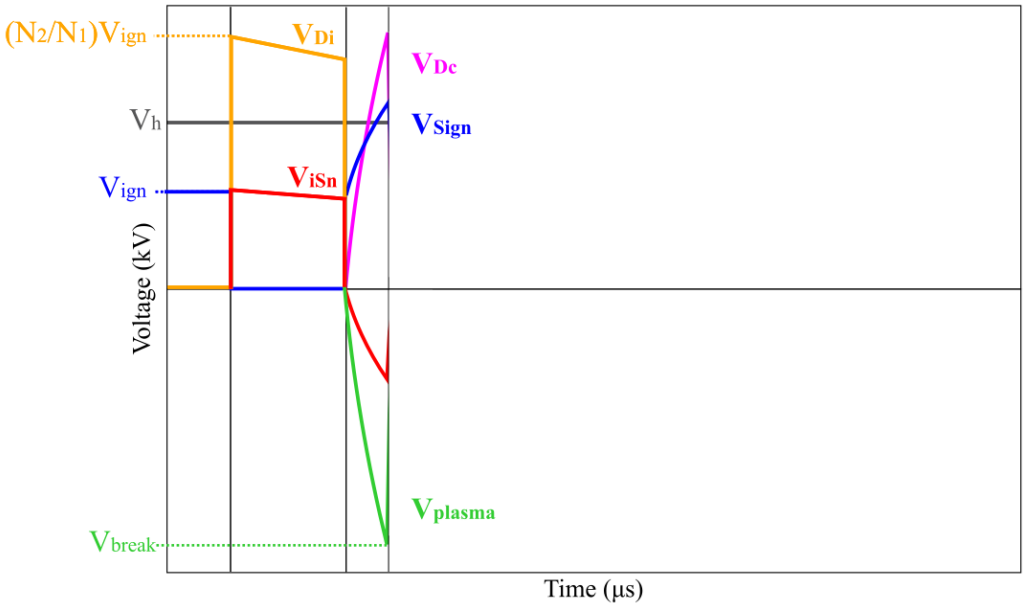

Figure 3.10: Third step of double pulse generator operation - voltage waveforms

Figure 3.9 shows the snubber current rising until the plasma breakdown occurs. Figure 3.10 shows the plasma voltage rising proportionally to the voltage across the snubber resistance. The coupling diode must hold-OFF the voltage applied to the plasma in this step.

Fourth step

The fourth step starts as the plasma ignition occurs; the stored energy is diverted from the snubber to the secondary due to the rapid drop in load impedance (solid lines in Figure 3.11). The plasma current will experience a sudden spike during the ignition and afterwards stabilise, decreasing slowly as the magnetic energy is discharged through the plasma (Figure 3.12), and the plasma voltage will drop rapidly with the plasma resistance (Figure 3.13). The maximum ignition plasma current will be determined by the ignition transformer ratio $I_{plasma} < I_{L\mu} \cdot N_1/N_2$.

The level of plasma ionisation after ignition will depend on the plasma current value during this step. A higher ignition plasma density will improve the reproducibility of the heater pulse; therefore, the choice of transformer ratio must be a compromise between the required voltage value in the third step and a suitable current value in the fourth.

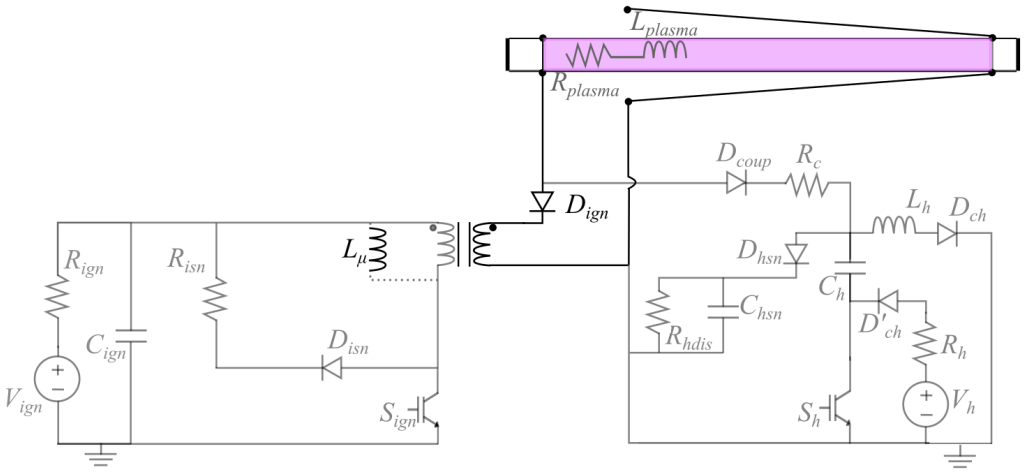

Figure 3.11: Fourth step of double pulse generator operation - schematic

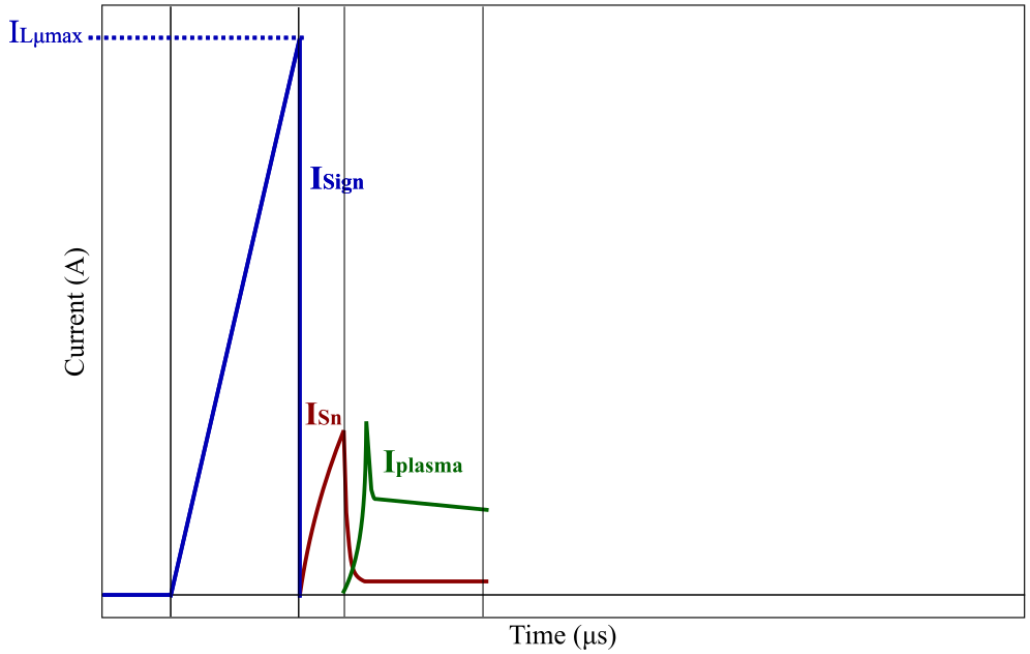

Figure 3.12: Fourth step of double pulse generator operation - current waveforms

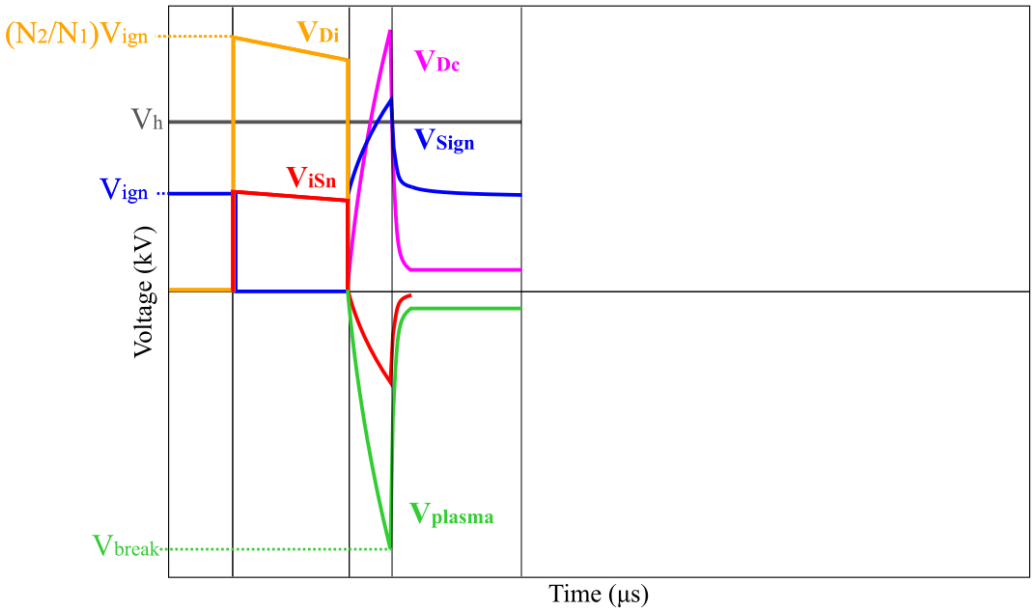

Figure 3.13: Fourth step of double pulse generator operation - voltage waveforms

Fifth step

After the plasma is established, the fifth step is initiated by turning ON the heater switch S_h. The negative pulse capacitive discharge enforces a plasma voltage of approximately $V_{plasma} = -V_{Ch}$, with V_{Ch} being the voltage charged in the capacitor, equal to V_h at the beginning of this step (solid lines in Figure 3.14). The low impedance set before allows the current to rise to $500\,\mathrm{A}$ with minimum jitter, increasing the plasma electron density to the values required.

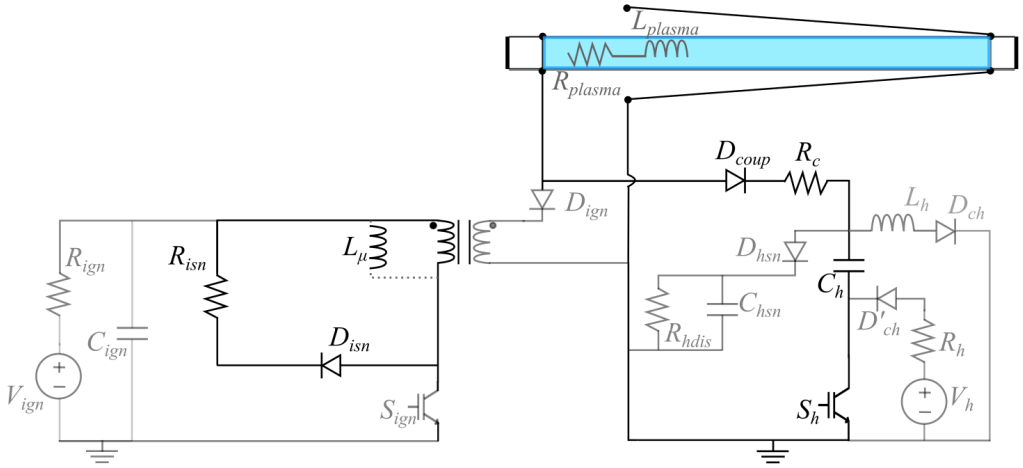

Figure 3.14: Fifth step of double pulse generator operation - schematic

During this step, the voltage applied by the heater pulse will invert the polarisation of the diode D_{ign}, effectively turning it OFF. This will activate the ignition diode D_{isn}, causing the current from the ignition transformer magnetising inductance to be diverted to it. On the other hand, the diode D_{coup} will activate during this step allowing the heater pulse to be delivered to the plasma. This combination allows the independent operation of the heater module.

Ideally, the plasma would have a constant R_{plasma}, the heating capacitor C_h would have an approximately infinite capacitance, and there would be no parasitic inductance L_{plasma}. In these conditions, and neglecting the tube parasitic capacitance C_{AKpar}, the heater pulse would be a square pulse until the switch turn-OFF (that starts the sixth step). However, these ideal conditions do not apply, and the shape of the heater pulse will be affected by the heater capacitance, the plasma tube inductance and the plasma resistance variation.

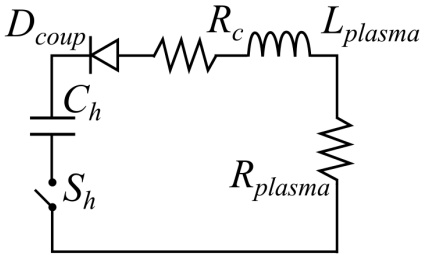

Figure 3.15: Simplified heater capacitive discharge in an RL load

To understand the effect of these elements in the heater pulse we consider the simplified schematic of Figure 3.15. The equations in (3.6) describe the behaviour of the capacitive discharge [143], considering i the current through the circuit and v_C the capacitor voltage:

$$\begin{aligned} v_c &= L\frac{di}{dt} + (R_c + r_{plasma})i \\ \frac{di}{dt} &= \frac{v_C - (R_c + r_{plasma})i}{L_{plasma}} \\ \frac{dv_c}{dt} &= \frac{i}{C} \end{aligned} \tag{3.6}$$

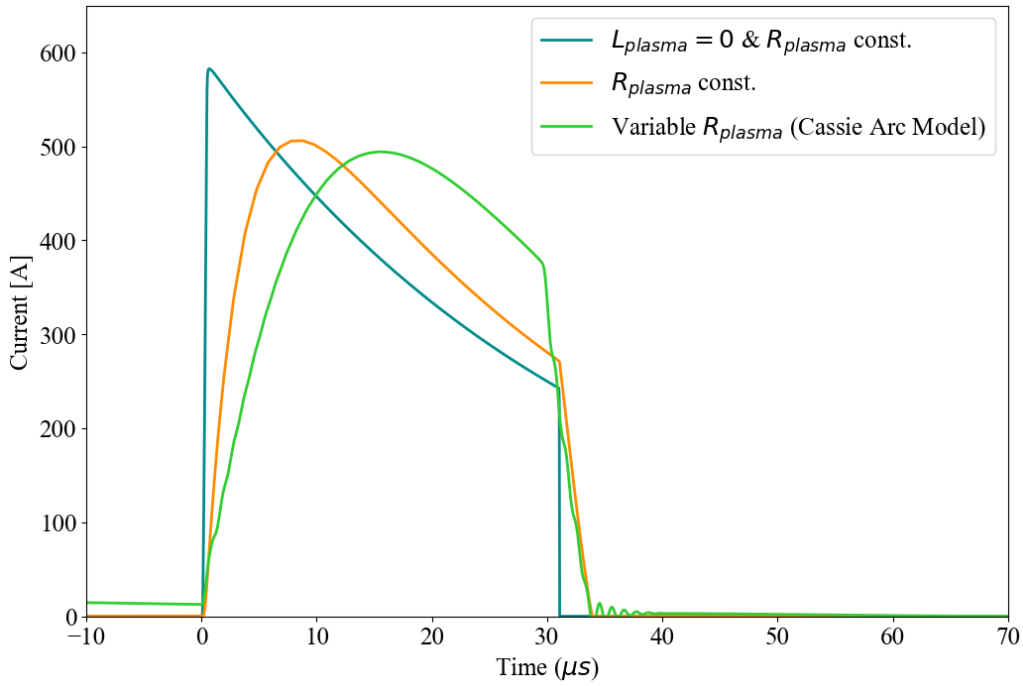

Figure 3.16: Comparison between the heater pulse shape with a constant resistance (with and without parasitic inductance) and a plasma model

Even after ignition, the plasma resistance (r_{plasma}) varies up to an order of magnitude as the plasma density increases significantly under the influence of the heating pulse. As discussed in the Chapter 2, there are several methods to predict and model plasma resistance [129, 142]. The Cassie arc model is described by the differential equation (2.3). This equation can be computed as (3.7), to obtain an expression for dr/dt:

$$\frac{dr}{dt} = \frac{r}{\theta}\left(1 - \left(\frac{v(t)}{V_0}\right)^2\right). \tag{3.7}$$

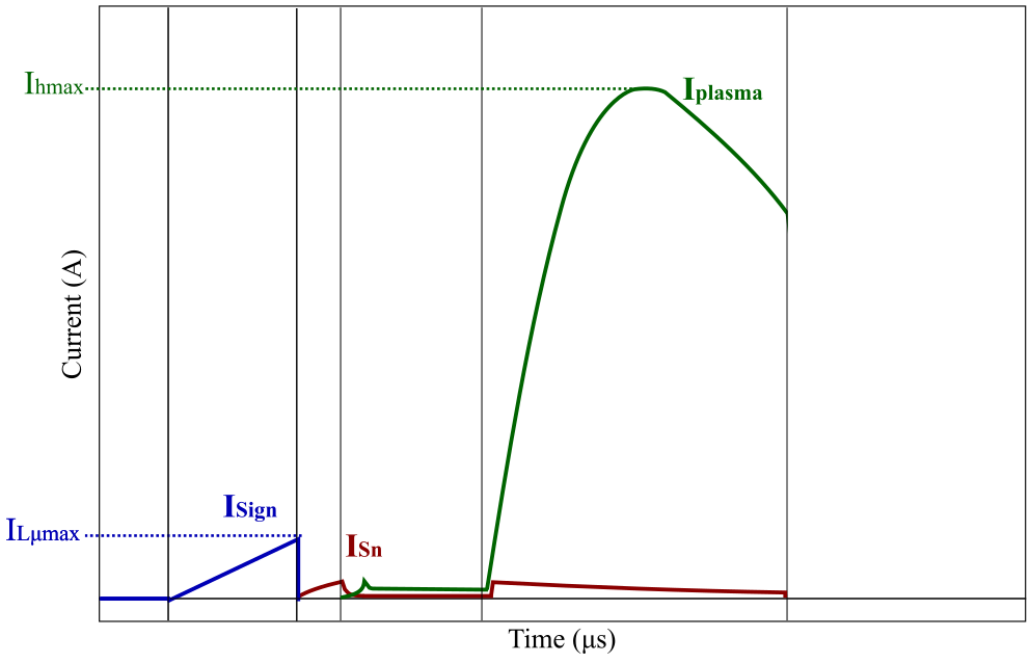

Figure 3.17: Fifth step of double pulse generator operation - current waveforms

Using PSpice simulations it is possible to observe how the introduction of this variable resistance affects the heater pulse shape (Figure 3.16).

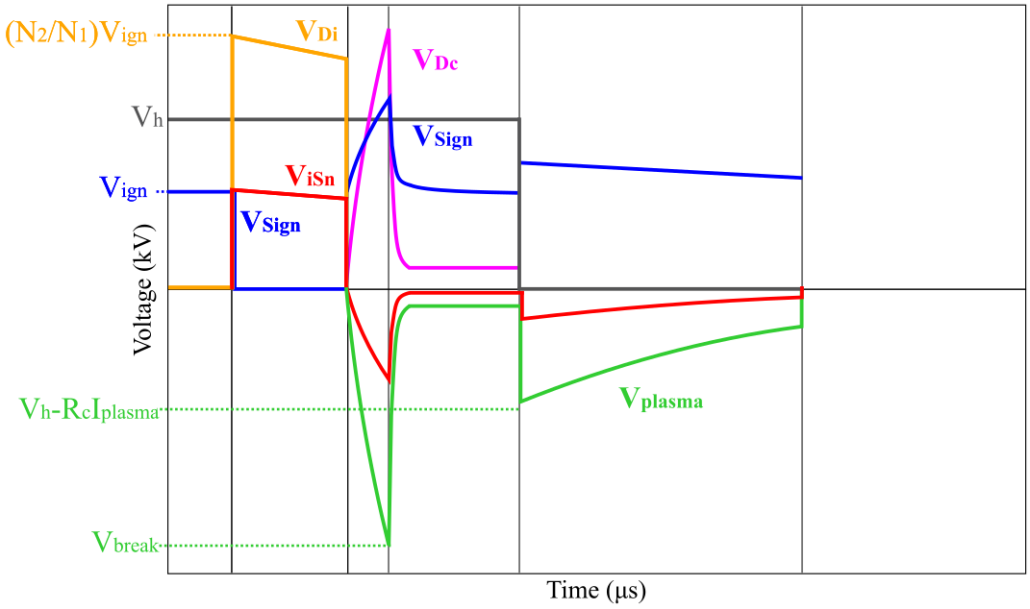

Figure 3.18: Fifth step of double pulse generator operation - voltage waveforms

Figure 3.17 shows the heater pulse shape, obtained by the Cassie arc model, and the reactivation of the snubber diode. In some conditions the stored energy in the magnetising inductance may be depleted before the end of the heater pulse which will cause a faster drop in the snubber current. Figure 3.18 shows the voltage rise across the ignition switch and the snubber resistor, caused by the heater pulse.

Sixth step

In step six, the heater switch (S_h) is deactivated. The capacitive and inductive parasitics of the plasma will prevent it from dropping to zero immediately (Figure 3.16). Therefore, the current in this step will be affected by the rate of discharge of these parasitic elements and the variation of plasma resistance.

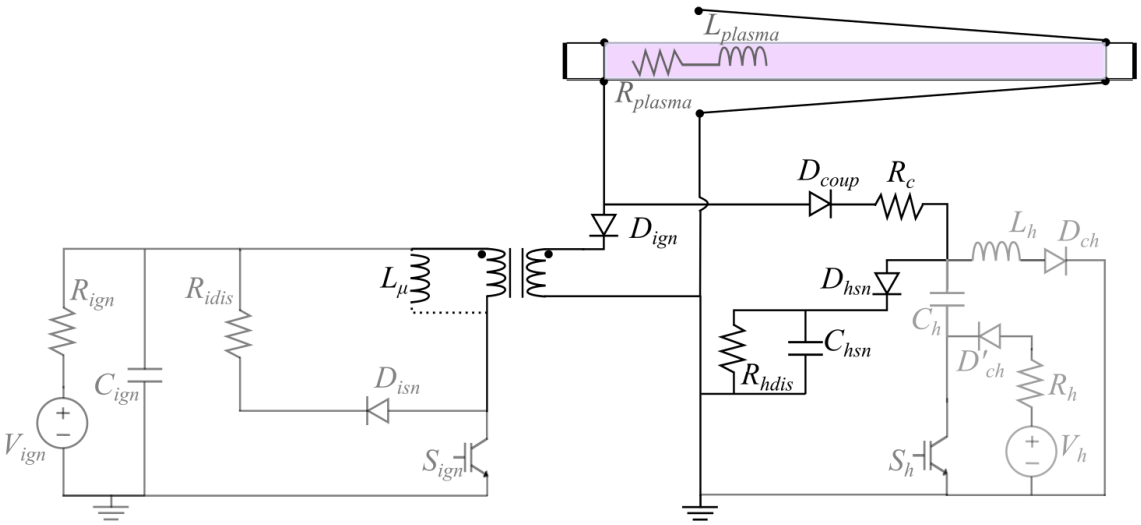

Figure 3.19: Sixth step of double pulse generator operation - schematic

When the plasma voltage falls below the voltage of the secondary winding, the ignition diode is reactivated,

causing the magnetising inductance current, which was previously directed to the ignition snubber, to be diverted to the plasma. Consequently, if there is residual magnetic energy from the transformer remaining, it will discharge through the conductive plasma.

Turning OFF the heater switch S_h will also activate the heater snubber (due to parasitic inductances on the current path) damping the overvoltage and protecting the heater semiconductors, the inductor L_h limits the current rise through the charging diodes. Once the stored energy is insufficient to sustain the plasma, the load ceases to be conductive and the remaining stored energy discharges again through the ignition snubber.

Figure 3.20 and Figure 3.21 show the expected theoretical waveforms for all the double pulse generator operation steps.

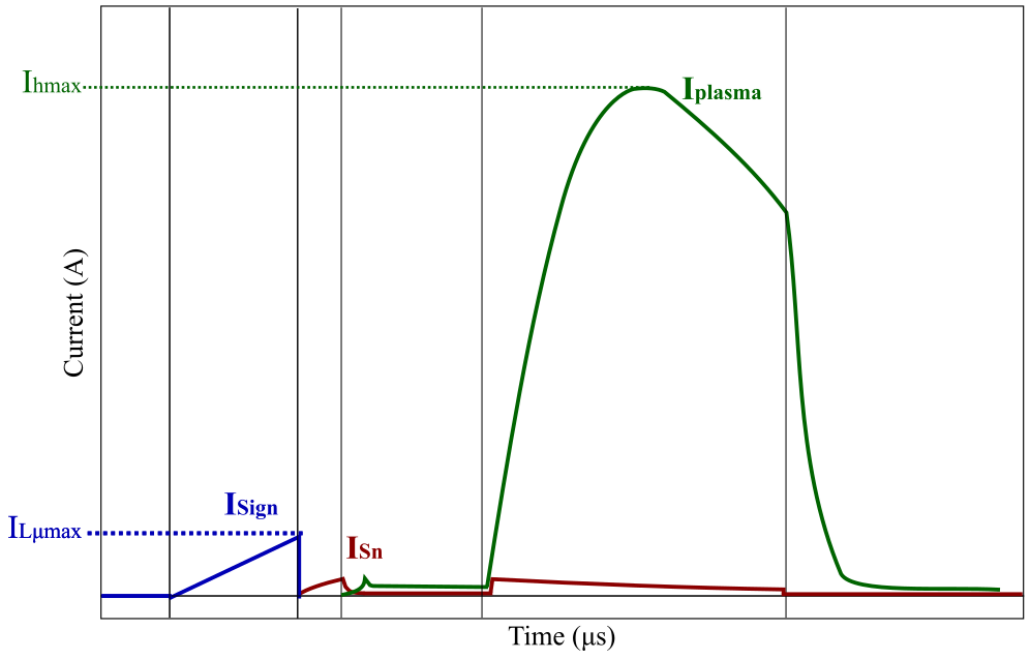

Figure 3.20: Sixth step of double pulse generator operation - current waveforms

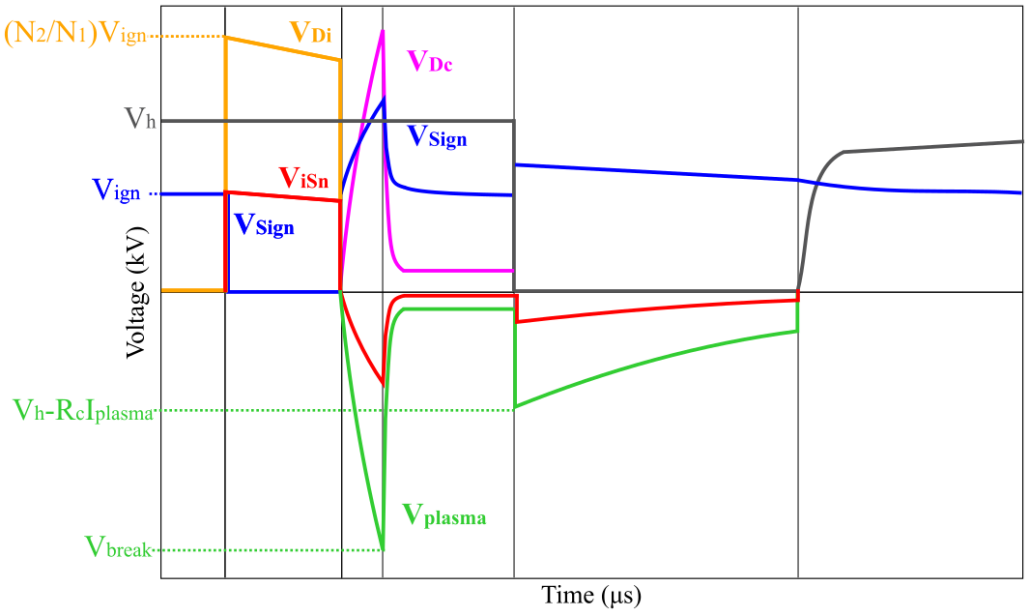

Figure 3.21: Sixth step of double pulse generator operation - voltage waveforms

In Chapter 4 the design of the plasma setup and the sizing of the different pulse generator elements is presented, taking into consideration the application objectives and the operation described in this chapter. In Chapter 5, the simulation and experimental traces are analysed and compared to the theoretical prediction from Figures 3.20 and 3.21.

CHAPTER 4

Discharge plasma source development

This chapter outlines the design and sizing of the key components that make up the DPS, including the plasma setup, pulse generator, and current balancing modules. It provides the foundational design considerations necessary for the development of the DPS, ensuring its readiness for testing and integration into the proton beam experiment.

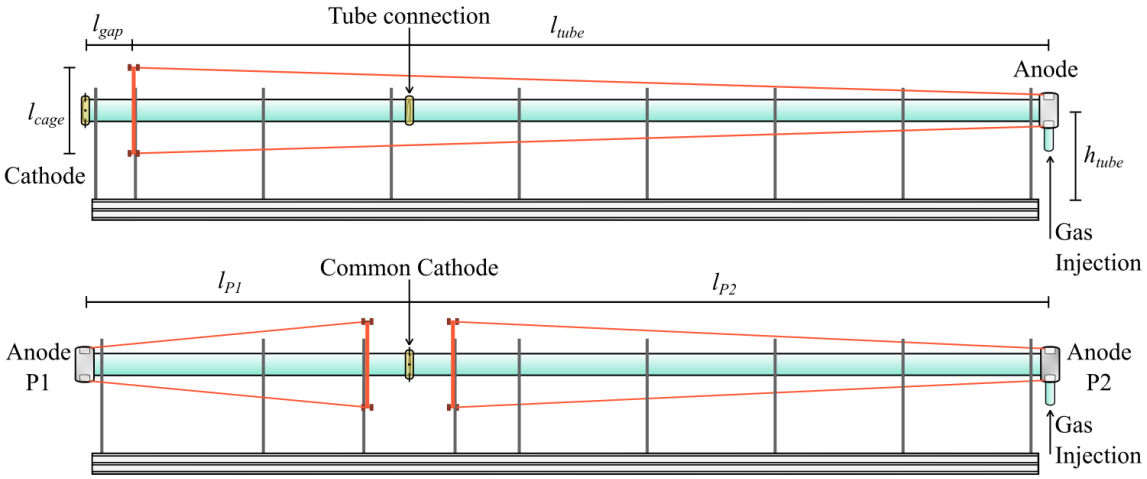

Figure 4.1: DPS geometry

4.1 Plasma setup design considerations

Different applications will require plasma to be generated under very distinct conditions. These conditions (pressure, gas, geometry, etc.) affect the plasma quality and are set by application requirements or technical/physical limitations. The AWAKE requirements, introduced challenges regarding the plasma electron density and the pulse generator reproducibility that motivated the use of the double pulse design, analysed in the previous chapter.

Plasma length

The plasma is generated between two electrodes, inside a dielectric tube. The maximum length between the electrodes (and the tube length) was set as $l_{tube} = 10\,\mathrm{m}$, which is currently the AWAKE acceleration length. A discharge plasma length can be altered simply by changing the position of the electrodes. Since varying the plasma length allowed for relevant diagnostics in the AWAKE experiment, the DPS was designed to have a degree of

flexibility in the positioning of the electrodes (as in Figure 4.1). The DPS tube has the capacity for three different plasma lengths: $10\,\mathrm{m}$ - full length, $l_{P1} = 3.5\,\mathrm{m}$ and $l_{P2} = 6.5\,\mathrm{m}$. Due to the AWAKE experimental restrictions, the plasma scalability potential will be assessed by combining lengths l_{P1} and l_{P2} to determine the possibility of operating two neighbouring synchronous plasmas.

Electrode design

An AWAKE-suitable plasma source must be able to let particle beams cross its length. Therefore, the electrodes must not block the passage of the proton bunches. The anode used is a metallic cylinder at one end of the tube. Connected to the anode is the anode cage: four wires connected to the anode that extend along the tube up to a short distance from the cathode ($l_{gap} = 25\,\mathrm{cm}$) in a $l_{cage} = 25\,\mathrm{cm}$ metallic square centred by the tube.

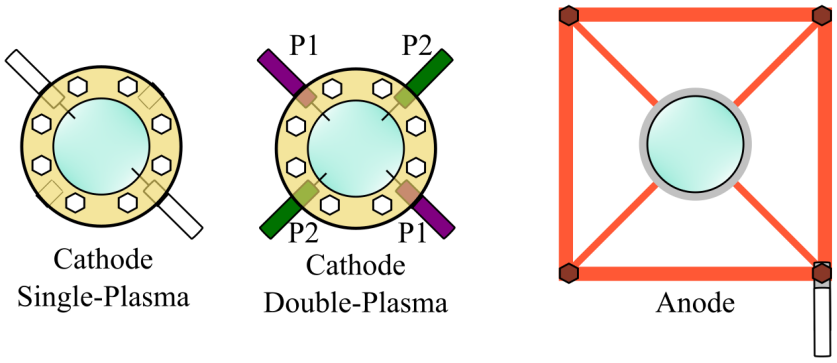

Figure 4.2: Cathode and anode geometry

During the discharge, electrons are delivered to the plasma through the cathode. In an arc discharge, the cathode will develop hotspots. A cylindrical design similar to the anode would result in an undefined and unpredictable hotspot location. Therefore, the cathode is designed with two tungsten pins. Preliminary tests revealed that a single-pin configuration produces non-uniform plasma distribution near the cathode. A coupled inductor is used for current balancing to ensure equal plasma generation across both pins. In a shared cathode (for two-plasma configurations) the plasma pins are assembled alternatively. The Figure 4.2 represents the electrode geometries described.

Cabling, grounding and parasitic components

The electronic equipment used in the AWAKE experiment must be screened from the radiation emitted in the proton beam line. Consequently, the pulse generators, the power supplies and the control systems were separated by a concrete wall from the plasma. The power cables are connected to the plasma through gaps below the wall. The $6.5\,\mathrm{m}$ and $3.5\,\mathrm{m}$ plasma lengths used $8.5\,\mathrm{m}$ parallel-pair cables, and the $10\,\mathrm{m}$ length used two similar cables, combined by an extension box. Before connecting to the plasma, the cables connect to the CBM box, containing the current balancing modules and the ground connection of the setup. Figure 4.3 is a scheme of the connections described.

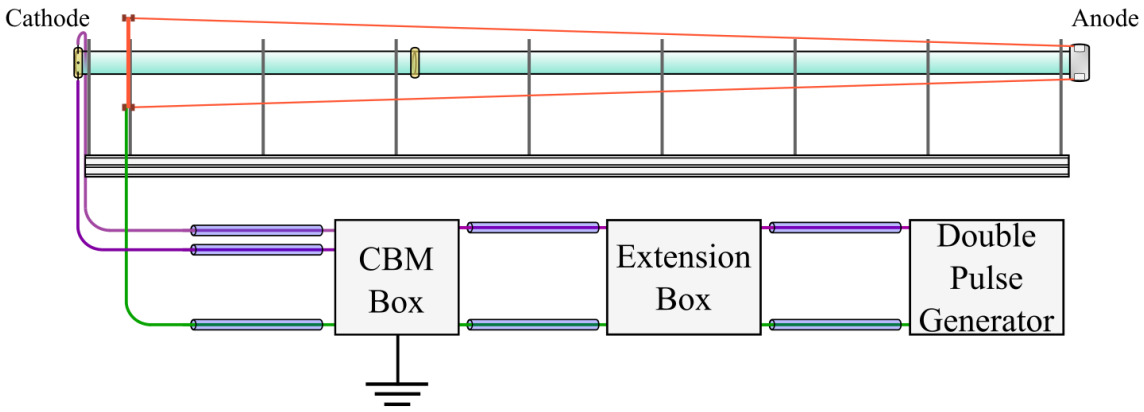

Figure 4.3: Configuration of the plasma source connection to the power input, with parasitic elements

The overall equivalent inductance of the full plasma current path was estimated to be $L_{plama} \approx 24.5\,\mu\mathrm{H}$. The parasitic capacitances were measured between the tube electrodes and the CBM box ($C_{par} = 393\,\mathrm{pF}$), in each set of cable pairs ($C_{cable} = 577\,\mathrm{pF}$), and in the extension box ($C_{extbox} = 203\,\mathrm{pF}$). For simplicity, we consider a single parasitic capacitance of $C_{A-Kpar} = 1.75\,\mathrm{nF}$ for the $10\,\mathrm{m}$ configuration, and $C_{A-Kpar} = 0.97\,\mathrm{nF}$ for the $6.5\,\mathrm{m}$ and $3.5\,\mathrm{m}$ configurations (no extension box and only one cable pair).

Gas system

The gas types used for the DPS were noble gases: helium, argon and xenon. Most discharges were performed using argon, which can reach the nominal AWAKE plasma electron density. Helium is a lighter element, used to observe the effect of ion motion in the self-modulation instability of the plasma. Xenon reached the highest value of plasma electron density. The DPS operates at relatively low pressures ($1 - 100\,\mathrm{Pa}$). These pressures are appropriate for the AWAKE experiment requirements, particularly for argon and xenon (closer to the minimum of the Paschen curves for the $10\,\mathrm{m}$ configuration).

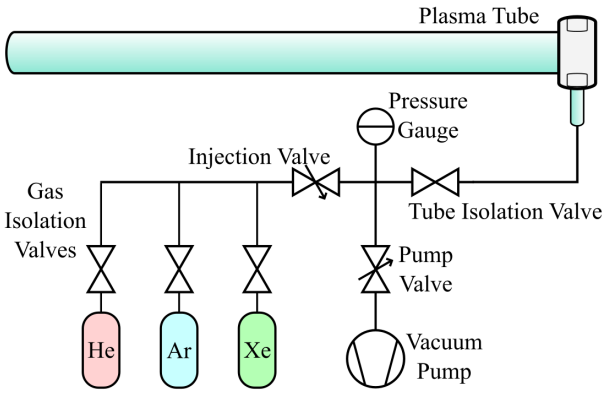

Figure 4.4: DPS gas injection system

The gas injection system is composed of a vacuum pump, three gas bottles, one for each gas, valves and a pressure gauge (Figure 4.4). Before starting the tube discharges, the gas and pressure must be set. The first step is to empty the tube and injection lines with the vacuum pump, then the gas isolation valves are used to select the gas type to be used. The injection and pump are variable proportional valves used to tune the required gas pressure (that is measured in the pressure gauge).

4.2 Double pulse generator design considerations

Having outlined the double pulse generator and its operational principles, as well as the application requirements and the experimental set-up characteristics, this section focuses on the specific considerations for its essential components design: ignition step-up transformer, energy storage capacitors, snubber circuits, IGBT switches, and ignition and coupling diodes.

4.2.1 Ignition step-up transformer

One of the essential elements of the ignition module flyback-type topology is the step-up transformer (Figure 4.5). The design of the ignition transformer differs from a typical transformer design since it operates as a magnetic energy storage device. Therefore, the magnetic inductance is the main parameter to consider. The transformer must also step up the ignition switch-OFF voltage and have a frequency bandwidth appropriate for the desired voltage rise-time.

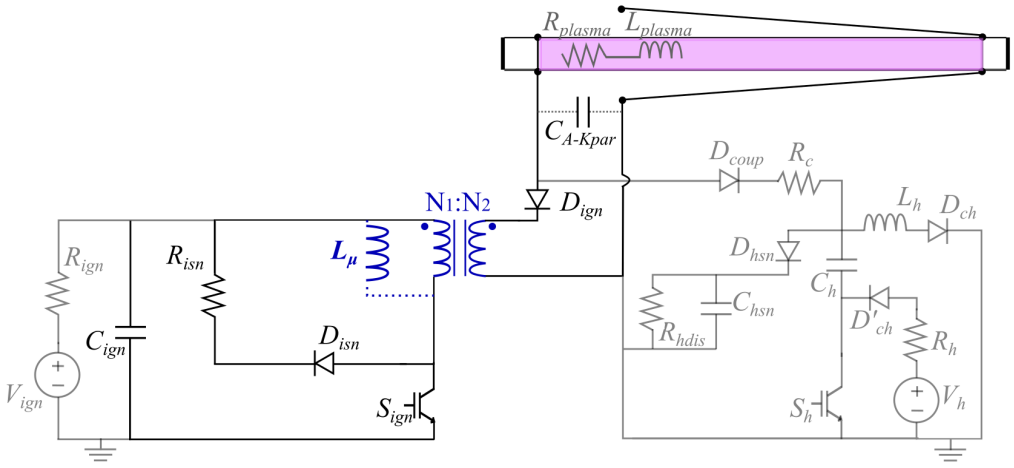

Figure 4.5: Ignition step-up transformer in the double pulse generator

The selection of the magnetic core and the number of primary turns (N_1) is dependent on the desired inductance (L_μ) and energy storage [24, 144]. From Faraday's Law, considering ϕ the magnetic flux in the core of the transformer, V_{ign} the power supply voltage applied to the primary winding of the transformer, and $I_{L\mu}$ the current across the same winding:

$$\begin{cases} N_1 \frac{d\phi}{dt} = V_{ign} \Rightarrow \phi = \frac{V_{ign}\Delta t}{N_1} \\ L_\mu \frac{dI_{L\mu}}{dt} = V_{ign} \Rightarrow I_{L\mu} = \frac{V_{ign}\Delta t}{L_\mu} \end{cases} \quad \Rightarrow \quad \phi = \frac{L_\mu I_{L\mu}}{N_1}. \tag{4.1}$$

The ideal maximum magnetic flux within the core can be expressed as the product of the core's cross-sectional area (A_{Fe}) and the saturation flux density (B_{max}) $\rightarrow \phi = A_{Fe}B_{max}$:

$$A_{Fe}B_{max} = \frac{L_\mu I_{L\mu}}{N_1} \Leftrightarrow N_1 = \frac{L_\mu I_{L\mu}}{A_{Fe}B_{max}}. \tag{4.2}$$

The magnetising inductance is a function of the core magnetic cross-section, magnetic path length (M_{gl}), magnetic permeability (μ), and the number of turns squared:

$$L_\mu = \mu N_1^2 \frac{A_{Fe}}{M_{gl}}. \tag{4.3}$$

Replacing N_1 from (4.2) in (4.3), and rearranging the terms, an equation relating the core dimensions, core flux density, and magnetic permeability to the maximum magnetising inductance energy (W_L) is obtained:

$$\begin{aligned} L_\mu &= \mu \left(\frac{L_\mu I_{L\mu}}{A_{Fe} B_{max}} \right)^2 \frac{A_{Fe}}{M_{gl}} \Leftrightarrow \\ \Leftrightarrow \frac{M_{gl} A_{Fe} B_{max}^2}{2\mu} &= \frac{1}{2} L_\mu I_{L\mu}^2 = W_L. \end{aligned} \tag{4.4}$$

Using equation (4.4), it is possible to select the pulse transformer energy rating, defined as the product of the core volume ($A_{Fe}M_{gl}$) to the core ratio $B_{max}^2/(2\mu)$. The magnetic core energy rating must be equal to the maximum magnetising inductance energy $L_\mu I_{L\mu}^2/2$. Therefore, it is possible to identify a suitable core (or combination of cores).

The equation (4.2) can be used subsequently to obtain the required number of primary turns. The voltage step-up will be determined by the value of R_{isn} and the transformer ratio (N_2/N_1). Designing a transformer with a high step-up ratio requires careful consideration due to the associated increase in leakage inductances and parasitic capacitances.

4.2.2 Ignition and heater capacitors

The ignition storage capacitor (in blue in Figure 4.6) value is obtained by solving (3.2) to obtain (4.5):

$$C_{ign} = \frac{t_{SignON}^2}{2L_\mu(1 - \frac{V_{Cign}}{V_{ign}})}. \tag{4.5}$$

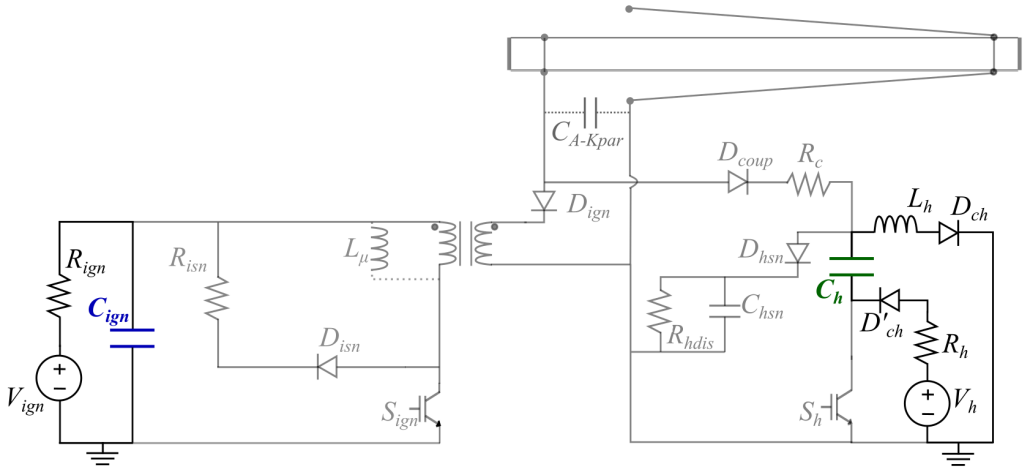

Figure 4.6: Ignition and heater capacitors in the double pulse generator

The heater storage capacitor (in green in Figure 4.6) is sized according to (4.6):

$$C_h = \frac{I_h t_{ShON}}{\Delta V_h}, \tag{4.6}$$

where ΔV_h is the allowed variation of the heater capacitor voltage during one pulse and t_{ShON} is turn-ON time of the heater switch.

4.2.3 Ignition snubber resistor

Topologies similar to the ignition module, based on the opening of inductive current paths, typically use snubbers as semiconductor protection circuits. This is an essential element due to the overvoltage caused by the high value of the current derivative at the turn-OFF. Snubbers will offer an alternative path to the current, limiting the overvoltage to a safe value for the semiconductors.

For this application, besides serving as protection, the snubber must also contribute to setting the gain value V_{isnMax}/V_{ign} (V_{isnMax} is the peak snubber voltage) after the S_{ign} turn-OFF. Therefore, the snubber topology used is a resistor and a diode in series (Figure 4.7). The parallel capacitor, typically used in these snubbers, was excluded to improve the V_{plasma} rise speed. The resistance value is obtained from equation (4.7):

$$R_{isn} = \frac{V_{isnMax}}{I_{iSn}}, \tag{4.7}$$

where I_{iSn} is the current across the RD-snubber. The required V_{isnMax} value comes from the target V_{plasma} divided by the transformer ratio N_2/N_1.

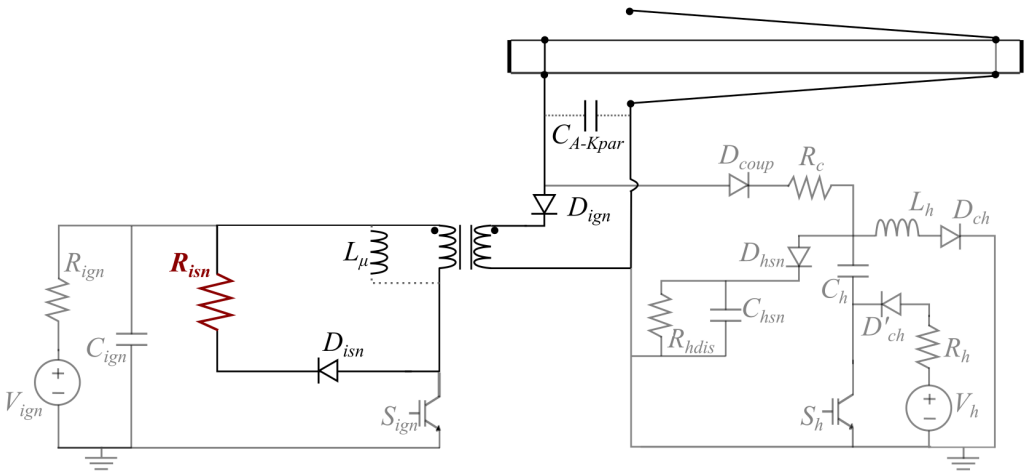

Figure 4.7: Ignition snubber in the double pulse generator

4.2.4 Heater RCD snubber and charging protection inductor

Due to the long length of the plasma and the pulse generator output cables, the heater module will have a high parasitic inductance (L_{plasma}). Consequently, the heater switch turn-OFF generates a voltage spike. The purpose of this snubber is to protect the heater semiconductors from this transient. The snubber capacitance is obtained from the expression (4.8), where V_{ShMax} is the maximum voltage applied to S_h, and I_{hMax} is the maximum current from the heater pulse.

$$\frac{1}{2}L_{plasma}I_h^2 = \frac{1}{2}C_{hsn}V_{ShMax}^2 \Rightarrow C_{hsn} = \frac{L_{plasma}I_h^2}{V_{ShMax^2}} \tag{4.8}$$

The resistor R_{hdis} sets the snubber time constant value and should be at least five times lower than a full

operation period ($RC < T/5$), allowing a safe discharge of the snubber capacitance.

The L_h heater charging protection inductor prevents the turn-OFF voltage spike from turning ON the charging diodes. The L_h inductor will limit the voltage rise to no more than V_{ShMax} while the heater snubber is active (Δt_{hsn}). Therefore, the inductance value comes from the equation (4.9):

$$V_{Sh} = L_h \frac{dI_{Dch}}{dt} \rightarrow L_h = \frac{V_{ShMax} \Delta t_{hsn}}{I_{DchMax}}, \tag{4.9}$$

where I_{Dch} is the current on the charging diodes. The values of R_h, C_h and L_h must have a damping coefficient high enough that the charging of the capacitor is non-oscillant.

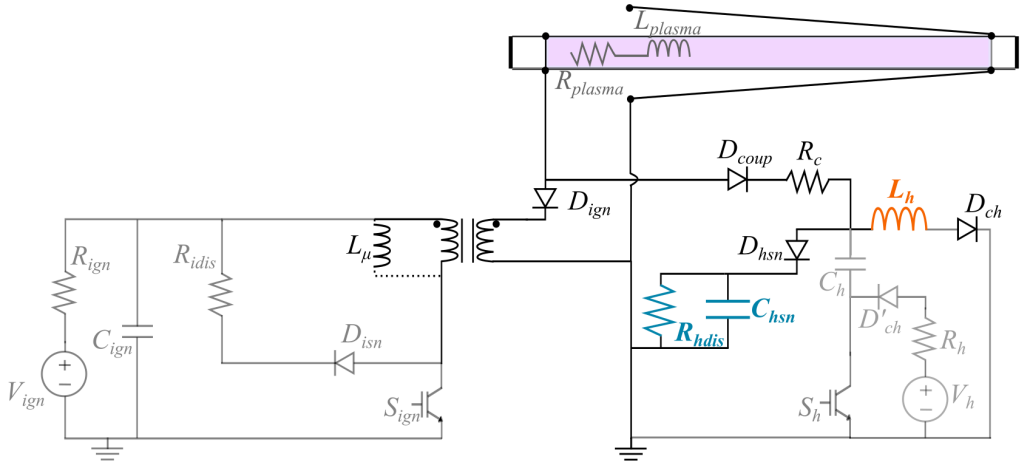

Figure 4.8: Heater snubber and protection inductor in the double pulse generator

4.2.5 Switch and diode modules

Fast-switching semiconductors typically do not have voltage ratings above 5 kV. However, it is possible with series and parallel assemblies to distribute the voltage and current (respectively) through several devices, increasing the overall power rating mostly without affecting the switching speed. Each individual semiconductor device will show a particular behaviour, and strategies are required to assemble them in series or in parallel. For the double pulse generator, the focus is mainly on silicon carbide (SiC) Schottky diodes for the snubber, ignition and coupling diodes and Insulated Gate Bipolar Transistors (IGBTs) for the ignition and heater switches.

The diodes chosen must have suitable switching times and current and voltage ratings. The variation of the forward voltage with increasing temperature is typically negative. Therefore, it is inadvisable to connect diodes in parallel without recurring to current balancing techniques which introduce parasitic elements and complexity to these modules. Thus, the current rating of the diodes should be selected to avoid using a parallel assembly. However, since the applied voltages exceed the capabilities of a single device, multiple diodes are connected in series to achieve the required voltage handling.

The number of series diodes is determined from the expression (4.10) [95], where n is the number of diodes, V_{ap} is the applied reverse voltage, V_{RRM} is the maximum repetitive reverse voltage, and ζ the margin factor:

$$n \geq \frac{V_{ap}}{\zeta V_{RRM}} \tag{4.10}$$

A parallel resistor (R_{bal}) should be included to assure a balanced voltage through every series diode. The

voltage through each resistor due to reverse current should not exceed the V_{RRM} of each diode. The reverse voltage V_R in n diodes is given by (4.11):

$$V_R \approx \frac{V_{ap} - \zeta V_{RRM}}{n-1}, \tag{4.11}$$

and the value of the balancing resistors is determined from the expression (4.12):

$$R_{bal} < \frac{\zeta V_{RRM} - V_R}{V_R} R_{eqOFF} \rightarrow R_{bal} < \frac{n\zeta V_{RRM} - V_{ap}}{V_{ap} - \zeta V_{RRM}} R_{eqOFF}, \tag{4.12}$$

where the equivalent diode-OFF resistance (R_{eqOFF}) is the value of the maximum repetitive reverse voltage divided by the reverse current I_R rating.

The ignition switch is activated during the second step and is turned off on the transition to the third step. The turn-OFF must be done swiftly since the time reproducibility of the plasma breakdown is dependent on this transition. Like with the series assembly of diodes (expression 4.10), the number of IGBT devices in series or in parallel must be high enough that the sum of the maximum ratings of voltage and current, respectively, is larger than the maximum applied value, with a proper margin. Unlike the diodes, the IGBTs have a positive temperature coefficient which allows them to be assembled in parallel directly. Nevertheless, symmetric assembly conditions, reduced parasitic inductance and isolated gate driving are crucial to guarantee safe operation in parallel. The IGBT series connections will have voltage balancing resistors and overvoltage protection TVS diodes, sized to hold-OFF a smaller voltage per stage than the limit of one single IGBT.

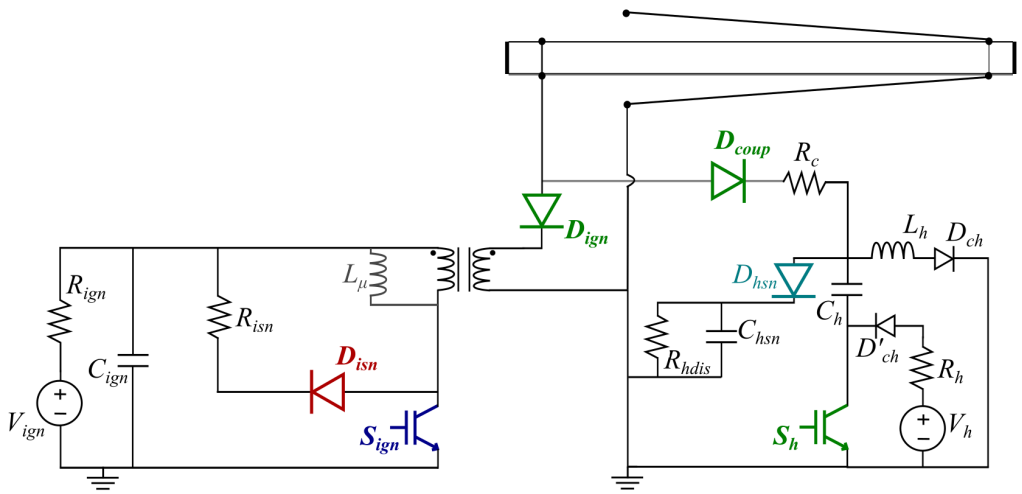

Figure 4.9: Main semiconductor modules in the double pulse generator

There are two main concerns regarding the driving of the switch modules: the first is that the switching must be simultaneous in all IGBT devices to avoid overvoltage/current at one stage and to reduce the pulse jitter. On the driving level, this is pursued by using one single high-voltage pulse distributed to all IGBT stages through a 1:1 galvanic isolation transformer unit. The second is the susceptibility to noise, inherent to pulsed power technology, particularly with loads that are non-linear and prone to parasitic elements. To mitigate this, switch trigger driving is made via fibre optics, ensuring isolation from the main double pulse generator circuitry.

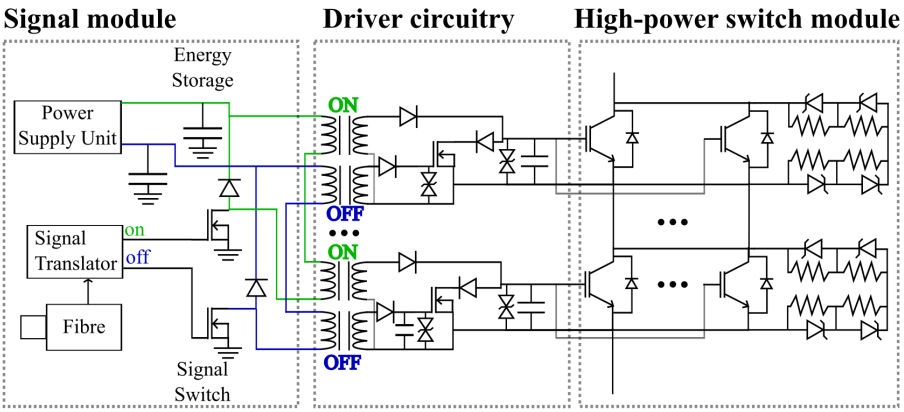

Figure 4.10: Switch driver simplified schematic

The drive electronics for both switch modules are therefore composed of the stages presented in Figure 4.10: i) signal module; ii) driver circuitry; and iii) high-power switch module. Each driver as a turn-ON and a turn-OFF signal that activate the IGBT gate and the MOSFET gate, respectively.

4.3 Current balancing modules design considerations for two-plasma configuration

One of the main requirements for an alternative AWAKE plasma source is scalability in length. The current balancing module (CBM) addresses this requirement by allowing the generation of a series of neighbouring plasmas with shared electrodes, aiming for uniform plasma formation and density across each length. Due to the dynamic plasma impedance and high voltages and currents involved in the plasma generation, the current balancing is performed by a passive technique: high-frequency differential mode magnetic chokes (DMC) [122], consisting of two coupled inductors (Figure 4.11), each linked to one plasma.

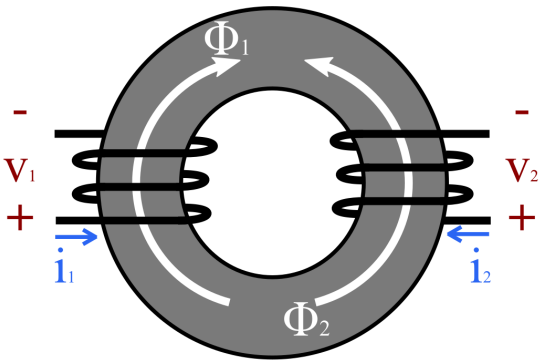

Figure 4.11: Representation of a differential mode choke - with similar currents the magnetic fluxes will cancel out

The initial approach for scalability is to have two synchronous parallel plasma with one DMC. Using a two-plasma configuration the best setup has the common cathode in the centre (where the highest voltage amplitude is applied) and the plasma anodes on each ends. Under this setup, each coupled inductor would be connected to one plasma anode (Figure 4.12), to equalise the current between the common cathode and each anode.

Constraints from the AWAKE experiment led to the asymmetric configuration represented in Figure 4.12, with

plasma lengths of 3.5 and $6.5\,\mathrm{m}$. This asymmetry affects the design of the DMC drastically. Under similar plasma lengths, the main design focus of the coupled inductor would be reducing leakage inductances and guaranteeing a good frequency response and good coupling between the windings.

With asymmetric lengths, the contrast in plasma resistance will cause much higher current differences, particularly during the heater pulse. Therefore, the coupled inductors of the DMC must present inductance values significantly higher, enough to induce the required voltages to balance the two currents.

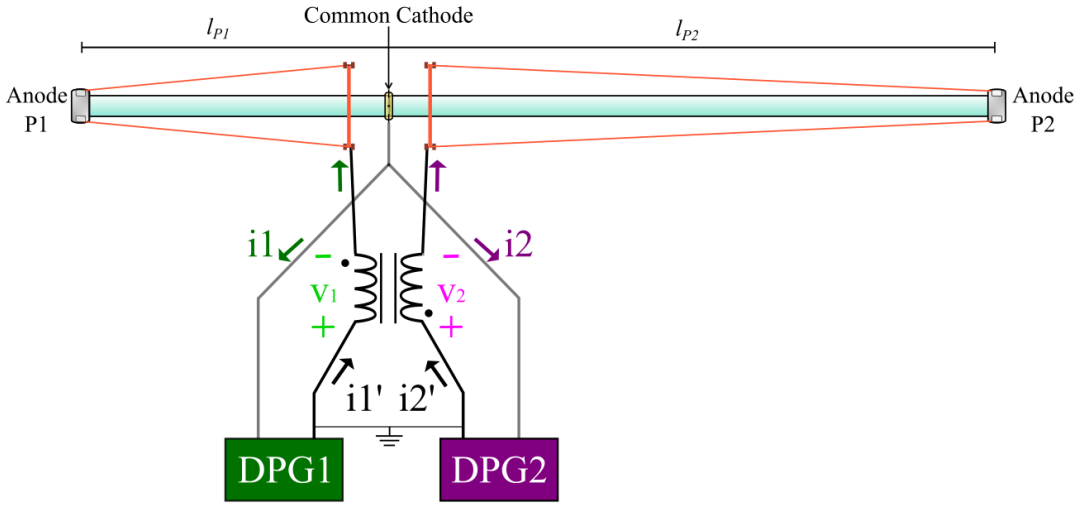

Figure 4.12: Double plasma configuration with current balancing coupled inductors

Figure 4.13 represents the current balancing coupled inductors, under steady-state, after the ignition pulse. The two plasma sections act like two separate resistive impedances (R_{p1} and R_{p2}). From Kirchoff's Law, instantaneous voltages of the pulse generators (v_{g1} and v_{g2}) are given by (4.13):

$$\begin{cases} v_{g1} = v_1 + R_{p1} i_1 \\ v_{g2} = v_2 + R_{p2} i_2. \end{cases} \tag{4.13}$$

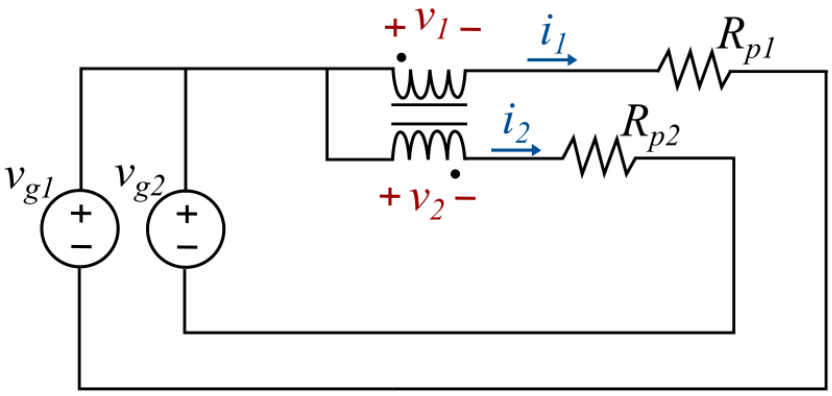

Figure 4.13: Current balancing coupled inductors in steady-state

With two windings and a similar number of turns, the flux linkage (ψ_1 and ψ_2) for each one is:

$$\begin{cases} \psi_1 = L_1 i_1 - L_M i_2 \\ \psi_2 = -L_M i_1 + L_2 i_2 \,, \end{cases} \tag{4.14}$$

where L_M is the coupling inductance, and L_1 and L_2 are the self-inductance of each winding. Using the same number of turns $L_1 = L_2$, from equation 4.14, if the current on both inductors is similar (in amplitude and orientation) the magnetic flux on the DMC core will cancel out (Figure 4.11) and the winding impedance will be defined only by the leakage elements.

Neglecting parasitic capacitances and resistances, the application of Faraday's Law for coupled inductors is:

$$v = \frac{d\psi}{dt}, \tag{4.15}$$

where v is the winding instantaneous voltage, i is the instantaneous current, and ψ is the instantaneous flux linkage. The voltage difference between the two windings is expressed by 4.16:

$$\begin{cases} v_1 = L_1 \frac{di_1}{dt} - L_M \frac{di_2}{dt} \\ v_2 = -L_M \frac{di_1}{dt} + L_2 \frac{di_2}{dt} \end{cases} \quad \Rightarrow \quad v_1 - v_2 = (L_1 + L_M)(\frac{di_1}{dt} - \frac{di_2}{dt}). \tag{4.16}$$

Any discrepancies in the current through the two windings will generate opposing self-induced voltages within the coupled inductors. These self-induced voltages act to cancel out the current difference, ensuring similar currents in the two branches and, consequently, balanced currents in the plasma lengths.

Considering $v_{g1} = v_{g2}$ and $L_M = kL_1$, an expression for the required coupling inductance is obtained from 4.13 and 4.16:

$$\begin{aligned} R_{p2} i_2 - R_{p1} i_1 &= L_M (k+1)(\frac{di_1}{dt} - \frac{di_2}{dt}) \\ \Rightarrow L_M &= \frac{R_{p2} i_2 - R_{p1} i_1}{(k+1)\frac{d}{dt}(i_1 - i_2)}. \end{aligned} \tag{4.17}$$

4.4 Application of design considerations to the AWAKE discharge plasma source

The required plasma parameters presented in Chapter 1 (namely $10\,\mathrm{m}$ length discharges, $7 \times 10^{14}\,\mathrm{cm}^{-3}$ plasma density, synchronisation with the proton beams) and the double pulse generator operation described in section 3.3, combined with the limitations of the electrical devices, set the system specifications on the Table 4.1. The design of the pulse generator will take into account these values for the different elements of both the pulse generators and the current balancing module.

Table 4.1: System Specifications

Parameter	Symbol	Value	Unit
Target ignition voltage	V_{plasma}	20	kV
Target primary current	$I_{L\mu}$	60	A
Maximum primary current	$I_{L\mu}$	130	A
Ignition secondary current Range	I_{sec}	$10 - 25$	A
Heating current range	I_h	$200 - 1200$	A
Heating current target	I_h	500	A
Ignition switch-ON duration range	t_{SignON}	$5 - 12.5$	μs
Ignition switch-ON duration typical	t_{SignON}	10	μs
Heater switch-ON duration range	t_{ShON}	$25 - 50$	μs
Heater switch-ON duration typical	t_{ShON}	30	μs
Target ignition lag time	t_{lag}	2	μs

Ignition and heater power supply units

The power supplies selected for the ignition and heater pulse generators were the Utravolt *6C24-P30* ($V_{ignMax} = 6\,\text{kV}$, $P = 30\,\text{W}$, $I_{outMax} = 5\,\text{mA}$) and *8C24-P250-I5* ($V_{ignMax} = 8\,\text{kV}$, $P = 250\,\text{W}$, $I_{outMax} = 25\,\text{mA}$). They were selected due to their compactness, relatively low ripple ($< 1\%$), and simple control interface. The repetition rate of the pulse generator operation ($\sim 0.1\,\text{Hz}$) allows for relatively low charging currents.

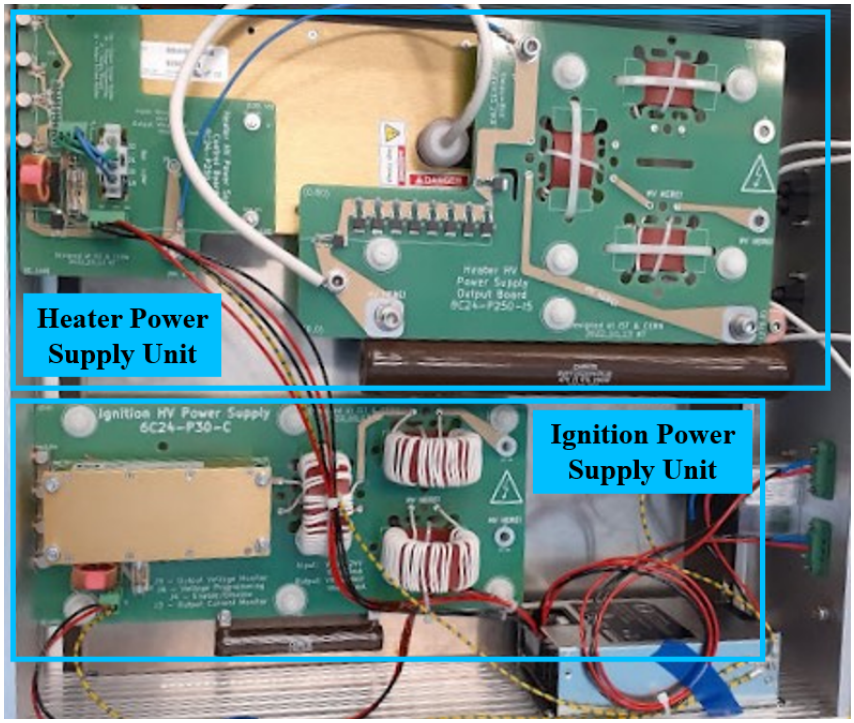

Figure 4.14: Ignition and heater power supply units

The DPS was designed to operate in a wide range of configurations (different plasma lengths, pressures, and gases). To allow for a large operation range, the ignition and heating pulse generators were designed to operate below the maximum voltage of the power supplies for the target voltage and current values. Therefore, the typical

supply voltage values are $V_{ign} = 3.5\,\mathrm{kV}$ and $V_h \approx 6.0\,\mathrm{kV}$. However, the sizing of the pulse generator components must always consider the maximum ratings of the power supplies.

Step-up transformer and ignition snubber resistor

Considering the standard operation ignition voltage ($V_{ign} = 3.5\,\mathrm{kV}$), to reach the target primary current $I_{L\mu} = 60\,\mathrm{A}$ in the typical switch-ON time of $t_{SignON} = 10\,\mu\mathrm{s}$, from (3.1) the required transformer primary magnetising inductance is approximately $L_\mu \approx 580\,\mu\mathrm{H}$. Considering the maximum ignition power supply voltage ($V_{ign} = 6.0\,\mathrm{kV}$) and switch-ON time $t_{SignON} = 12.5\,\mu\mathrm{s}$, the primary current value obtained is $I_{L\mu} \approx 130\,\mathrm{A}$.

From (4.4), to obtain the required 5 J of magnetic energy ($L_\mu = 580\,\mu\mathrm{H}$ and $I_{L\mu} = 130\,\mathrm{A}$) the selected transformer core is a combination of four Micrometal's toroidal powder cores, two *T400-18* and two *T400-52*. Both models have the same dimensions ($M_{gl} = 25\,\mathrm{cm}$, $A_{Fe} = 3.46\,\mathrm{cm}^2$) and approximately the same $B_{max} \approx 1.5\,\mathrm{T}$, but different bandwidths. Therefore, the *T400-18* cores improve the high frequency response and the *T400-52* presents a higher permeability. Considering the combined cores to be equivalent to parallel inductors and their permeability values at the relevant frequencies to be about $\mu_{18} = 55\mu_0$ and $\mu_{52} = 75\mu_0$, for *T400-18* and *T400-52* respectively, the target energy of 5 J is reached. The number of turns to reach the required inductance comes from (4.2), obtaining $N_1 \approx 36$.

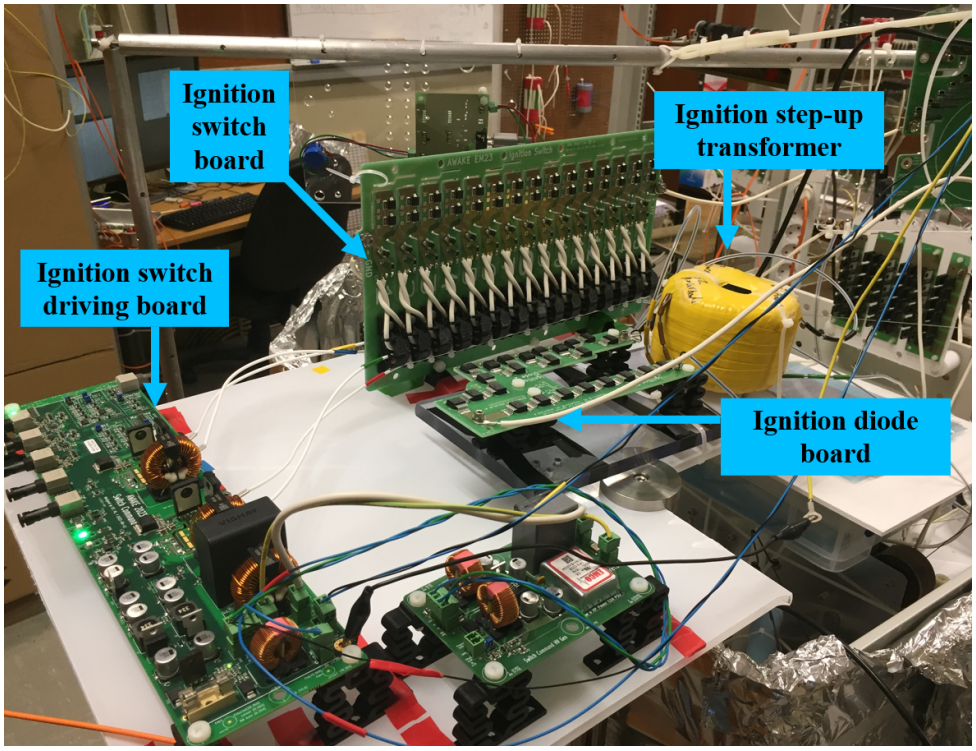

Figure 4.15: Testing ignition pulse generator components using the 5 m plasma in the IST DPS Lab

The low-jitter plasma ignition requires over 20 kV in standard operation, since the ignition power supply delivers 3.5 kV, the diode resistor snubber and pulse transformer must provide a step-up ratio of around 6. Pulse transformers show increasingly high leakage inductances and parasitic capacitances for high step-up ratios, both should be minimised to allow a fast rise of the load voltage. Therefore, moderate pulse transformer step-up ratios, like $N_2/N_1 = 3.5$, should be considered [47] resulting in $N_2 = 126$. This value would also enable a high enough secondary current ($\sim 20\,\mathrm{A}$ theoretical maximum in standard operation) to set the plasma to a low impedance arc

state.

Considering a transformer ratio of $N_2/N_1 = 3.5$, for an output voltage of $V_{plasma} = 20\,\text{kV}$ and a $I_{L\mu} = 60\,\text{A}$, a maximum ignition snubber current of $I_{iSn} \approx 30\,\text{A}$ is expected (considering a part of the inductor current is used to charge the parasitic tube capacitance C_{A-Kpar}). From (4.7) the required value of the ignition snubber resistor is $R_{isn} \approx 200\,\Omega$. From (4.7), considering $I_{L\mu} = 130\,\text{A}$ and a $I_{iSn} \approx 65\,\text{A}$, we determine the maximum output voltage $V_{plasma} \approx 46\,\text{kV}$.

Figure 4.15 is a photograph of the ignition step-up transformer being tested in the IST DPS-Laboratory.

Semiconductor devices selection and design

The diodes and the switches are an essential part of the pulse generators operation. They must sustain relatively high voltages and currents, and be able to switch in nanoseconds. As mentioned in Chapter 2, to enhance their voltage or current ratings they can be assembled in series and/or in parallel (respectively). Assembling the semiconductors this way entails some complications due to the possibility of imbalances between devices and the required switch synchronisation. Different strategies to mitigate these effects were employed. One strategy was the use of parallel resistors (for the diodes) or TVS diodes (for the switches) to balance the voltage between the semiconductors. To reduce the imbalance even further different components of the switches were tested and grouped with those of more similar performance, the components included the driver transformer cores and MOSFETs (Figure 4.10), the balancing TVS diodes, and the IGBT switches. The diodes and the switches were assembled in printed-circuit boards (PCBs) that were designed to have reduced parasitics (particularly in the driving circuitry) and similar layout for all the semiconductor devices. A separate board receives the fibre optics triggers and delivers the driving pulse to the IGBTs (Figure 4.16).

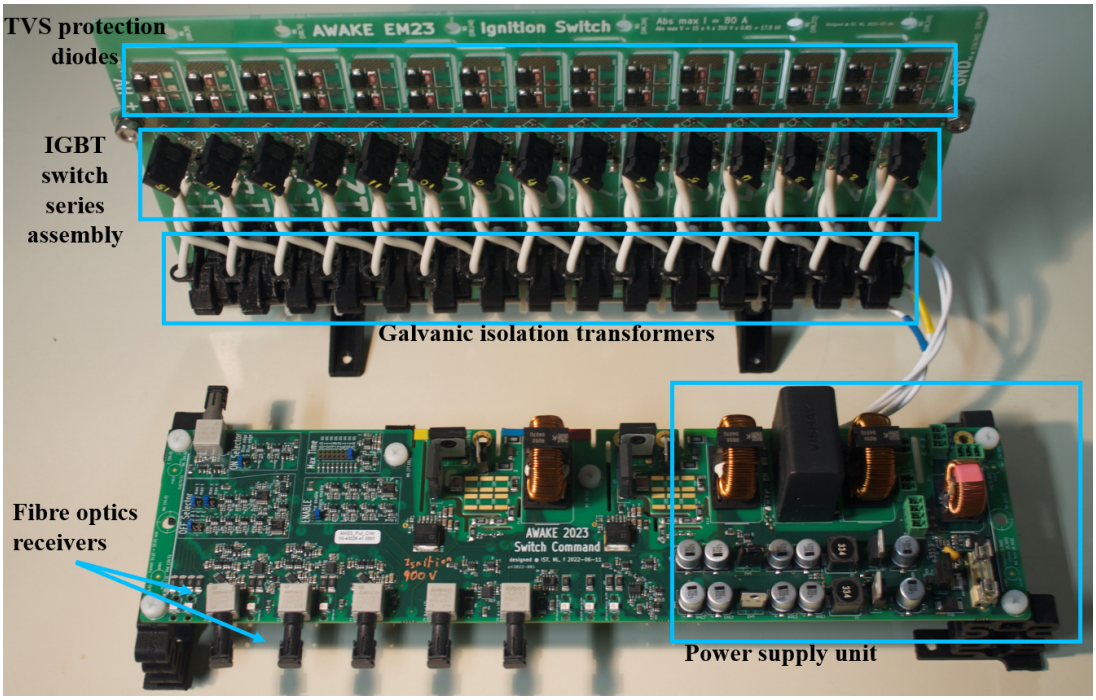

Figure 4.16: Driving signal board (bottom) connected to the ignition switch board (top) through galvanic isolation transformers

The ignition snubber diode must hold-OFF the power supply maximum voltage (6.0 kV) and have a switch time below 10 ns. The available device was GeneSiC's *GD60MPS17H*, with a $V_{RRM} = 1.7\,\text{kV}$. To hold-OFF

safely the voltage these diodes must be assembled in series. Considering a margin factor of $\zeta = 0.6$, the appropriate number of series diodes for the ignition snubber diode is 6.

The heater snubber diode also uses GeneSiC's *GD60MPS17H*. It must hold-OFF the power supply maximum voltage ($8.0\,\mathrm{kV}$), support up to $600\,\mathrm{A}$ of current and have a switch time below $10\,\mathrm{ns}$. To hold-OFF safely the voltage these diodes must be assembled in series. Considering the same margin factor of $\zeta = 0.6$, the number of series diodes for the heater snubber diode is 8.

For the coupling diode module, the available device was GeneSiC's *GD60MPS17H* as well. This module must hold-OFF the ignition voltage during steps 3 and 4 and will be activated during the fifth step. As the variation of the forward voltage with increasing temperature is negative it is not advisable to connect diodes in parallel directly, without recurring to current balancing techniques. Since the coupling diode module must sustain the heater pulse high current, the first criterion for the diode selection was the forward current rating, which is $I_{FSM} = 3\,\mathrm{kA}$. The coupling diode module must sustain the maximum ignition voltage $46\mathrm{kV}$. Since the diode voltage rating is $V_{RRM} = 1700\,\mathrm{V}$ and considering a margin factor of $\zeta = 0.6$, from (4.10) the number of series devices is $n = 45$.

The ignition diodes available were GeneSiC's *GB05MPS33-263*, these were chosen due to their short switching time ($t_s < 10\,\mathrm{ns}$), and voltage and current ratings of $V_{RRM} = 3300\,\mathrm{V}$ and $I_{FSM} = 50\,\mathrm{A}$ ($t_p = 10\,\mathrm{ms}$) respectively. The ignition diode module will hold-OFF the voltage during the second step of the operation, while the ignition switch is ON, and the transformer inductance is being charged. Considering the maximum ignition source voltage $V_{ign} = 6\,\mathrm{kV}$, the maximum voltage that can be applied to the diode is $V_{Dign} = V_{Cign}N_2/N_1 = 21kV$. Since the fast breakdown of the plasma is highly dependent on the power delivered by the ignition pulse, in an attempt to reduce the on-resistance of D_{ign}, the margin factor used was $\zeta = 0.8$. Therefore, the number of series diodes is $n = 8$. The ignition diode must sustain a current up to $\sim 37\,\mathrm{A}$ ($I_{L\mu} \cdot N_1/N_2$).

The diode modules have voltage balancing resistors calculated from the expression (4.12), the values chosen for the ignition diode and the coupling diode were $20\,\mathrm{M\Omega}$ (*HV733ATTE2005F*) and $750\,\mathrm{k\Omega}$ (*RCV2512750KFKEGAT*).

The ignition switch was designed to sustain up to $13\,\mathrm{kV}$ of collector-emitter voltage at the turn-OFF, and a current up to $130\,\mathrm{A}$. From the available IGBT devices, the one selected was IXYS' *IXYX25N250CV1*, featuring a

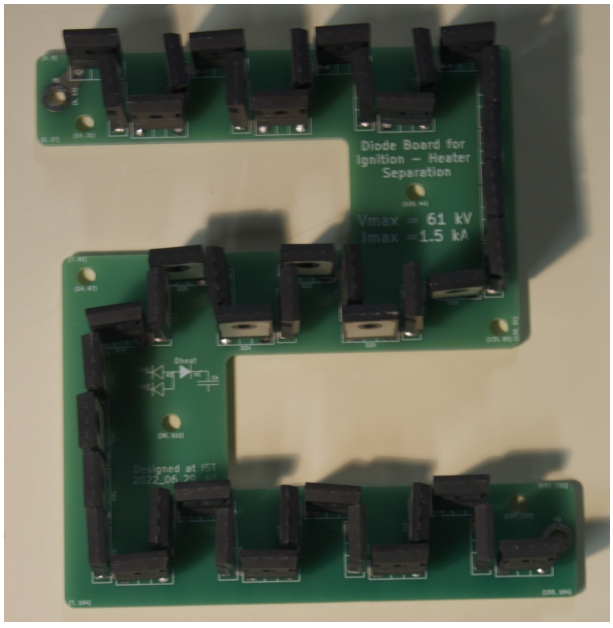

Figure 4.17: Coupling diode PCB

collector-emitter voltage limit of $V_{CEmax} = 2500\,\mathrm{V}$), and a continuous collector current $I_{CM} = 235\,\mathrm{A}$. The current rating proves adequate for the application, eliminating the requirement for parallel association. However, the *IXYX25N250CV1*'s voltage rating of $2500\,\mathrm{V}$ is insufficient, leading to the use of 15 IGBTs in series. The required fast turn-OFF of the ignition switch justifies a conservative margin factor. To ensure precise static and dynamic voltage balancing across the 15 stages, each IGBT incorporates a series of TVS diodes (Comchip Technologies *ATV50C351J-HF*) assembled in parallel, along with resistors $R_S = 1\,\mathrm{M\Omega}$ (Bourns' *CHV2512-FX-1004ELF*).

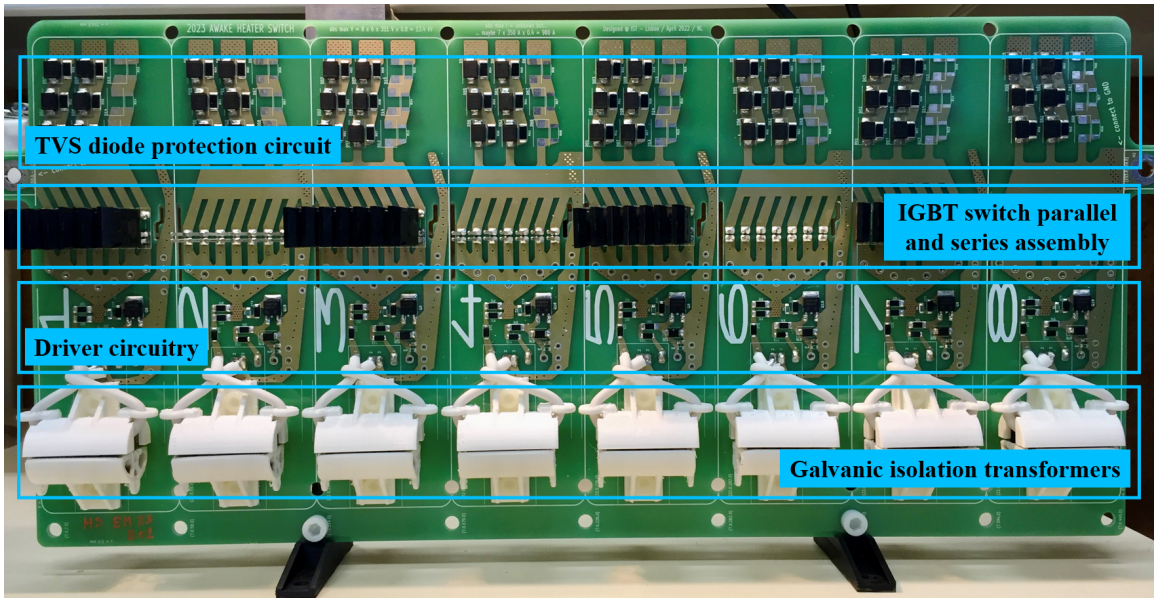

Figure 4.18: Heater switch PCB

The heater switch was designed to withstand up to $1.2\,\mathrm{kA}$. The chosen IGBT device for this application is IXYS' *IXYX40N450HV0*, featuring a collector-emitter voltage $V_{CEmax} = 4500\,\mathrm{V}$, and a peak collector current $I_{CM} = 350\,\mathrm{A}$. To meet the specified current demands safely, the switch requires a parallel association of 7 IGBTs (using a 0.5 margin). In contrast to diodes, IGBT semiconductors exhibit a positive variation of conduction voltage with increasing temperature, reducing the necessity for intricate current balancing techniques. At turn-OFF, the heater switch must sustain up to $\sim 17\,\mathrm{kV}$ of collector-emitter voltage (equation (4.8)). To satisfy voltage requirements (with a 0.5 margin), an 8 IGBT series association is used. To ensure the voltage balancing across the series stages we use a similar protection circuit of TVS diodes and parallel resistors.

Charging protection inductor and current limiting resistor

The L_h inductor prevents the heater turn-OFF voltage spike from activating the charging diodes. Considering $V_{ShMax} = Vh = 8\,\mathrm{kV}$, the duration of the snubber activation $\Delta t_{hsn} = 6\,\mu\mathrm{s}$ and a maximum allowed current of $I_{DchMax} = 0.5\,\mathrm{A}$, from (4.9) the inductance obtained is $L_h = 100\,\mathrm{mH}$. With these values of R_h, C_h and L_h, the damping coefficient is high enough that the charging of the capacitor is overdamped.

Since the plasma does not have a constant resistance (tends to a low value as the current rises), the limiting resistor will prevent the heater current from rising above the semiconductor devices limits. Considering the maximum power supply voltage of $8.0\,\mathrm{kV}$ and a minimum plasma impedance of $\sim 3\,\Omega$, a resistance of $3.3\,\Omega$ will limit the current to the maximum value $\sim 1.2\,\mathrm{kA}$.

Current balancing coupled inductors

The coupled inductors that balance the current between the two plasma sections must be sized to allow the minimum current variation. As a result of constraints from the AWAKE experiment, the first experimental run of this technology will employ an asymmetric configuration with plasma lengths of $3.5\,\mathrm{m}$ and $6.5\,\mathrm{m}$ [22, 24]. In this situation, the winding voltage difference is mainly determined by the length difference (proportional to the plasma resistance). We can expect the main contributor to the current balancing to be the inductor connected to the $3.5\,\mathrm{m}$ plasma, which will induce a higher voltage to compensate for its less resistive node. Therefore, we expect the maximum value of the coupled inductor voltage difference to be $v_1 - v_2 = v_G(R_{p1}/Rp2)$.

Considering the maximum power supply voltage $v_G = 8\,\mathrm{kV}$, a maximum allowed current variation of 4% (for $I_h = 500\,\mathrm{A}$), a pulse duration of $50\,\mu\mathrm{s}$, and a coupling factor $k = 0.5$, from (4.17) the minimum coupling inductance value is $L_M = 7.2\,\mathrm{mH}$.

The selected cores used for the coupled inductors were Vacuumschmelze's *T60006-L2050-W565*. To reach the inductance required and avoid core saturation $N_c = 20$ cores were stacked, with $N_t = 8$ turns the expected coupling inductance is $L_M = 12.8\,\mathrm{mH}$. This margin (0.6) was used to mitigate other potential imbalances (cable distribution, inductor coupling, pulse generator and plasma parasitics, etc.).

Table 4.2: Ignition pulse generator component values

Parameter	Symbol	Value	Unit	Reference
Ignition power supply	V_{ign}	$0-6$	kV	*6C24-P30*
Ignition voltage typical	V_{ign}	3.5	kV	*6C24-P30*
Ignition power supply resistor	R_{ign}	50	kΩ	-
Ignition transformer magnetizing inductance	L_μ	580	μH	(3.1)
Ignition transformer number of primary turns	N_1	36	-	(4.2)
Ignition transformer ratio	N_2/N_1	3.5	-	-
Ignition storage sapacitor	C_{ign}	2	μF	(4.5)
Ignition snubber resistor	R_{isn}	200	Ω	(4.7)
Ignition diode maximum reverse voltage	$V_{RRM-ign}$	3.3	kV	*GB05MPS33-263*
Ignition diode maximum forward current	$I_{FSM-ign}$	50	A	*GB05MPS33-263*
Ignition diode number of series devices	n_{Dign}	8	-	(4.10)
Ignition diode balancing resistor	R_{bal}	20	MΩ	(4.12)
Ignition snubber diode maximum reverse voltage	$V_{RRM-isn}$	1.7	kV	*GD60MPS17H*
Ignition snubber diode number of series device	n_{Disn}	6	-	(4.10)
Ignition switch IGBT maximum collector-emitter voltage	$V_{CEmax-ign}$	2.5	kV	*IXYX25N250CV1*
Ignition switch IGBT maximum collector current	I_{CM-ign}	235	A	*IXYX25N250CV1*
Ignition switch number of series IGBTs	$n_{ignIGBT}$	15	-	(4.10)

Table 4.3: Heater pulse generator component values

Parameter	Symbol	Value	Unit	Reference
Heater power supply	V_h	$0-8$	kV	*8C24-P250-I5*
Heater power supply resistor	R_h	100	kΩ	-
Heater storage capacitor	C_h	4	μF	(4.6)
Heater charging protection inductor	L_h	100	mH	(4.9)
Heater snubber capacitor	C_{hsn}	100	nF	(4.8)
Heater snubber discharge resistor	R_{hdis}	100	kΩ	-
Heater snubber diode maximum reverse voltage	$V_{RRM-hsn}$	1.7	kV	*GD60MPS17H*
Heater snubber diode maximum forward current	$I_{FSM-hsn}$	600	A	*GD60MPS17H*
Heater snubber diode number of series device	n_{Dhsn}	8	-	(4.10)
Heater switch IGBT maximum collector-emitter voltage	$V_{CEmax-h}$	4.5	kV	*IXYX40N450HV0*
Heater switch IGBT maximum collector current	I_{CM-h}	350	A	*IXYX40N450HV0*
Heater switch number of parallel IGBTs	$n_{pIGBT-h}$	7	-	-
Heater switch number of series IGBTs	$n_{sIGBT-h}$	8	-	(4.10)
Heater current limiting resistor	R_c	3.3	Ω	-

Table 4.4: Coupling Diode and Current Balancing Module Component Values

Parameter	Symbol	Value	Unit	Reference
Coupling diode maximum reverse voltage	$V_{RRM-coup}$	1.7	kV	*GD60MPS17H*
Coupling diode maximum forward current	$I_{FSM-coup}$	600	A	*GD60MPS17H*
Coupling diode number of series device	n_{Dcoup}	45	-	(4.10)
Coupleng diode balancing resistor	R_{bal}	750	kΩ	(4.12)
Current balancing module mutual inductance	L_M	12.8	mH	(4.17)
Current balancing module number of stacked cores	N_c	20	-	*T60006-L2050-W565*
Current balancing module number of turns	N_t	8	-	*T60006-L2050-W565*

CHAPTER 5

Experimental results of the double pulse generator

This chapter presents the simulation and experimental results of the developed double pulse generator. The simulations were done in *PSpice* and the experimental data was collected in the CERN DPS-Laboratory (Figure 5.1), using the setup described in Chapter 4. The pulse generators include current sensors (Pearson's current monitor *3972*) to measure the ignition switch, snubber, and output (plasma) currents. Additionally, a high-voltage probe (Tektronix's *P6015A*) was installed to measure the voltage across the plasma. These results contribute to the characterisation of the system and enhance the understanding of the plasma behaviour.

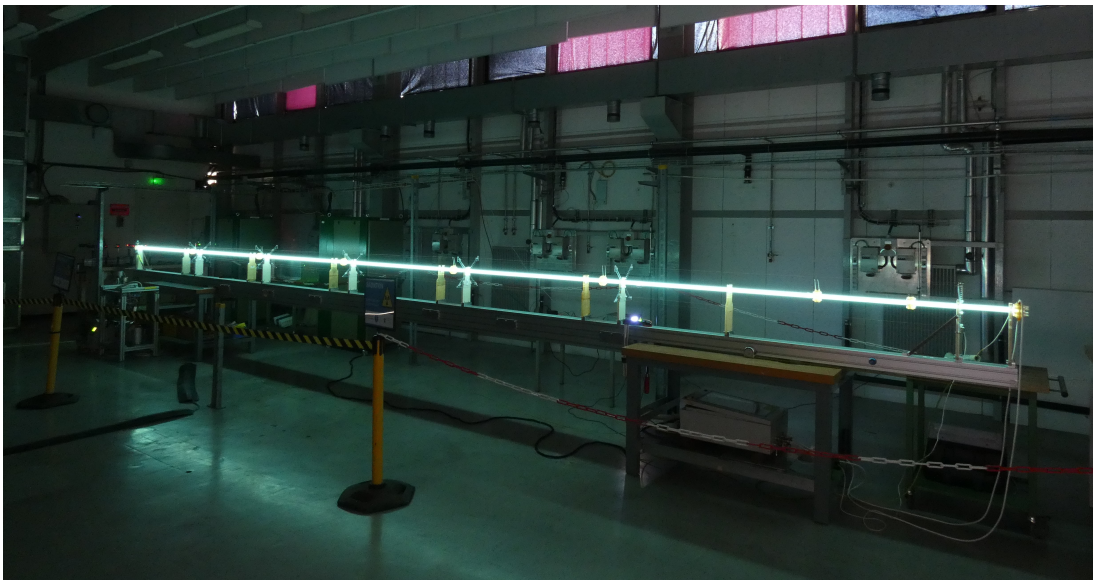

Figure 5.1: Plasma discharge in CERN DPS laboratory - Xe, $p = 16\,\mathrm{Pa}$, $I_h = 500\,\mathrm{A}$, $l_{plasma} = 10\,\mathrm{m}$

5.1 Analysis of a standard DPS discharge - simulation and experimental results

Firstly, we study a standard discharge, with argon at $p = 24\,\mathrm{Pa}$ and a target heater current of $I_h = 500\,\mathrm{A}$. Simultaneously, we analyse a PSpice simulation using a Cassie arc plasma model, described in Chapter 2.

In the simulation and experimental current and voltage waveforms from Figures 5.2 to 5.4, it is possible to observe the six steps of operation described in Chapter 3 and validate the design considerations from Chapter 4.

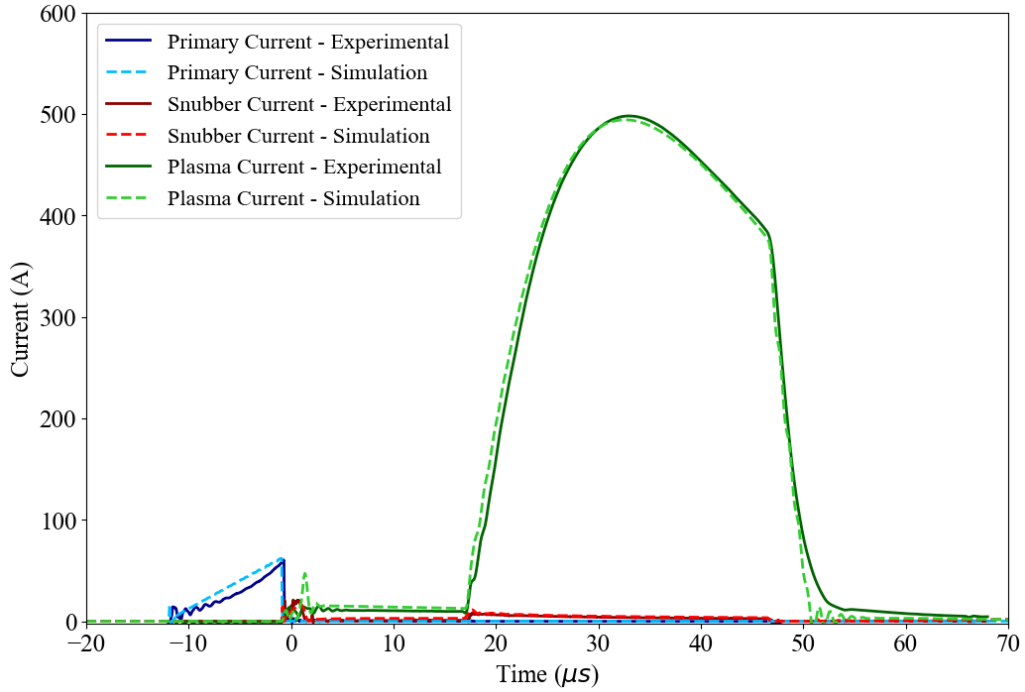

Figure 5.2: Simulation and experimental current waveforms; Ar, $p = 24\,\mathrm{Pa}$, $I_h = 500\,\mathrm{A}$, $l_{plasma} = 10\,\mathrm{m}$ - Sim: Vign=3.5 kV, Vh=6.9 kV; Exp: Vign=3.5 kV, Vh=6.08 kV

Analysing Figure 5.2, the model shows only a small difference in the heater plasma current ($\sim 1.4\%$ difference at the current maximum). However, observing the detail in Figure 5.3, it is noticeable that the ignition pulse plasma current difference between the simulation and the experimental measurements is more significant ($\sim 10.1\%$ at $t = 10\,\mu\mathrm{s}$), demonstrating that the model loses accuracy for lower current values. Furthermore, at the plasma ignition (after the ignition switch turn-OFF) the simulation plot presents a current spike that is not present in the experimental measurements. This is due to the sudden variation in plasma resistance, further supporting the higher accuracy of the plasma model during the heater pulse, when plasma resistance changes more gradually. For the plasma voltage (in Figure 5.4), the differences between simulation and experimental results follow the same pattern, being higher in the plasma ignition ($\sim 20\%$ difference in the maximum voltage) and lower during the heater pulse ($\sim 7\%$ difference in the heater pulse maximum).

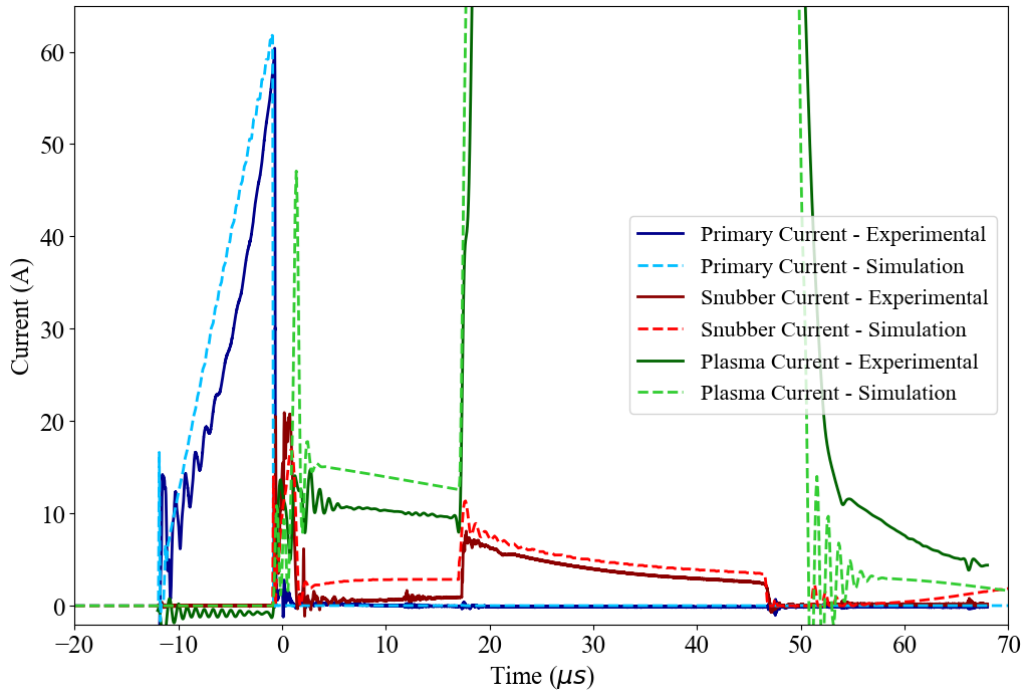

Figure 5.3: Simulation and experimental current waveforms (detail); Ar, $p = 24\,\mathrm{Pa}$, $I_h = 500\,\mathrm{A}$, $l_{plasma} = 10\,\mathrm{m}$ - Sim: Vign=3.5 kV, Vh=6.9 kV; Exp: Vign=3.5 kV, Vh=6.08 kV

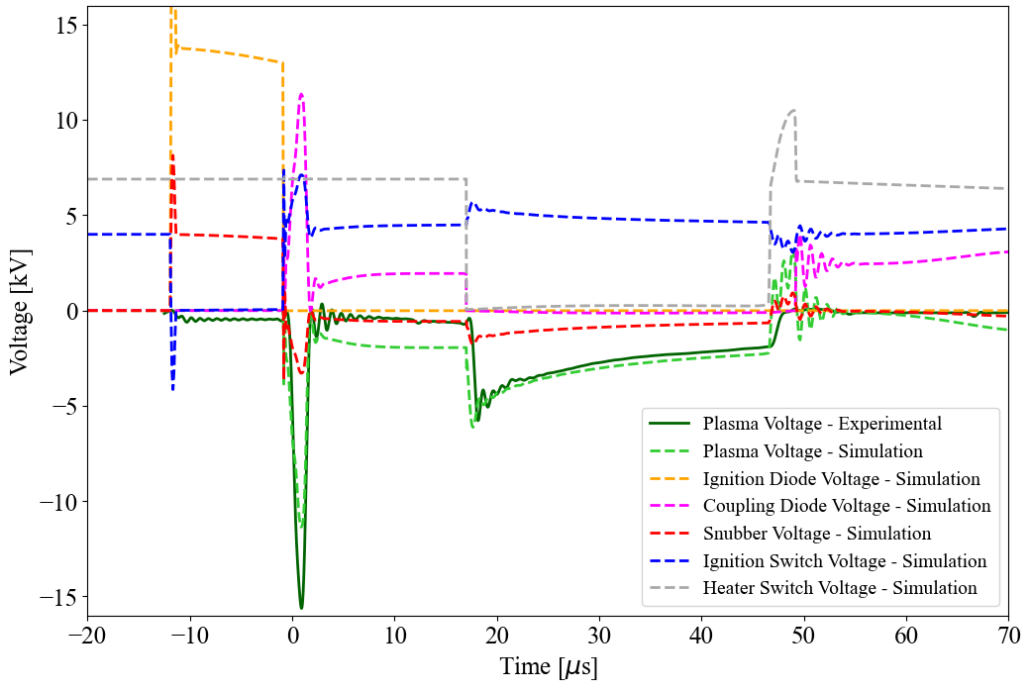

Figure 5.4: Simulation and experimental voltage waveforms; Ar, $p = 24\,\mathrm{Pa}$, $I_h = 500\,\mathrm{A}$, $l_{plasma} = 10\,\mathrm{m}$ - Sim: Vign=3.5 kV, Vh=6.9 kV; Exp: Vign=3.5 kV, Vh=6.08 kV

A typical discharge will operate as described by the design equations of Chapter 3. Testing different parameters and their effect is essential to further analyse the behaviour and operation range of the pulse generator.

5.2 No-load ignition pulse discharge

When the gas breakdown voltage is reached, and the plasma ignites, the output voltage drops rapidly. Thus, to characterise the voltage waveform of the ignition pulse without the influence of the plasma ignition, discharges were conducted under conditions where plasma breakdown does not occur. For an argon pressure lower than $0.1\,\mathrm{Pa}$ the plasma does not breakdown at the standard operation ignition output voltage.

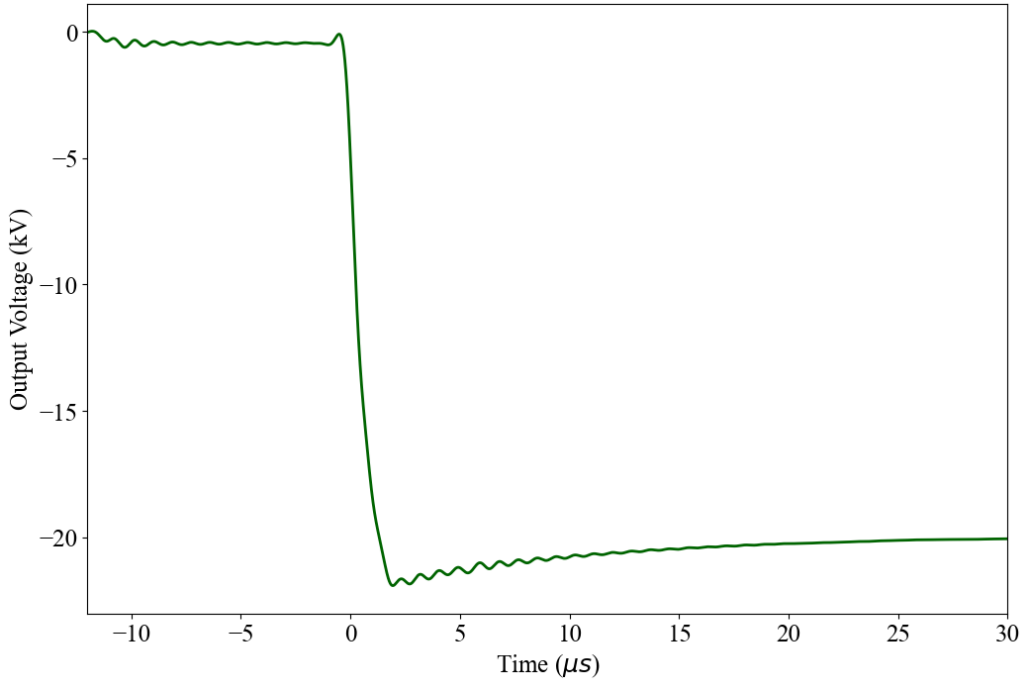

Figure 5.5: Output voltage waveform for ignition pulse without plasma breakdown, $V_{ign} = 3.5\,\mathrm{kV}$, $V_{peak} = -21.86\,\mathrm{kV}$, the voltage rises with a slope of $dV/dt = -8.66\,\mathrm{kV}/\mu\mathrm{s}$

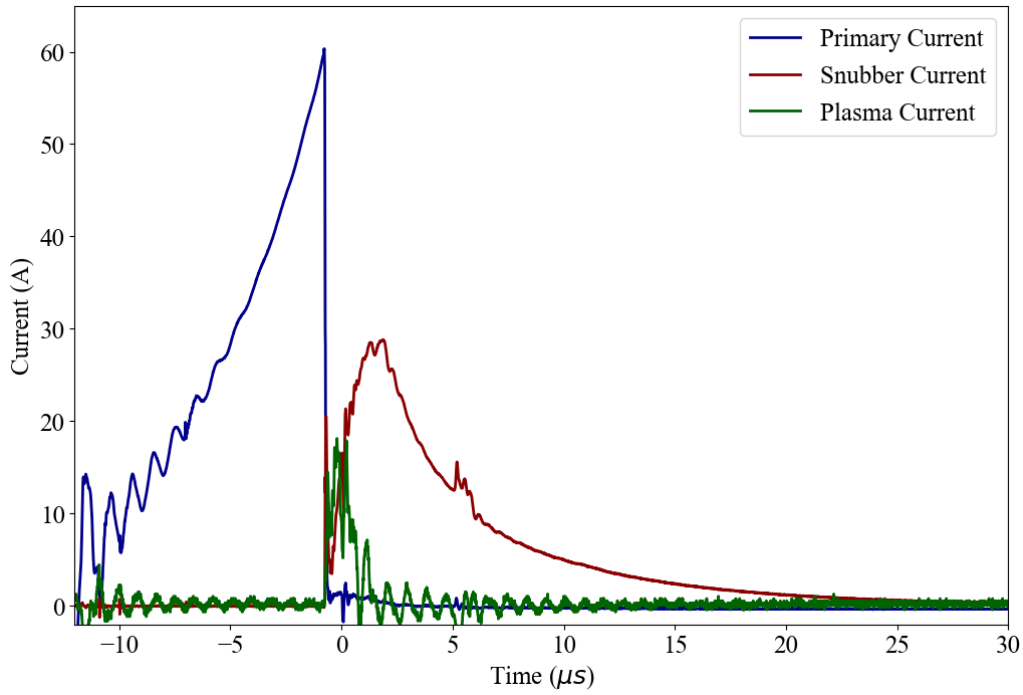

Figure 5.6: Primary, snubber and output current waveforms for ignition pulse without plasma breakdown, $V_{ign} = 3.5\,\mathrm{kV}$

Therefore, at these pressure values the ignition system will operate without initiating plasma formation. Under these conditions, the output voltage reflects only the contributions of the parasitic components, including the tube, cabling, voltage probe, and oscilloscope. Figure 5.5 illustrates the (negative) voltage rise following the ignition switch turn-off ($t = 0$). The pulse reaches a peak voltage of $V_{peak} = -21.9\,\mathrm{kV}$, consistent with the design specifications described in Chapter 3 (equations (3.3) and (3.5)) and the specifications of Chapter 4 - specifically, the target ignition voltage and the lag time ($t_{lag} = 1.96\,\mu\mathrm{s}$).

The current traces from Figure 5.6 also give insights into the behaviour of the pulse generator. Even with no conditions to ignite a plasma, there is a current on the secondary to charge and quickly discharge the C_{A-Kpar} tube capacitance. The peak current in the secondary is equal to $I_{prim} \times N_1/N_2 \approx 17\,\mathrm{A}$. As the capacitor starts discharging, the current diverts back to the snubber. The snubber current reaches a peak value of $I_{iSn} = 28.8\,\mathrm{A}$ and slowly discharges as the magnetising inductance energy gets depleted.

5.3 Plasma breakdown voltage - pressure scan

For slightly higher pressures it is possible to breakdown the plasma and the ignition pulse will operate differently. It is important to confirm that the pulse generator can operate at the required pressure range for AWAKE.

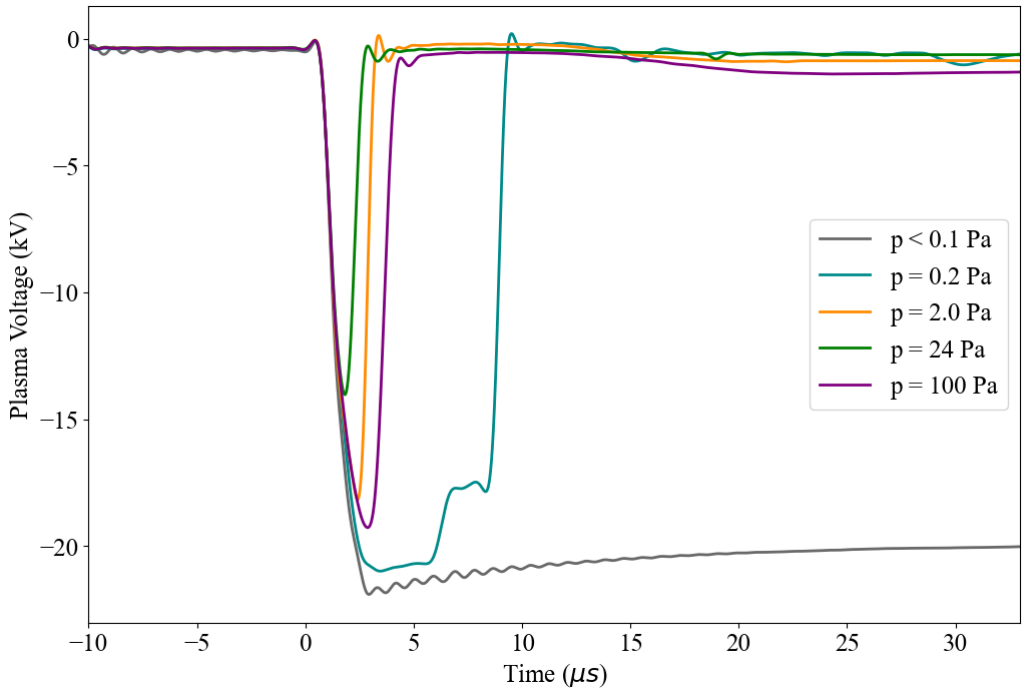

Figure 5.7: Plasma voltage waveforms of ignition pulse for different pressure values; Ar, $l_{plasma} = 10\,\mathrm{m}$, $V_{ign} = 3.5\,\mathrm{kV}$

According to Paschen's Law [38], the breakdown voltage of a gas discharge varies as a function of the product of the electrode gap distance and the gas pressure (pd). Still, factors like the geometry of the discharge and the electrodes also affect the breakdown value. For the first Paschen curves, the gas pressure and gap distance was varied between parallel metal plates. However, the discharge plasma source has distinct electrode and tube geometries that justify a new experimental study of its threshold voltages. Furthermore, typically the Paschen curve studies are performed for DC voltage (or long pulses) and the DPS requires fast plasma ignition, which significantly increases the breakdown voltage measured [41].

To study the effect of changing the pd in the DPS setup, discharges were performed for different argon pressure values, using the same ignition pulse. In Figure 5.7 it is possible to observe the effect that different pressures have on the plasma ignition.

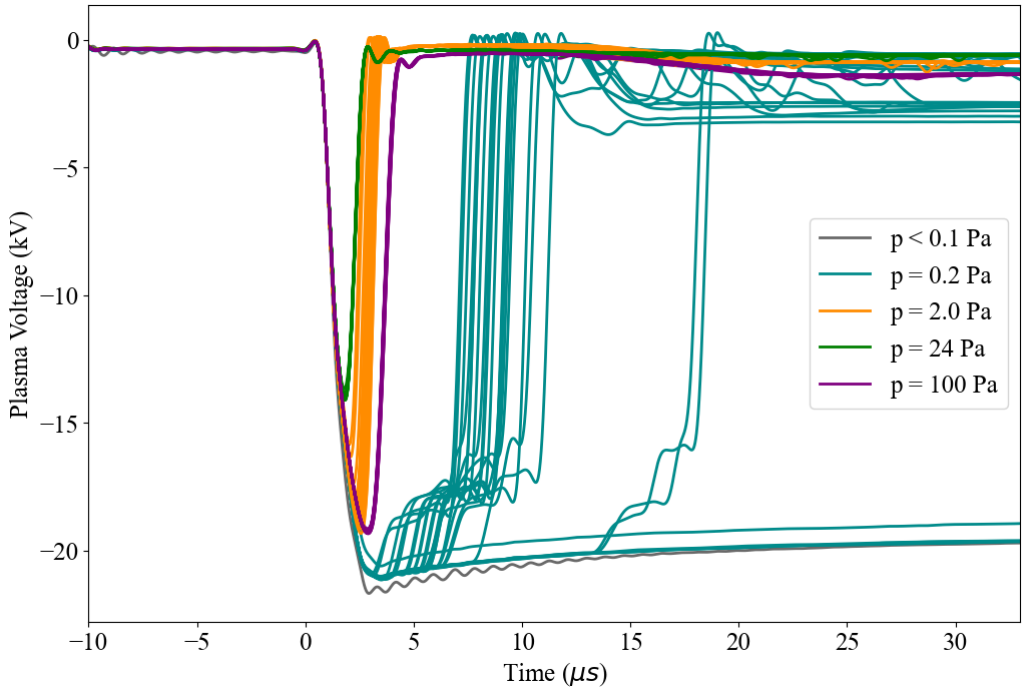

Figure 5.8: Plasma voltage waveforms of ignition pulse for different pressure values; Ar, $l_{plasma} = 10\,\mathrm{m}$, $V_{ign} = 3.5\,\mathrm{kV}$ - 25 discharges per pressure, 10 s repetition rate, average $t_{lag} = [8.8, 2.9, 2.2, 3.7]\,\mu\mathrm{s}$

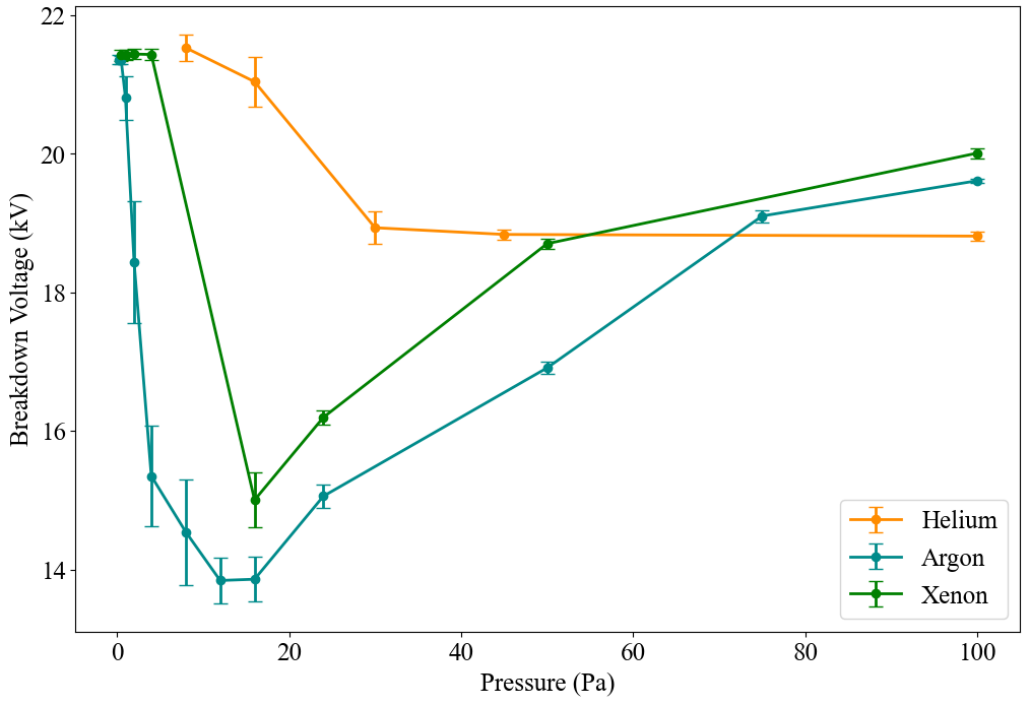

Figure 5.9: Voltage breakdown vs pressure for helium, argon, and xenon; $l_{plasma} = 10\,\mathrm{m}$, $V_{ign} = 3.5\,\mathrm{kV}$

For higher pressures (100 Pa) the breakdown voltage is relatively higher than for the standard 24 Pa used in most of the tests, likewise for lower pressures like 2 Pa. For even lower pressures 0.5 Pa the plasma breakdown

only occurs after V_{plasma} reaches its peak and stabilises, causing the lag between ignition pulse and plasma breakdown to be much longer for such pressures. Furthermore, we can see in Figure 5.8, that when the breakdown occurs after the rising edge it causes an increase in the ignition jitter. For this reason, the DPS will operate under voltage and pressure conditions that lead to the plasma breakdown occurring in the rising edge of the ignition pulse, thus relying on faster breakdown mechanisms, less dependent on probabilistic conditions.

Plasma breakdown voltage tests were performed for helium and xenon as well. Figure 5.9 shows how the plasma breakdown voltage evolves with the pressure for each gas, in a $10\,\mathrm{m}$ length. This study, combined with the plasma density requirements of the AWAKE, determined the pressure values most suitable for the experiment. We conclude from Figure 5.9, that xenon can be operated with better performance at $16\,\mathrm{Pa}$. Argon should be used in pressures between $8\,\mathrm{Pa}$ and $24\,\mathrm{Pa}$. In this range, lower pressures present the advantage of a lower breakdown voltage, but higher pressures benefit from higher reproducibility. Helium must operate at higher pressures than the other gases used, with $45\,\mathrm{Pa}$ being the most balanced.

For lower-pressure xenon, in Figure 5.9, there is a plateau at $\sim 21\,\mathrm{kV}$. This value is the peak voltage of the ignition pulse and signals that the breakdown occurred after the rising edge. However, these low pressures are not suitable to obtain the AWAKE plasma densities. Thus, the operation range between $[8,\ 24]\,\mathrm{Pa}$ for argon and xenon, and $[30,\ 45]\,\mathrm{Pa}$ for helium, are adequate for the application objectives.

5.4 Primary peak current effect on ignition pulse

From equations (3.3) and (3.5), the shape of the ignition pulse is determined by the following parameters ignition snubber resistance (R_{isn}), transformer's turn ratio (N_2/N_1), and the maximum primary current ($I_{L\mu}$). The primary current can be tuned by varying the ignition power supply voltage (V_{ign}) and ignition switch-ON duration (t_{ignON}).

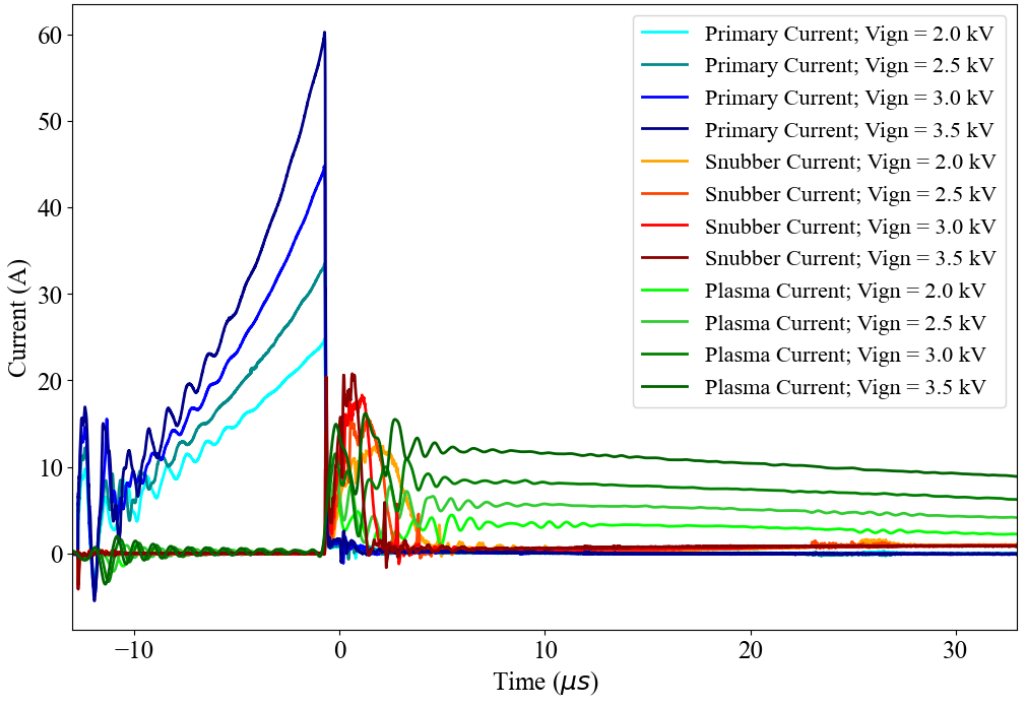

Figure 5.10: Ignition pulse current waveforms - V_{ign} scan; Ar, $p = 24\,\mathrm{Pa}$, $l_{plasma} = 10\,\mathrm{m}$

Figure 5.10 represents the ignition switch, ignition snubber, and plasma currents for four different values of ignition power supply voltage, the Figure 5.11 shows the plasma voltage waveforms for the same parameters.

These results demonstrate how the ignition supply voltage affects the ignition output. As expected, the plasma current is proportional to the primary peak current, and so is the snubber maximum current. Higher primary peak currents will also result in a larger plasma breakdown voltage. This increase in breakdown voltage is caused by a faster voltage rise and consequent reduction in plasma ignition lag - Table 5.1.

Table 5.1: Primary current effect on ignition output

$\mathbf{V_{ign}}$ **[V]**	$\mathbf{I_{L\mu}}$ **[A]**	$\mathbf{V_{plasma}}$ **[kV]**	t_{lag} $[\mu\mathbf{s}]$
2	24.9	-9.4	4.1
2.5	33.7	-11.0	2.85
3	44.9	-13.7	2.03
3.5	59.6	-15.6	1.72

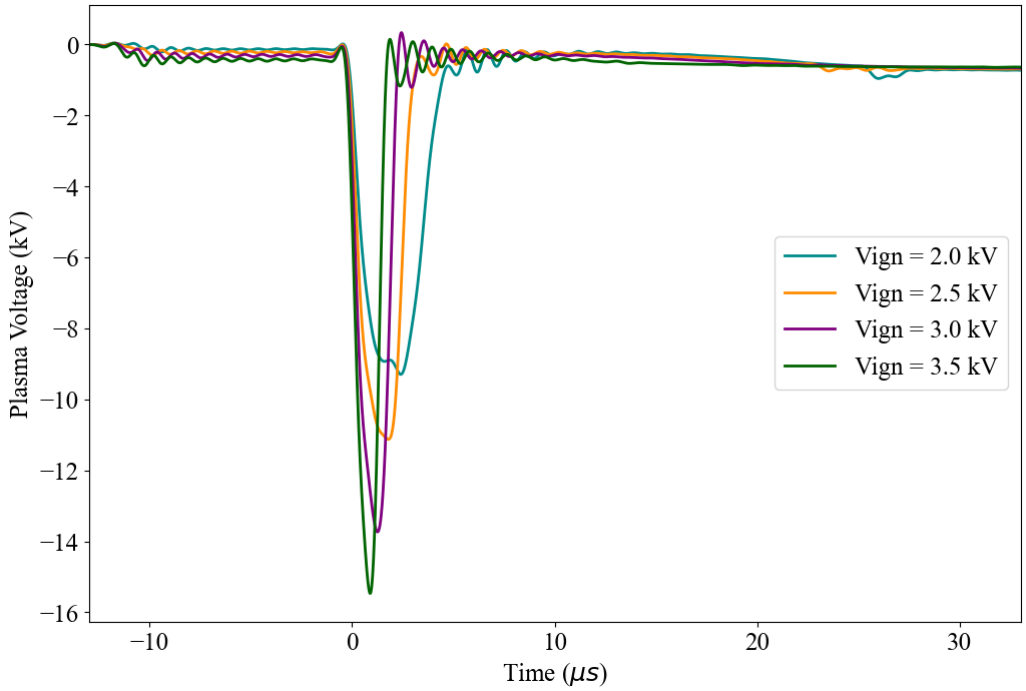

Figure 5.11: Ignition pulse plasma voltage waveforms - V_{ign} scan; Ar, $p = 24\,\text{Pa}$, $l_{plasma} = 10\,\text{m}$

In Figures 5.12 and 5.13, the ignition switch-ON time varied, but the ignition supply voltage was adapted to preserve a similar primary peak current in each discharge. For the same peak primary currents, we obtain similar output plasma voltage pulses (Figure 5.13 - with a peak voltage variation $< 3.5\%$). These results demonstrate that the primary peak current value defines the output pulse shape, regardless of the ignition switch-ON time.

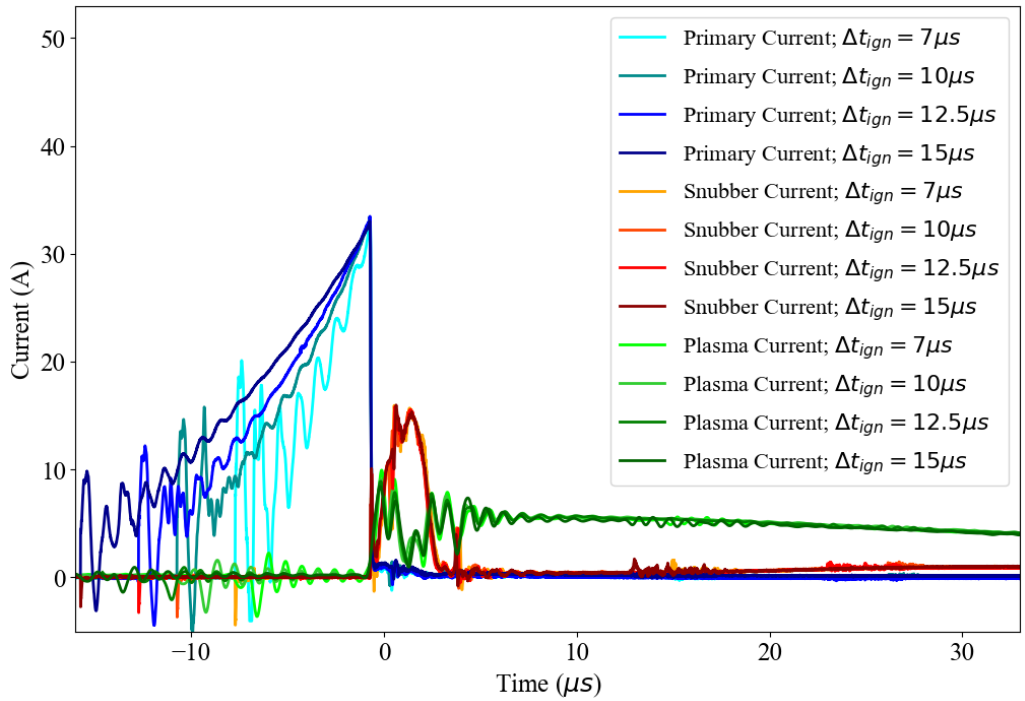

Figure 5.12: Ignition pulse current waveforms - Δt_{ign} scan; Ar, $p = 24\,\text{Pa}$, $l_{plasma} = 10\,\text{m}$, $V_{ign} = [4.2, 3.0, 2.5, 2.0]\,\text{kV}$

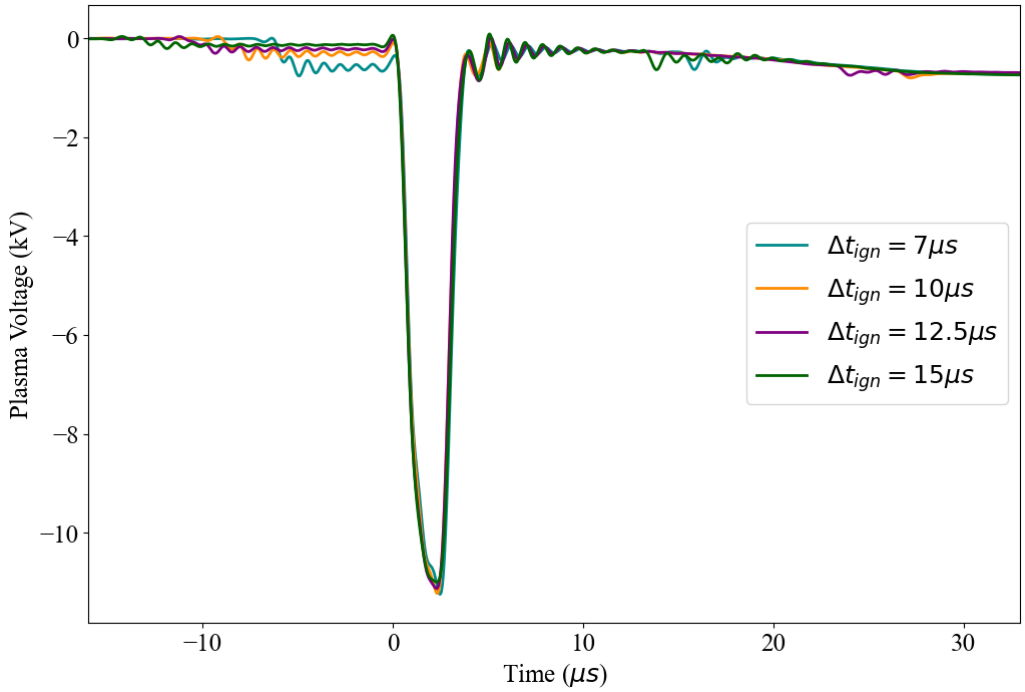

Figure 5.13: Ignition pulse plasma voltage waveforms - Δt_{ign} scan; Ar, $p = 24\,\text{Pa}$, $l_{plasma} = 10\,\text{m}$, $V_{ign} = [4.2, 3.0, 2.5, 2.0]\,\text{kV}$

5.5 Primary peak current effect on heater pulse

After the ignition pulse, the plasma resistance drops substantially, enabling the start of the heater pulse. However, the shape of the ignition pulse affects the shape and reproducibility of the heater pulse. Using the same ignition pulse parameters of Figure 5.10, but including the heater pulse we obtain the current increase up to $I_h = 500\,\text{A}$. We

can observe in Figure 5.14 how the heater pulse current rise is slower for lower-power ignition pulses due to their initial lower plasma resistance. Figure 5.15 shows how the snubber current during the heater pulse drops faster for lower ignition voltages. This is because the stored energy in the ignition transformer magnetising inductance is depleted faster.

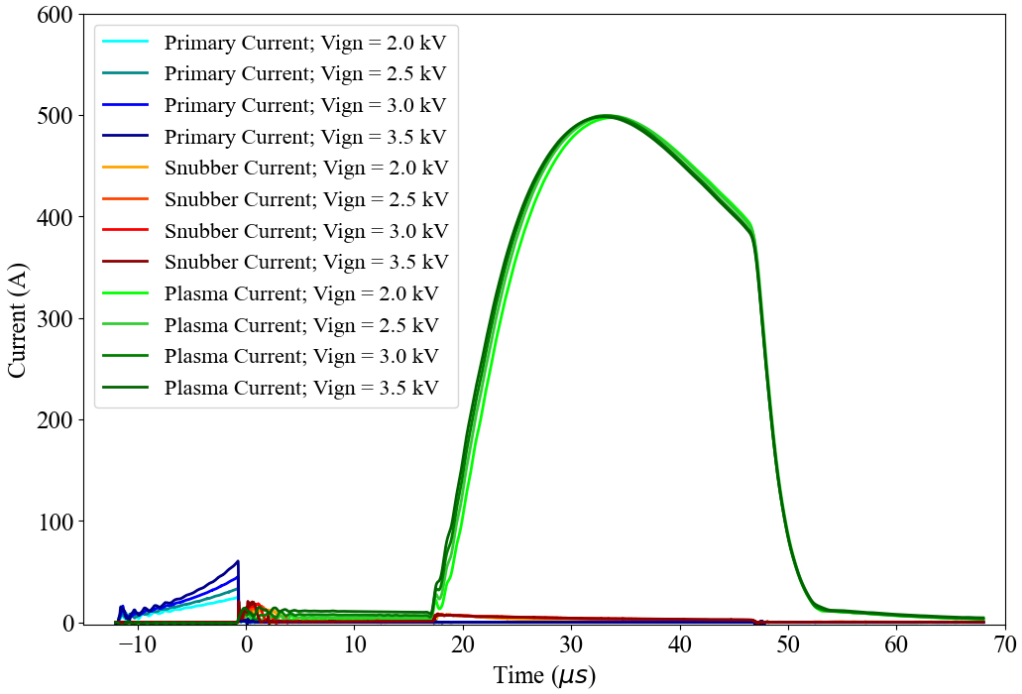

Figure 5.14: Double pulse current waveforms - V_{ign} scan; Ar, $p = 24\,\text{Pa}$, $I_h = 500\,\text{A}$, $l_{plasma} = 10\,\text{m}$, $V_h \approx 6.1\,\text{kV}$

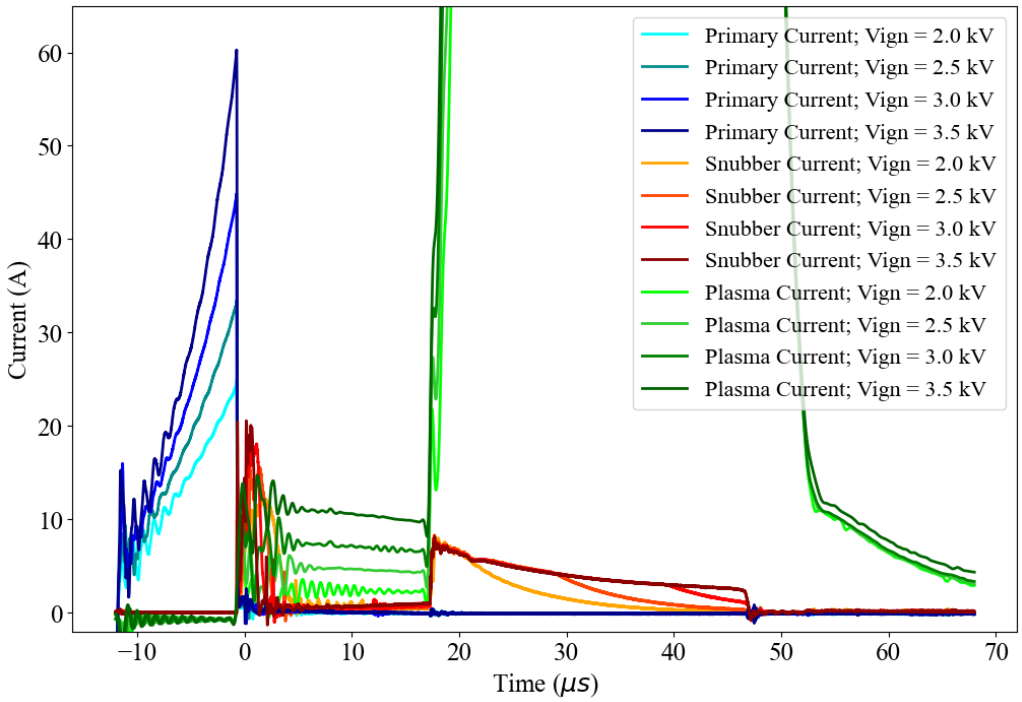

Figure 5.15: Double pulse plasma current waveforms - V_{ign} scan; Ar, $p = 24\,\text{Pa}$, $I_h = 500\,\text{A}$, $l_{plasma} = 10\,\text{m}$, $V_h \approx 6.1\,\text{kV}$ (detail)

Higher power ignition pulses reduce the heater pulse jitter and the maximum current variation. By analysing

the results from Table 5.2 we conclude that to have a current variation below 1% and a jitter below $20\,\mathrm{ns}$ an $I_{L\mu} > 44.9\,\mathrm{A}$ is required.

Table 5.2: Heater pulse current reproducibility as a function of V_{ign} and $I_{L\mu}$ for 25 discharges with 10 s repetition rate

$\mathbf{V_{ign}}$ **[V]**	$\mathbf{I_{L\mu}}$ **[A]**	$\mathbf{I_h}$ **variation [A]**	$\mathbf{I_h}$ **variation [%]**	$\mathbf{I_h}$ **jitter [ns]**
2	24.9	11.53	2.25	25.6
2.5	33.7	5.62	1.12	25.6
3	44.9	4.88	0.97	19.2
3.5	59.6	2.93	0.53	19.2

5.6 Measurements of the plasma resistance during the heater pulse

The plasma resistance still varies significantly during the heater pulse due to the increase in plasma electron density. Dividing the voltage measurements with the current values during a discharge it is possible to determine the plasma resistance evolution along the heater pulse period (bold lines in Figure 5.16). Before and after the heater pulse (faded lines in Figure 5.16), the voltage and current traces are highly susceptible to noise due to their relatively lower values, making the resistance measurement inaccurate.

In Figure 5.16 we can observe the variation for different heater pulse peak currents. As expected, a higher current density leads to reduced plasma resistance: the $I_h = 200\,\mathrm{A}$ and the $I_h = 500\,\mathrm{A}$ pulses have a minimum plasma resistance of $6.8\,\Omega$ and $2.8\,\Omega$ respectively. The minimum plasma resistance does not decrease proportionally with the increase in current, suggesting that for higher current densities and, consequently, higher ionisation fractions, the plasma resistance tends to an asymptotic limit, under the experimental conditions practised.

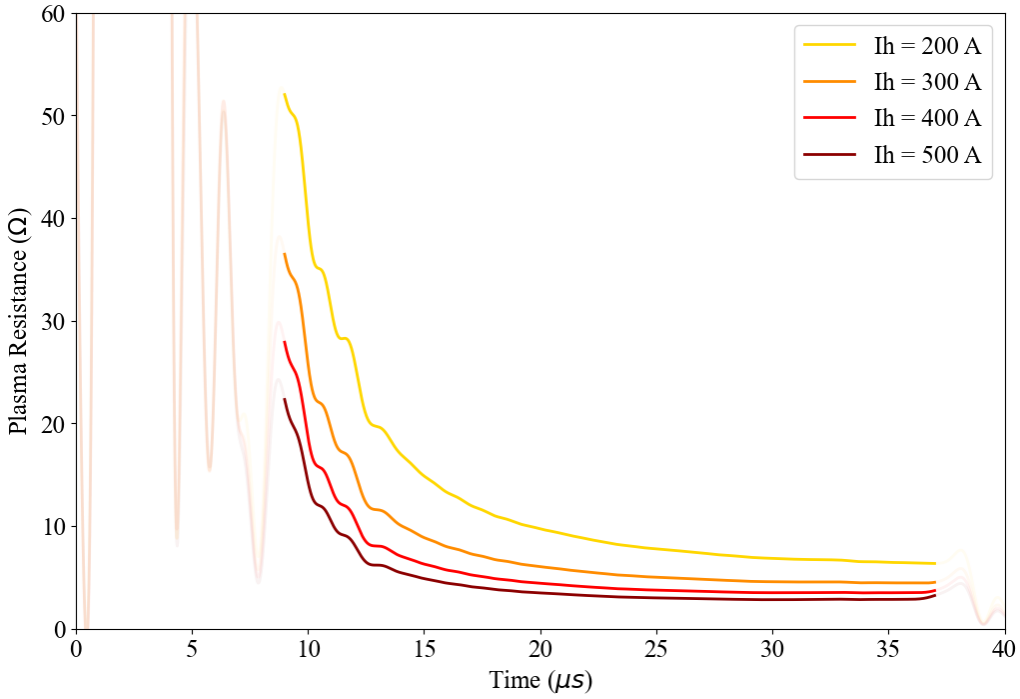

Figure 5.16: Plasma resistance during the heater pulse - I_h scan; Ar, $p = 24\,\mathrm{Pa}$, $l_{plasma} = 10\,\mathrm{m}$, $V_h = [3.20, 4.32, 5.36, 6.40]\,\mathrm{kV}$

5.7 Double plasma configuration - 3.5 m + 6.5 m

It is possible to test the current balancing module (CBM) sized in Chapter 4, by changing the configuration to the two-plasma setup (Figure 4.1). The experimental objectives of AWAKE required the possibility of using three distinct lengths of plasma (3.5 m, 6.5 m, and 10 m). The asymmetric two-plasma configuration was a consequence of this requirement. For this experiment, we measure the voltage across each winding and the current of each plasma section. As explored in chapters 2 and 4, the CBM is composed of coupled inductors and must be able to

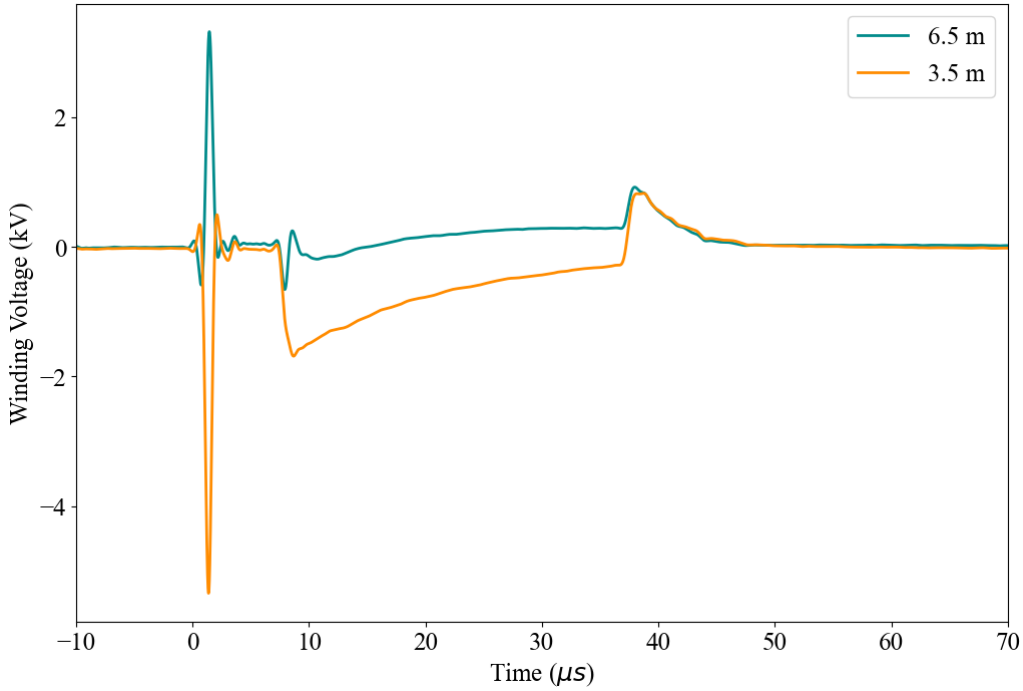

Figure 5.17: CBM winding voltage - two-plasma configuration; Ar, $p = 24\,\mathrm{Pa}$, $I_h = 500\,\mathrm{A}$, $l_{plasma} = (3.5 + 6.5)\,\mathrm{m}$, $V_{ign} = 3.0\,\mathrm{kV}$, $V_h = 4.6\,\mathrm{kV}$

compensate for the different impedances of the two different lengths (3.5 m/6.5 m). Discrepancies in current generate opposing self-induced voltages in the CBM windings. Even without the different lengths, the differences in the parasitics of the current path of each winding and plasma length create current imbalances every time there is a fast current transient, causing flux differences and inducing voltages in the CBM windings. In Figure 5.17, we observe that during the plasma ignition process ($t = 0$), and the switching of the heater (switch-ON at $t = 7.5\,\mu\mathrm{s}$ and switch-OFF at $t = 37.5\,\mu\mathrm{s}$) there are voltage spikes in both windings. At the plasma ignition the voltage reaches a higher absolute value in the winding corresponding to the 3.5 m section ($V_{w-3.5m} = -5.34\,\mathrm{kV}$ and $V_{w-6.5m} = 3.32\,\mathrm{kV}$), to compensate for the lower threshold voltage required in this section. During the heater pulse the voltage in the winding corresponding to the 6.5 m section tends to stabilize in a relatively low value while the winding for the 3.5 m plasma has a higher voltage induced (with a maximum at $V_{w-3.5m} = 1.68\,\mathrm{kV}$) due to the lower resistance of the section.

Figure 5.18 depicts the current and voltage traces across each CBM winding. These results indicate a maximum current difference of $\Delta I_h \approx 16.5\,\mathrm{A}$ during the heater pulse (average variation value within 10 discharges), with the higher current on the shorter length (3.5 m) plasma. The heater pulse voltage waveforms in Figure 5.18, indicate that the voltages applied to both plasmas were modified to mitigate the current unbalancing to a suitable

level. Given the lower impedance of the 3.5 m plasma, its corresponding winding experiences a higher increase in voltage, thus decreasing the 3.5 m plasma applied voltage, to attain current balancing with the higher impedance branch (6.5 m).

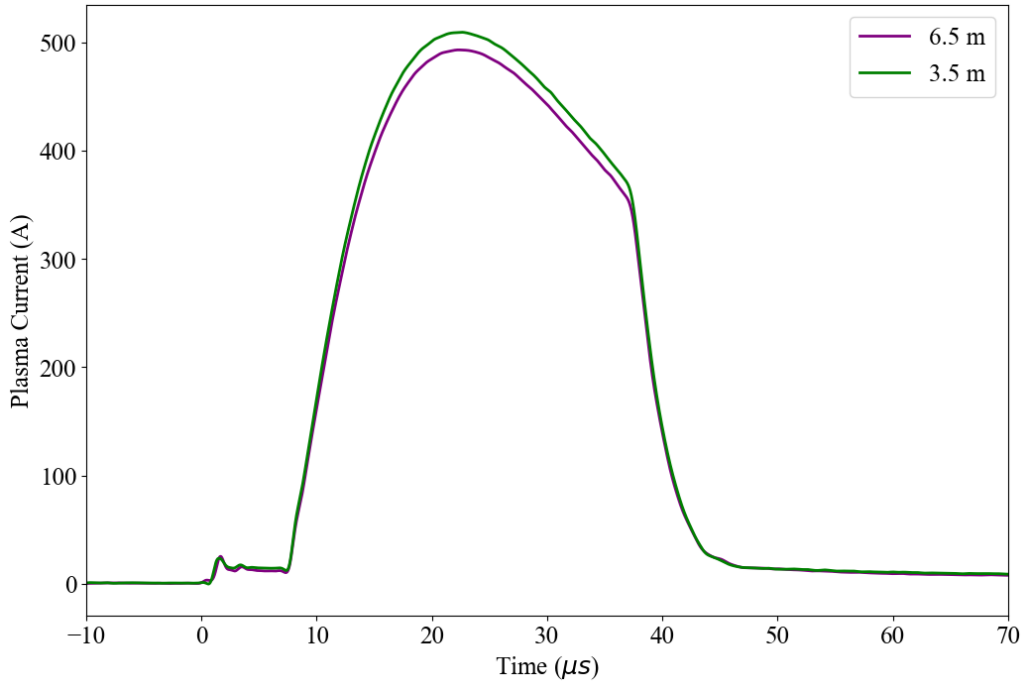

Figure 5.18: CBM plasma current - two-plasma configuration; Ar, $p = 24\,\mathrm{Pa}$, $I_h = 500\,\mathrm{A}$, $l_{plasma} = (3.5 + 6.5)\,\mathrm{m}$, $V_{ign} = 3.0\,\mathrm{kV}$, $V_h = 4.6\,\mathrm{kV}$

We conclude that the CBM was able to distribute the plasma currents with a 3.3% difference, even under asymmetric plasma sections.

The results of this chapter, along with plasma density measurements performed in parallel, qualified the plasma source design and served as preparation for the installation and operation of the DPS in the AWAKE experiment.

CHAPTER 6

AWAKE Run 2b results with the discharge plasma source

After successful testing and characterisation of the discharge plasma source (DPS) using the double pulse generator, it was possible to install and test the new plasma source in the AWAKE experiment, with the propagation of high-energy proton beams. This was part of the AWAKE Run 2b [22] and was the first time a length scalable plasma source prototype was tested in the AWAKE experiment. The main objective of this test was to demonstrate the DPS potential as an alternative plasma source by observing the self-modulation instability (SMI) of the proton bunch [42].

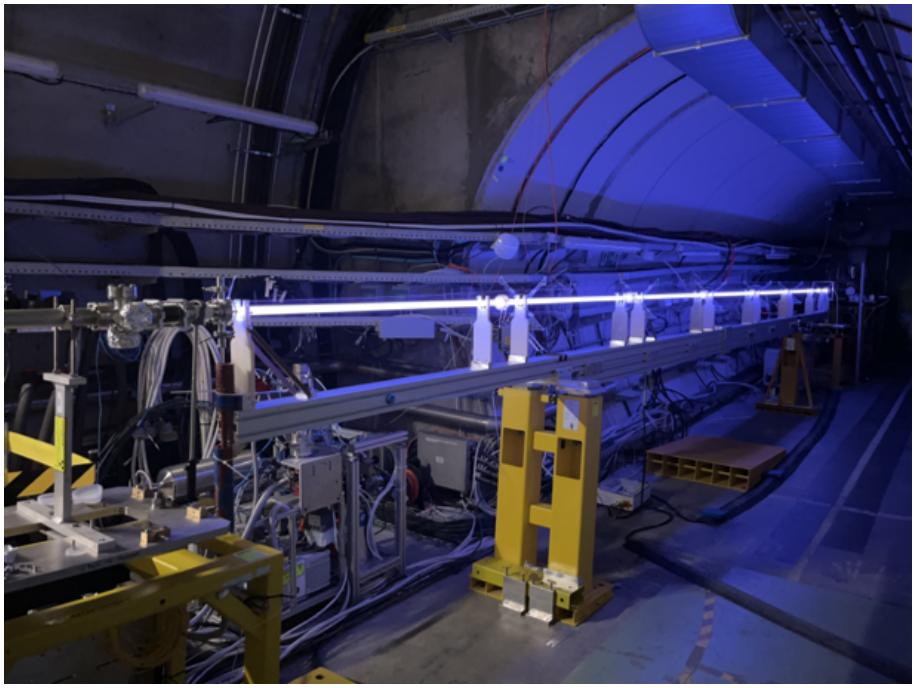

Figure 6.1: Plasma discharge in the AWAKE experiment - Ar, $p = 24\,\mathrm{Pa}$, $I_h = 500\,\mathrm{A}$

The double pulse generator operation range allowed the use of different plasma lengths (3.5 m, 6.5 m, and 10 m) and gases (xenon, argon, and helium). Furthermore, by adjusting the discharge current and its timing relative

to the arrival of the proton beam, a broad range of plasma electron densities could be investigated [42]. Additionally, the double plasma configuration was successfully tested using simultaneously 3.5 m and 6.5 m plasma lengths. Although the total plasma length was limited to $10\,\mathrm{m}$ by the experimental setup, the ability to develop two simultaneous plasmas was an important step in the pursuit of obtaining plasma length scalability.

Since the heater pulse was the most relevant for the physics studies of AWAKE, the $t = 0$ in the plots of this chapter shifted from the start of the ignition pulse to the start of the heater pulse (heater switch-ON).

6.1 Discharge plasma source performance in AWAKE

The DPS experiment in the AWAKE lasted three weeks (from May 1^{st} to May 21^{st}), generating over 21 thousand plasmas. The DPS was installed in AWAKE replacing the $10\,\mathrm{m}$ rubidium plasma source temporarily. The proton bunches are extracted from CERN's Super Proton Synchrotron (SPS) accelerator and have an energy of $400\,\mathrm{GeV}$. Proton extraction occurs every $15 - 30\,\mathrm{s}$, and they travel through the plasma from the cathode to the anode in the $10\,\mathrm{m}$ single plasma configuration. In the two-plasma configuration, the protons travel from the anode of the $3.5\,\mathrm{m}$ to the anode of the $6.5\,\mathrm{m}$.

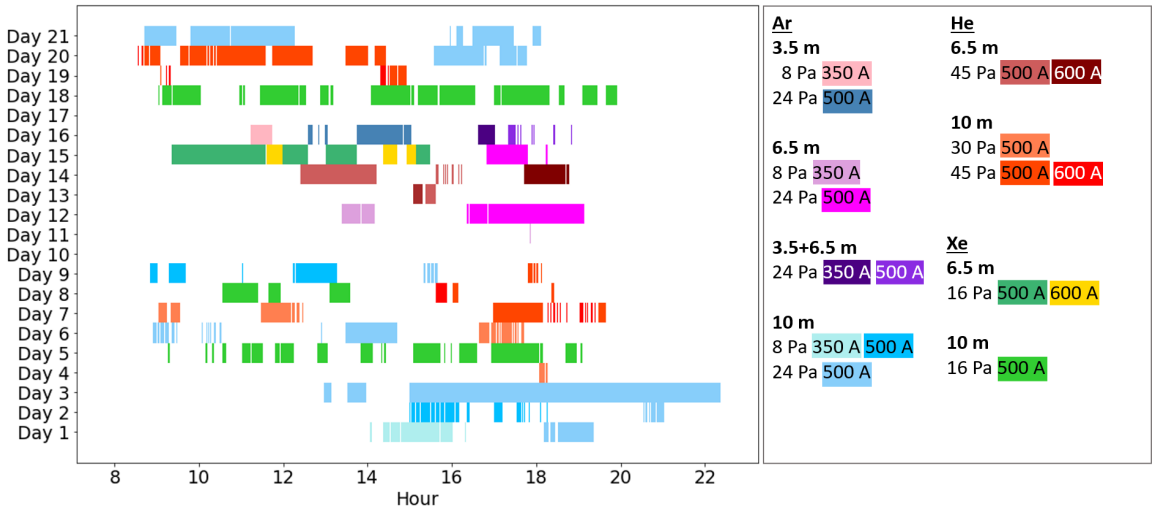

Figure 6.2: Distribution of plasma discharges in time during the AWAKE DPS-experiment

Figure 6.2 displays the plasma discharges performed over the three weeks. The colours represent the different setups and parameters used in the experiment. The 10-meter configuration was the most used (from the 1^{st} to the 9^{th} day and from the 18^{th} to the 21^{st}) with 11 678 discharges. Argon was the most used gas (7 163 discharges), and most discharges (14 589) were made at $I_h = 500\,\mathrm{A}$. The days 4, 10, 11, and 17, were days without protons where only a few test discharges were done. The change from the single plasma to the two-plasma configuration was made on the 10^{th} and 11^{th}, and on the 17^{th}, it was changed back from the two-plasma to the single plasma configuration.

6.2 Double pulse generator operation range

The parameter flexibility of the DPS allowed the study of a variety of effects in the propagation of the proton beam in plasma, that benefited from the plasma being contained in a glass tube [145], the wide density range [146], and

the different gas types [147] and plasma lengths [148]. However, the different configurations lead to small changes in the shape and characteristics of the pulses.

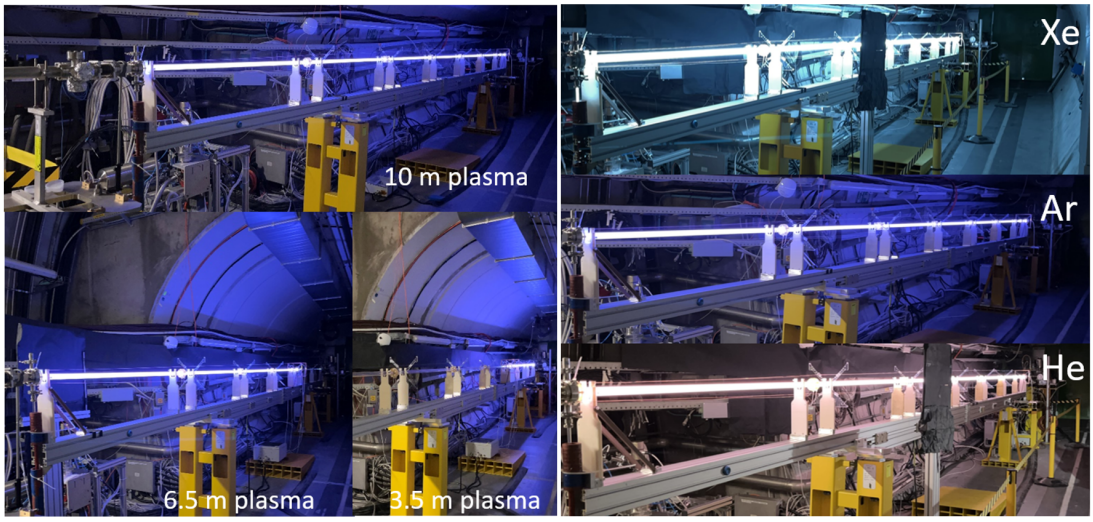

Figure 6.3: Photographs of plasma discharges with argon using 3.5 m, 6.5 m and 10 m configurations on the left and of plasma discharges with 10 m length using helium, argon and xenon, on the right - at the AWAKE experiment

6.2.1 Plasma length comparison

Considering plasma discharges in argon at $p = 24\,\mathrm{Pa}$, with a maximum current of $I_h = 500\,\mathrm{A}$, for the three plasma lengths, we obtain Figure 6.4. The variation in plasma length primarily affects the plasma resistance following ignition. Consequently, achieving the same peak current value of $500\,\mathrm{A}$ requires a lower applied voltage for shorter lengths ($V_{h-3.5m} = 4.22\,\mathrm{kV}$, $V_{h-6.5m} = 5.07\,\mathrm{kV}$, and $V_{h-10m} = 6.32\,\mathrm{kV}$). This difference in impedance, and hence the required applied voltage, is reflected in the heater pulse waveforms shown in Figure 6.4.

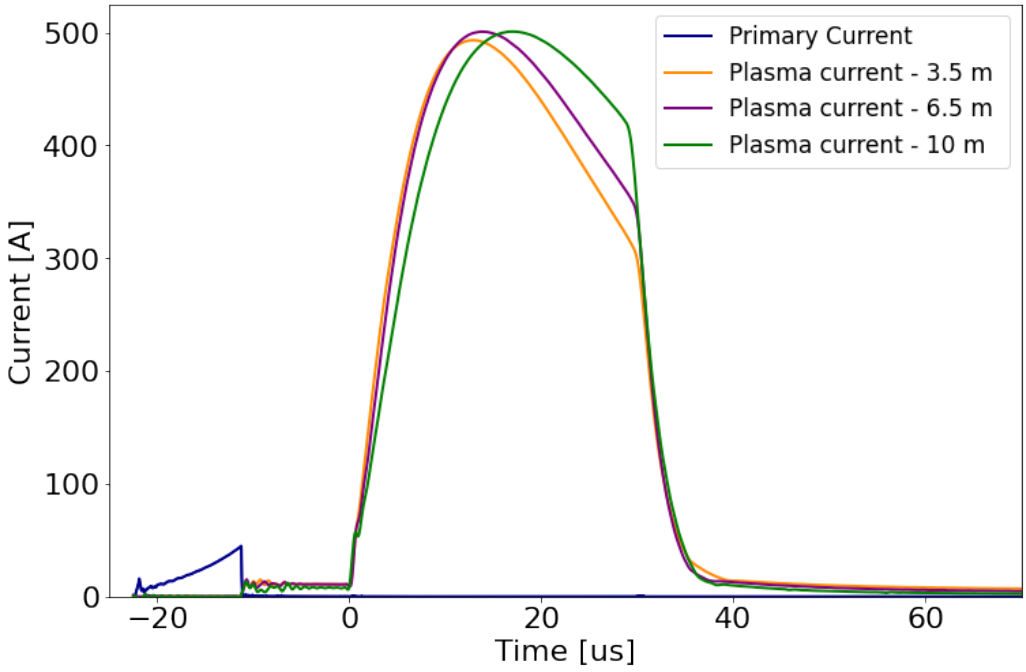

Figure 6.4: Primary and plasma currents - Ar (24 Pa) in 3.5 m ($V_h = 4.22\,\mathrm{kV}$), 6.5 m ($V_h = 5.07\,\mathrm{kV}$) and 10 m ($V_h = 4.22\,\mathrm{kV}$ lengths

Plasmas with lower impedance reach the $500\,\mathrm{A}$ current target more quickly - plasma current maximum instant

for the 3.5 m, 6.5 m, and 10 m respectively is: $t_{max} = 12.9\,\mu$s, $t_{max} = 13.4\,\mu$s, and $t_{max} = 16.9\,\mu$s; however, due to the reduced charge in the capacitor C_h (from the lower heater voltage applied) the pulse current decreases more rapidly in the shorter plasmas compared to the longer ones (the plasma current at the heater turn-OFF is $I_{hOFF} = 320.6$ A, $I_{hOFF} = 357.4$ A, and $I_{hOFF} = 319.7$ A, for the 3.5 m, 6.5 m and 10 m plasmas respectively).

6.2.2 Gas-type comparison

The gases used in this experiment were helium, argon and xenon. Helium, as the lighter gas, must be at a higher pressure to ignite as observed in Chapter 5. Even at higher pressures, helium discharges still require a higher ignition voltage to obtain a consistent plasma discharge, as shown in Figure 6.5 where the primary current used for helium was $I_{L\mu} = 60$ A, while for argon and xenon $I_{L\mu} = 45$ A was sufficient.

The difference in plasma resistance after ignition in these three cases is minimal, producing more similar shapes for each heater pulse, when compared with the plots from Figure 6.4. However, the different gases produce very different plasma electron density evolutions and ionisation fractions [42].

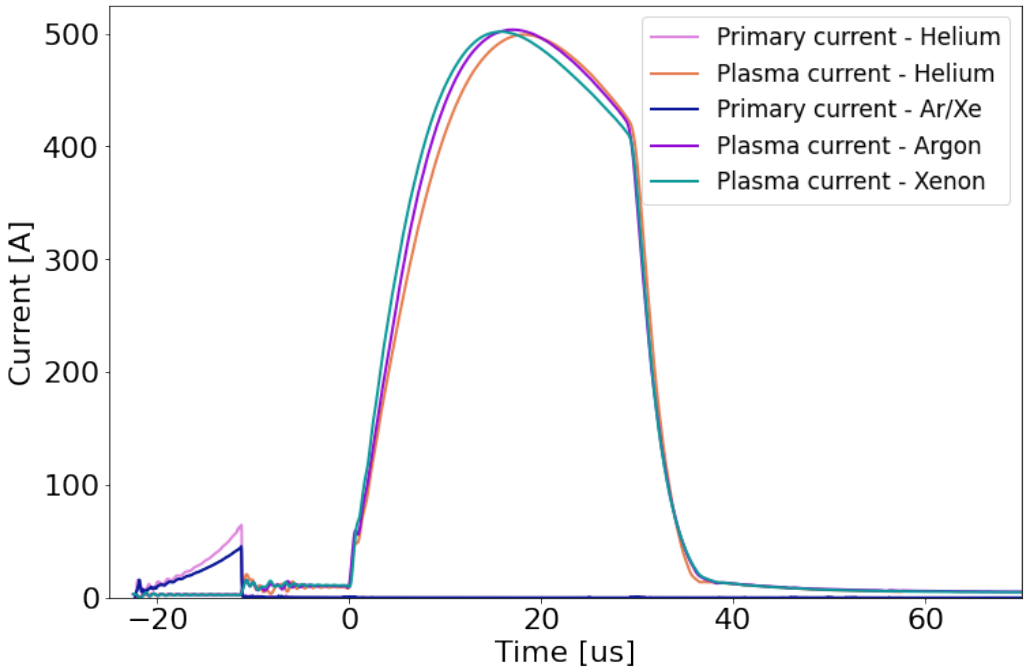

Figure 6.5: Primary and plasma currents for 10 m length in He (45 Pa, $V_h = 6.56$ kV), Ar (24 Pa, $V_h = 6.32$ kV), Xe ($V_h = 6.83$ kV)

6.3 Effect of the proton beam on the plasma current

In addition to the various configurations, a large range of densities was accessible by varying the beginning of the discharge with respect to the arrival of the proton beam, allowing to probe different moments of the discharge [42]. The proton beam travelling through the plasma can further ionise it (impact ionisation). In this section we will analyse how the plasma heater current is affected by the proton beam, using different gases. To visualize the passage of the proton bunch in the current plots we introduce the signal of a photo-diode, installed at the exit of the plasma source and used to detect the light emitted by the proton beam (red line in Figure 6.6).

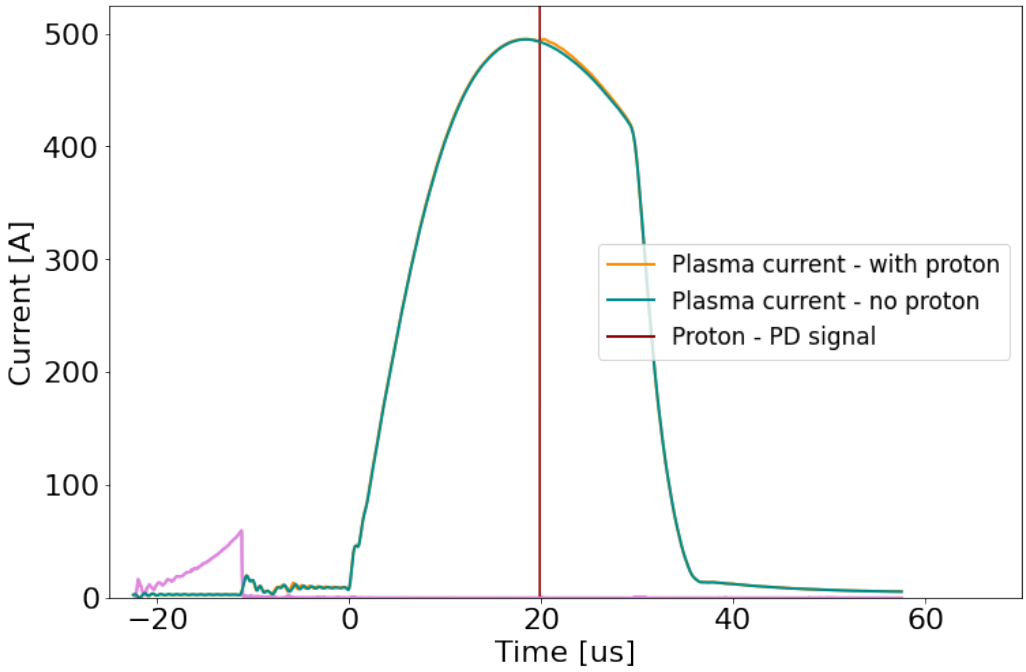

Figure 6.6: Plasma currents for 10 m length in He (45 Pa, $V_h = 6.56\,\mathrm{kV}$) with and without proton

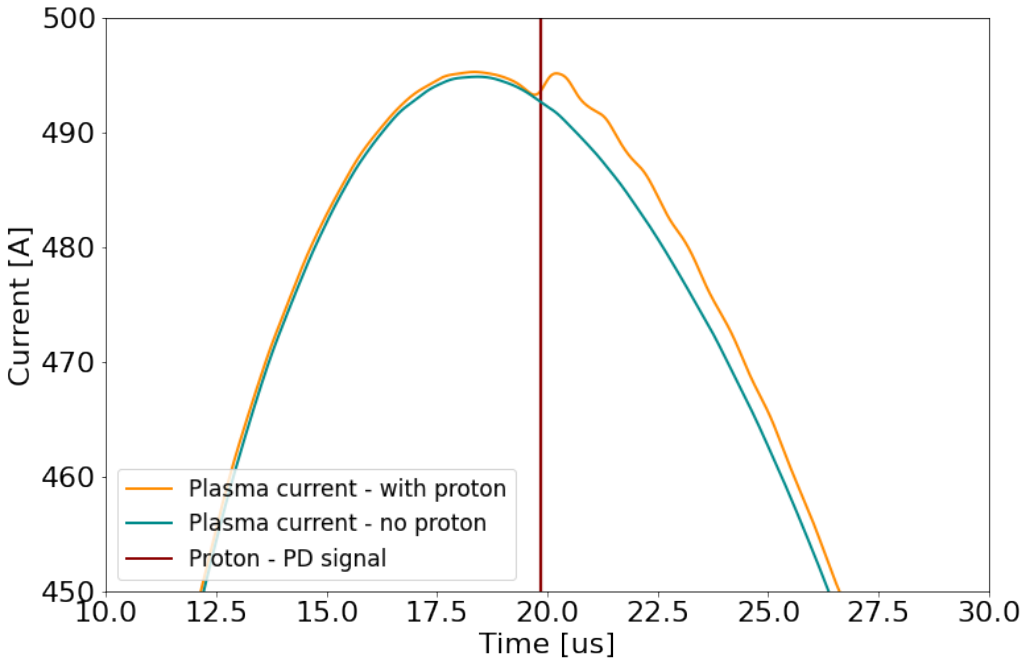

Figure 6.7: Detail of plasma currents for 10 m length in He (45 Pa, $V_h = 6.56\,\mathrm{kV}$) with and without proton

Ideally, the effect of the proton beams on the electrical system would be minimal. However, helium experiences a significant reduction in plasma resistance after the passage of the proton beam. This reduction is evident in Figure 6.7, with the sudden increase in current after the proton beam. The effect of the impact ionisation is noticeable due to the lower ionisation fraction associated with the helium plasmas, which generates a current increase of up to $3.9\,\mathrm{A}$ between plasmas with and without proton.

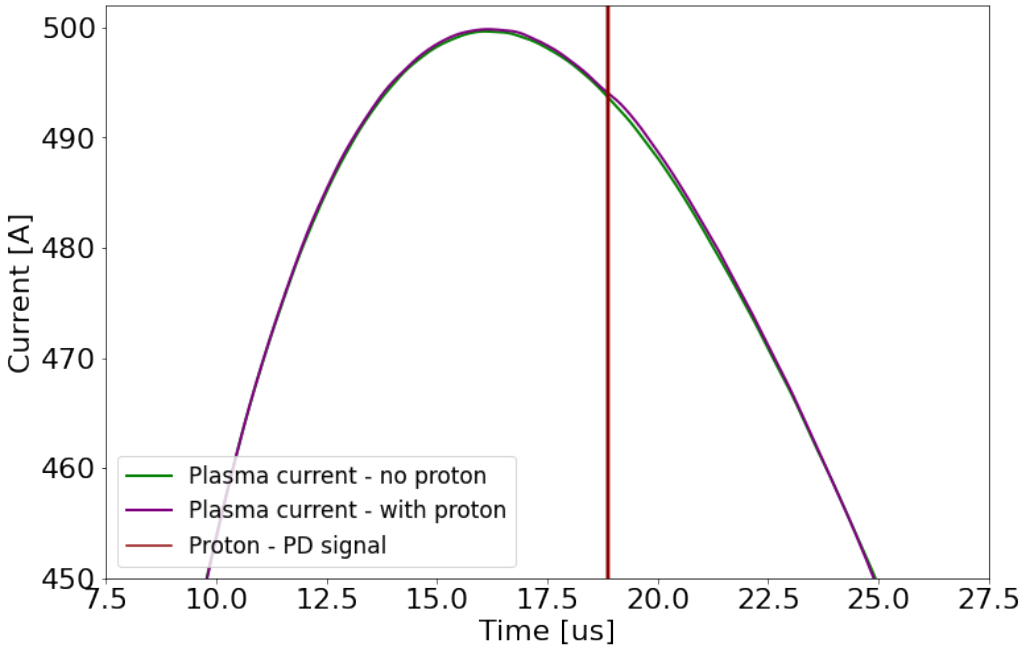

Figure 6.8: Detail of plasma currents for 10 m length in Ar (24 Pa, $V_h = 6.33\,\mathrm{kV}$) with and without proton

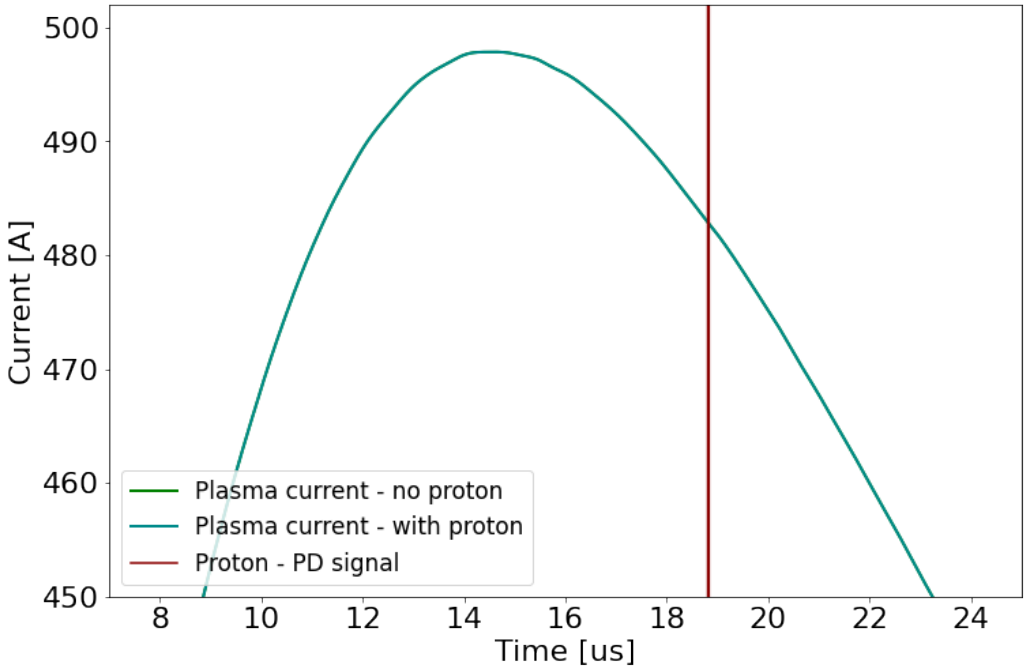

Figure 6.9: Detail of plasma currents for 10 m length in Xe (16 Pa, $V_h = 6.75\,\mathrm{kV}$) with and without proton

This effect is much less noticeable in argon (Figure 6.8 - $0.76\,\mathrm{A}$ difference in discharges with and without plasma), and completely neglectable in xenon (Figure 6.9) which presents the highest ionisation fraction of the three gases used.

6.4 Current reproducibility analysis

To assess the performance of the DPS in the AWAKE experiment, it is essential to evaluate the reproducibility of the heater pulse current. This analysis provides insight into the stability of the system operation under experimental conditions. Reproducibility is examined following the methodology outlined in Chapter 5, which involves measuring both the jitter and the variation in maximum current. Additionally, particular attention is given to the reproducibility at the point of proton beam passage, as this is a critical parameter for the success of the experiment.

As an example, we will analyse the discharges done in 24 Pa Ar, with the $10\,\mathrm{m}$ setup, on the 3^{rd} of May. Figure 6.10 presents the current waveforms of 300 discharges overlapped. Analysing these waveforms, we determine that the difference between the highest and the lowest heater pulse maximum current was $4.39\,\mathrm{A}$ (from an average of $500.04\,\mathrm{A}$) giving a maximum-current variation of 0.88%. It is also relevant to determine what was the current variation during the passage of the proton beam. Considering the moment of highest density (determined in [42]), the current variation was $2.7\,\mathrm{A}$ (average value $457.2\,\mathrm{A}$) translating into a 0.59% variation.

The rise of the heater pulse has a time jitter (with respect to the trigger) of $25.6\,\mathrm{ns}$. However, since the plasma generated must be synchronised with the passage of the proton bunch, it is more relevant to determine the heater rise jitter with respect to this event. This is possible using the photodiode signal, and the jitter calculated was $19.2\,\mathrm{ns}$.

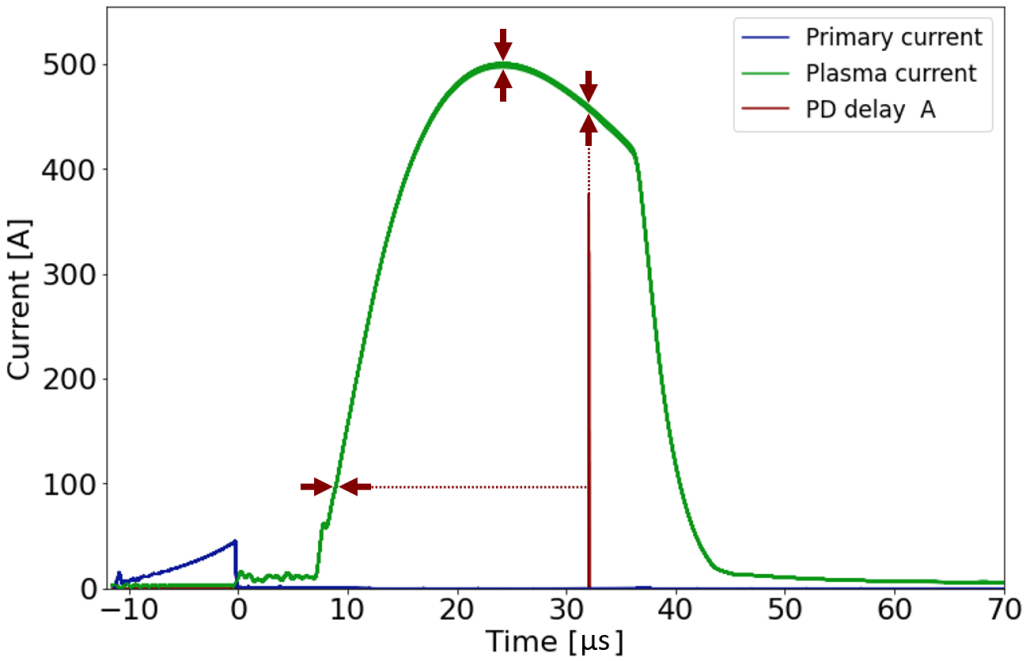

Figure 6.10: Plasma currents for 10 m length in Ar (24 Pa, $V_h = 6.32\,\mathrm{kV}$) - 300 discharges overlapped

This analysis was repeated with other configurations and settings, the results are presented in Table 6.1.

Discharges conducted in helium exhibited lower reproducibility when compared to other gases, primarily due to two factors: the significant impact of proton bunches on current variation and the helium higher breakdown voltage, which leads to lower power in the ignition plasma which affects the plasma electron density and resistance prior to the heater pulse, causing an increased jitter and a larger pulse magnitude variation. In contrast, the other plasma configurations demonstrated consistent reproducibility, with jitter remaining below 20 ns and current variation

below 1%. The variations that occur are possibly also attributed to physical effects such as pressure and temperature fluctuations over time and are further constrained by the resolution limits of the current measurement system.

Table 6.1: Heater pulse current reproducibility results

Length	**Gas-type**	**Pressure [Pa]**	**I_h average [A]**	**I_h variation [A]**	**I_h variation [%]**	**I_h jitter [ns]**
10 m	argon	24	500.04	4.39	0.88	19.2
10 m	xenon	16	499.16	2.20	0.44	19.2
10 m	helium	45	502.22	5.37	1.07	32.0
6.5 m	argon	24	499.66	1.71	0.34	12.8
3.5 m	argon	24	498.33	2.69	0.54	19.2

The DPS operation in the AWAKE experiment demonstrated its potential as an alternative plasma source for plasma wakefield experiments. The DPS measured good electrical reproducibility (jitter $< 20\,\mathrm{ns}$, and current $< 1\%$ for argon and xenon plasmas), robustness, and wide operational range. These qualities facilitated a variety of physics studies, providing valuable experimental results. These studies have contributed to advancing our understanding of plasma acceleration and of SMI in proton bunches, reflected in multiple articles at various stages of publication: [42, 43, 145–147]. It also demonstrated that helium was the least adequate gas tested (for an AWAKE plasma) due to its reproducibility values, sensibility to the proton beam, lower ionisation fraction, and plasma density measured. This experiment also demonstrated the potential for length scalability beyond the current $10\,\mathrm{m}$ limit. The outcomes of this experiment lay the foundation for future advancements in scalable plasma source technologies, paving the way for their continued development and integration into large-scale accelerator experiments [149].

CHAPTER 7

Conclusions

This thesis deals with the development of a semiconductor-based double pulse generator for the ignition and heating of a discharge plasma source for the AWAKE experiment. The pulse generator was designed and developed in IST, tested and validated for AWAKE compliance in CERN, and finally, it operated successfully in AWAKE for a three-week experiment that included the propagation of high-energy proton beams and discharges with multiple plasma tubes, producing valuable results and contributing to further advancements for plasma wakefield accelerators and high-energy physics [42, 43, 145–147]. Therefore, we conclude that the objectives defined in Chapter 1 were met.

7.1 Summary

The design of the pulse generators involved selecting the appropriate topologies and their switches. The development of the pulse generator also benefits from electrical simulations which require a suitable plasma model. Lastly, the two-plasma configuration requires current balancing. In Chapter 2, we analysed different pulse generator topologies and switches, as well as current balance techniques and plasma models for electrical simulations.

The double pulse generator was developed based on two distinct topologies: a flyback-type generator for the high-voltage, fast-rising ignition pulse ($20\,\mathrm{kV}$) and a capacitive negative discharge topology for the high-current heating pulse ($> 500\,\mathrm{A}$). In Chapter 3, we analyse this selection concerning the AWAKE plasma source requirements, and how both topologies were integrated in the double pulse generator. We also analyse the six step operation of the double pulse generator and the interaction between its different components.

With the double pulse generator operation detailed, it was possible to design its different components: IGBT switches, high-power diodes, step-up transformer, overvoltage snubbers, current balancing coupled inductor, etc. Chapter 4 presents the component sizing and selection, along with some relevant DPS plasma setup design considerations. PSpice simulations were conducted using a custom plasma model based on Cassie's Arc Model, to assist in the development and characterisation of the pulse generator.

Chapter 5 presents the main (electrical) results of the tests performed at the CERN DPS laboratory. The pulse generator operation can be observed as described, and the PSpice model currents were compared. The plasma current differences between simulation and experiment are more significant for the lower current associated with

the ignition pulse (presenting a 10% difference after stabilising) than for the heater pulse (with 1.4% difference at the current maximum), thus demonstrating a lower accuracy of the model under lower plasma currents.

Discharges without plasma gave insights into the ignition pulse voltage shape. It demonstrated that it could produce a voltage pulse of $V_{plasma} = 21.86\,\mathrm{kV}$ with a rise-time of $t_{lag} = 1.96\,\mu\mathrm{s}$, using a power supply voltage of $V_{ign} = 3.5\,\mathrm{kV}$ and an ignition switch-ON time of $t_{ignON} = 10\,\mu\mathrm{s}$.

Analysing the plasma breakdown voltage at different pressures also assisted in the characterisation of the discharges with different gases, demonstrating that the ignition pulse can generate a plasma under the required pressure range for the AWAKE plasma densities $[8, 24]\,\mathrm{Pa}$ for argon and xenon and $[30, 45]\,\mathrm{Pa}$ for helium.

A study of the ignition primary current shows how the current magnitude affects the ignition pulse and consequently the output pulse characteristics. Lower ignition power supply values lead to slower plasma breakdowns ($t_{lag} = 4.1\,\mu\mathrm{s}$ for $V_{ign} = 2\,\mathrm{kV}$ and $t_{lag} = 1.72\,\mu\mathrm{s}$ for $V_{ign} = 3.5\,\mathrm{kV}$) under a lower voltage ($V_{br} = 9.4\,\mathrm{kV}$ for $V_{ign} = 2\,\mathrm{kV}$ and $V_{br} = 15.6\,\mathrm{kV}$ for $V_{ign} = 3.5\,\mathrm{kV}$).

It was also possible to observe how the ignition power affects the heater pulse, particularly its reproducibility, showing that to meet the objectives of current variation $< 1\%$ and heater rise jitter $< 20\,\mathrm{ns}$ only $3\,\mathrm{kV}$ or $3.5\,\mathrm{kV}$ pulses are viable (demonstrating a current maximum variation of 0.97% and 0.53% respectively, and a jitter of $19.2\,\mathrm{ns}$).

The plasma resistance during the heater pulse was measured, comparing the effect of the heater current pulse value and the gas pressure. For the relevant argon pressures the plasma resistivity is approximately proportional to the pressure value. However, the effect of the different currents suggests that the plasma resistivity should progressively vary less for higher current densities.

Lastly the double plasma configuration was tested showing the performance of the current balancing module, allowing two plasma sections with a length difference of 53% to operate simultaneously with currents with only 3.4% variation. These results (along with the plasma density measurements performed together [42]) demonstrated the adequacy of the pulse generator for the AWAKE experiment.

The double pulse generator demonstrated significant flexibility, enabling experiments with different plasma lengths ($3.5\,\mathrm{m}$, $6.5\,\mathrm{m}$ and $10\,\mathrm{m}$ plasma setups, as well as a two-plasma $3.5 + 6.5\,\mathrm{m}$ configuration) and gases (helium, argon and xenon under different pressures between $1 - 45\,\mathrm{Pa}$). Furthermore, the plasma density evolution in a discharge allows for a relatively simple way to use different plasma densities, by adjusting the timing of the discharge relative to the proton beam arrival, allowing a wide range of experimental parameters. These characteristics lead to the installation of the DPS in the AWAKE experiment. Chapter 6 details the performance of the double pulse generator in AWAKE.

The DPS operated for 21 days, generating over 21 thousand plasma discharges. The different plasma lengths used demonstrated significant differences in the plasma resistance following ignition, made evident by the values of heater supply voltage ($V_{h-3.5m} = 4.22\,\mathrm{kV}$, $V_{h-6.5m} = 5.07\,\mathrm{kV}$, and $V_{h-10m} = 6.32\,\mathrm{kV}$) and the current rise speed of the heater pulse ($t_{max-3.5m} = 12.9\,\mu\mathrm{s}$, $t_{max-6.5m} = 13.4\,\mu\mathrm{s}$, and $t_{max-10m} = 16.9\,\mu\mathrm{s}$). In comparison, the different gases did not show a relevant difference in plasma resistance, but helium required a higher ignition voltage for a stable operation ($V_{ign} = 3.5\,\mathrm{kV}$ and $I_{L\mu} = 60\,\mathrm{A}$) than argon and xenon ($V_{ign} = 3.0\,\mathrm{kV}$ and $I_{L\mu} = 45\,\mathrm{A}$). Helium also demonstrated a higher sensibility to the proton beam, presenting a current spike of $3.9\,\mathrm{A}$ after its passage, argon only suffered a shift of $0.76\,\mathrm{A}$ and xenon did not measure any effect. The current

reproducibility was also determined by measuring the heater pulse rise jitter and the heater current maximum variation for the different gases and configurations. Only helium measured a jitter above $20\,\mathrm{ns}$ ($32\,\mathrm{ns}$) and a current variation above 1% (1.07%).

The DPS flexibility facilitated the study of relevant phenomena in proton beam propagation through plasma, including the development of transverse filamentation instability [146], the influence of ion motion on the SMI [147], and (enabled by the DPS glass tube) light diagnostics [145]. The two-plasma configuration was also tested, supporting the further use of coupled inductor current balancing for plasma length scalability.

7.2 Recommendations and future work

The pulse generators developed for the DPS demonstrated the ability to meet the AWAKE requirements of length, plasma electron density, and reproducibility. It was also possible to observe proton bunch self-modulation instability (SMI) signatures similar to the ones obtained with the AWAKE standard laser field ionisation plasma source, which was an essential part of the AWAKE DPS experiment, although not in the scope of this thesis.

However, the constraint of using asymmetric plasma lengths for the two-plasma configuration limited the AWAKE results under this setup. The current balancing module performed as expected and demonstrated its ability to have a viable two-plasma configuration, but future work must encompass symmetric plasma configurations to consolidate the knowledge acquired in length scalability of discharge plasma sources. To increase the plasma length to hundreds of meters, configurations with more than two plasmas must also be designed and tested.

The plasma model used was an essential tool for the development of the double pulse generator. However, due to the differences observed for lower currents, the development of a plasma model suitable for a wider range of currents is advisable for applications such as this one.

It was also observed the effect of temperature and pressure variations in the plasma density reproducibility, showing that future developments of the DPS must involve an accurate control of both these parameters, to achieve even better plasma density reproducibility results. Temperature control of the semiconductor components and the resistor R_c may also prove beneficial to further improve the current reproducibility. Increasing the ionisation fraction of the DPS plasmas could potentially have an effect on the reproducibility, by reducing the effect of small current variations in the plasma density.

Bibliography

[1] N. A. Solyak. Gradient limitations in room temperature and superconducting acceleration structures. *AIP Conference Proceedings*, 1086:365–372, 2009. ISSN 0094243X. doi: 10.1063/1.3080933.

[2] C. Adolphsen, D. Angal-Kalinin, K. Aulenbacher, T. Arndt, M. Arnold, R. Assmann, B. Auchmann, A. Ballarino, B. Baudouy, P. Baudrenghien, S. Bentvelsen, M. Benedikt, A. Blondel, A. Bogacz, F. Bossi, L. Bottura, S. Bousson, M. Bruker, O. Brunner, O. Brüning, G. Burt, S. Calatroni, A. Castilla, N. Catalan-Lasheras, E. Cenni, A. Chancé, N. Colin, S. Cordez, L. Corieri, B. Crosa, A. Crossu, J.-P. Delahaye, G. Devanz, A.-I. Etienne, P. Evtushenko, P. Fazilleau, M. Ferrario, A. Gallof, L. García-Tabarés, C. Geddes, F. Gerigk, F. Gianotti, E. Gschwendtner, A. Grudieva, M. Hogan, G. Hoffstaetter, S. Hooker, R. Ischebeck, K. Jakobs, P. Janota, E. Jensen, W. Kaabi, D. Kayran, M. Klein, J. Knobloch, M. Koratzinos, J. Kühn, B. Kuske, M. Lamont, A. Latina, P. Lebrun, W. Leemans, D. Lip, K. Long, D. Longuevergne, R. Losito, W. Lu, O. Lundh, F. Marhauser, E. Métral, J. Michni, B. Militsyn, N. Mouneta, P. Muggli, P. Musumeci, S. Nagaitsev, M. Neo, A. Neumann, D. Newbold, P. Nghiem, J. Osterhoff, M. Palmer, N. Pastrone, N. Pietralla, S. Prestemon, T. Proslier, L. Quettier, T. Raubenheimer, L. Rivier, B. Rimmer, B. Rochepault, C. Rogers, G. Rosaza, L. Rossi, R. Rubert, C. Senator, M. Seidl, B. Shepherd, J. Shiv, N. Shipman, S. Stapnes, D. Stratakis, A. Stocchi, I. Syratcheva, S. Tantawi, O. Tanaka, C. Tennant, E. Tsesmelis, C. Vaccarezza, A.-M. Valente, B. Védrine, J. Vieira, N. Vinokurov, Y. Wakayama, M. Wenskat, P. Williams, M. Wing, K. Yokoya, and F. Zimmerman. *European Strategy for Particle Physics - Accelerator R&D Roadmap*. CERN Yellow Reports: Monographs, 2022. ISBN 9789290836216. doi: doi.org/10.48550/arXiv.2201.07895.

[3] V. Barger, M. S. Berger, J. F. Gunion, and T. Han. Particle physics opportunities at μ+μ- colliders. *Nuclear Physics B - Proceedings Supplements*, 51(1):13–31, 1996. ISSN 09205632. doi: 10.1016/0920-5632(96)00412-4.

[4] K. R. Long, D. Lucchesi, M. A. Palmer, N. Pastrone, D. Schulte, and V. Shiltsev. Muon colliders to expand frontiers of particle physics. *Nature Physics*, 17(3):289–292, 2021. ISSN 17452481. doi: 10.1038/s41567-020-01130-x.

[5] I. V. Bazarov. Overview of energy recovery linacs. *Proceedings of the IEEE Particle Accelerator Conference*, 2005:382–386, 2005. doi: 10.1109/PAC.2005.1590441.

[6] J. M. Dawson and T. Tajima. Laser Electron Accelerator. *Physical Review Letters*, 43(4):267–270, 1979.

[7] P. Chen, J. Dawson, R. W. Huff, and T. Katsouleas. Acceleration of electrons by the interaction of a bunched electron beam with a Plasma. *Physical Review Letters*, 54(7):693, 1985. ISSN 03759601. doi: 10.1016/0375-9601(91)90914-T.

[8] F. Albert, M. E. Couprie, A. Debus, M. C. Downer, J. Faure, A. Flacco, L. A. Gizzi, T. Grismayer, A. Huebl, C. Joshi, M. Labat, W. P. Leemans, A. R. Maier, S. P. Mangles, P. Mason, F. Mathieu, P. Muggli, M. Nishiuchi, J. Osterhoff, P. P. Rajeev, U. Schramm, J. Schreiber, A. G. Thomas, J. L. Vay, M. Vranic, and K. Zeil. 2020 Roadmap on Plasma Accelerators. *New Journal of Physics*, 23(3), 2021. ISSN 13672630. doi: 10.1088/1367-2630/abcc62.

[9] V. Shiltsev and F. Zimmermann. Modern and future colliders. *Reviews of Modern Physics*, 93(1):15006, 2021. ISSN 15390756. doi: 10.1103/RevModPhys.93.015006.

[10] F. F. Chen. Excitation of large amplitude plasma waves. *Physica Scripta*, 1990(T30):14–23, 1990. ISSN 14024896. doi: 10.1088/0031-8949/1990/T30/003.

[11] E. Esarey, C. B. Schroeder, and W. P. Leemans. Physics of laser-driven plasma-based electron accelerators. *Reviews of Modern Physics*, 81(3):1229–1285, 2009. ISSN 00346861. doi: 10.1103/RevModPhys.81.1229.

[12] I. Blumenfeld, C. E. Clayton, F. J. Decker, M. J. Hogan, C. Huang, R. Ischebeck, R. Iverson, C. Joshi, T. Katsouleas, N. Kirby, W. Lu, K. A. Marsh, W. B. Mori, P. Muggli, E. Oz, R. H. Siemann, D. Walz, and M. Zhou. Energy doubling of 42 GeV electrons in a metre-scale plasma wakefield accelerator. *Nature*, 445 (7129):741–744, 2007. ISSN 14764687. doi: 10.1038/nature05538.

[13] A. J. Gonsalves, K. Nakamura, J. Daniels, C. Benedetti, C. Pieronek, T. C. De Raadt, S. Steinke, J. H. Bin, S. S. Bulanov, J. Van Tilborg, C. G. Geddes, C. B. Schroeder, C. Tóth, E. Esarey, K. Swanson, L. Fan-Chiang, G. Bagdasarov, N. Bobrova, V. Gasilov, G. Korn, P. Sasorov, and W. P. Leemans. Petawatt Laser Guiding and Electron Beam Acceleration to 8 GeV in a Laser-Heated Capillary Discharge Waveguide. *Physical Review Letters*, 122(8):84801, 2019. ISSN 10797114. doi: 10.1103/PhysRevLett.122.084801.

[14] R. D'Arcy, A. Aschikhin, S. Bohlen, G. Boyle, T. Brümmer, J. Chappell, S. Diederichs, B. Foster, M. J. Garland, L. Goldberg, P. Gonzalez, S. Karstensen, A. Knetsch, P. Kuang, V. Libov, K. Ludwig, A. M. De La Ossa, F. Marutzky, M. Meisel, T. J. Mehrling, P. Niknejadi, K. Põder, P. Pourmoussavi, M. Quast, J. H. Röckemann, L. Schaper, B. Schmidt, S. Schröder, J. P. Schwinkendorf, B. Sheeran, G. Tauscher, S. Wesch, M. Wing, P. Winkler, M. Zeng, and J. Osterhoff. FLASHForward: Plasma wakefield accelerator science for high-average-power applications. *Philosophical Transactions of the Royal Society A: Mathematical, Physical and Engineering Sciences*, 377(2151), 2019. ISSN 1364503X. doi: 10.1098/rsta.2018.0392.

[15] A. Caldwell, K. Lotov, A. Pukhov, and F. Simon. Proton-driven plasma-wakefield acceleration. *Nature Physics*, 5(5):363–367, 2009. ISSN 17452481. doi: 10.1038/nphys1248.

[16] E. Gschwendtner, E. Adli, L. Amorim, R. Apsimon, R. Assmann, A. M. Bachmann, F. Batsch, J. Bauche, V. K. Berglyd Olsen, M. Bernardini, R. Bingham, B. Biskup, T. Bohl, C. Bracco, P. N. Burrows, G. Burt, B. Buttenschön, A. Butterworth, A. Caldwell, M. Cascella, E. Chevallay, S. Cipiccia, H. Damerau, L. Deacon, P. Dirksen, S. Doebert, U. Dorda, J. Farmer, V. Fedosseev, E. Feldbaumer, R. Fiorito, R. Fonseca, F. Friebel, A. A. Gorn, O. Grulke, J. Hansen, C. Hessler, W. Hofle, J. Holloway, M. Hüther, D. Jaroszynski, L. Jensen, S. Jolly, A. Joulaei, M. Kasim, F. Keeble, Y. Li, S. Liu, N. Lopes, K. V. Lotov, S. Mandry, R. Martorelli, M. Martyanov, S. Mazzoni, O. Mete, V. A. Minakov, J. Mitchell, J. Moody, P. Muggli, Z. Najmudin,

P. Norreys, E. Öz, A. Pardons, K. Pepitone, A. Petrenko, G. Plyushchev, A. Pukhov, K. Rieger, H. Ruhl, F. Salveter, N. Savard, J. Schmidt, A. Seryi, E. Shaposhnikova, Z. M. Sheng, P. Sherwood, L. Silva, L. Soby, A. P. Sosedkin, R. I. Spitsyn, R. Trines, P. V. Tuev, M. Turner, V. Verzilov, J. Vieira, H. Vincke, Y. Wei, C. P. Welsch, M. Wing, G. Xia, and H. Zhang. AWAKE, The Advanced Proton Driven Plasma Wakefield Acceleration Experiment at CERN. *Nuclear Instruments and Methods in Physics Research, Section A: Accelerators, Spectrometers, Detectors and Associated Equipment*, 829:76–82, 2016. ISSN 01689002. doi: 10.1016/j.nima.2016.02.026.

[17] E. Adli, A. Ahuja, O. Apsimon, R. Apsimon, A. M. Bachmann, D. Barrientos, F. Batsch, J. Bauche, V. K. Berglyd Olsen, M. Bernardini, T. Bohl, C. Bracco, F. Braunmüller, G. Burt, B. Buttenschön, A. Caldwell, M. Cascella, J. Chappell, E. Chevallay, M. Chung, D. Cooke, H. Damerau, L. Deacon, L. H. Deubner, A. Dexter, S. Doebert, J. Farmer, V. N. Fedosseev, R. Fiorito, R. A. Fonseca, F. Friebel, L. Garolfi, S. Gessner, I. Gorgisyan, A. A. Gorn, E. Granados, O. Grulke, E. Gschwendtner, J. Hansen, A. Helm, J. R. Henderson, M. Hüther, M. Ibison, L. Jensen, S. Jolly, F. Keeble, S. Y. Kim, F. Kraus, Y. Li, S. Liu, N. Lopes, K. V. Lotov, L. Maricalva Brun, M. Martyanov, S. Mazzoni, D. Medina Godoy, V. A. Minakov, J. Mitchell, J. C. Molendijk, J. T. Moody, M. Moreira, P. Muggli, E. Öz, C. Pasquino, A. Pardons, F. Peña Asmus, K. Pepitone, A. Perera, A. Petrenko, S. Pitman, A. Pukhov, S. Rey, K. Rieger, H. Ruhl, J. S. Schmidt, I. A. Shalimova, P. Sherwood, L. O. Silva, L. Soby, A. P. Sosedkin, R. Speroni, R. I. Spitsyn, P. V. Tuev, M. Turner, F. Velotti, L. Verra, V. A. Verzilov, J. Vieira, C. P. Welsch, B. Williamson, M. Wing, B. Woolley, and G. Xia. Acceleration of electrons in the plasma wakefield of a proton bunch. *Nature*, 561(7723): 363–367, 2018. ISSN 14764687. doi: 10.1038/s41586-018-0485-4.

[18] P. Muggli, E. Adli, R. Apsimon, F. Asmus, R. Baartman, A. M. Bachmann, M. Barros Marin, F. Batsch, J. Bauche, M. Bernardini, B. Biskup, E. Blanco Vinuela, A. Boccardi, T. Bogey, T. Bohl, C. Bracco, F. Braunmüller, S. Burger, G. Burt, S. Bustamante, B. Buttenschön, A. Butterworth, A. Caldwell, M. Cascella, E. Chevallay, M. Chung, H. Damerau, L. Deacon, A. Dexter, P. Dirksen, S. Doebert, J. Farmer, V. Fedosseev, T. Feniet, G. Fior, R. Fiorito, R. Fonseca, F. Friebel, P. Gander, S. Gessner, I. Gorgisyan, A. A. Gorn, O. Grulke, E. Gschwendtner, A. Guerrero, J. Hansen, C. Hessler, W. Hofle, J. Holloway, M. Huther, M. Ibison, M. R. Islam, L. Jensen, S. Jolly, M. Kasim, F. Keeble, S. Y. Kim, F. Kraus, A. Lasheen, T. Lefevre, G. LeGodec, Y. Li, S. Liu, N. Lopes, K. V. Lotov, M. Martyanov, S. Mazzoni, D. Medina Godoy, O. Mete, V. A. Minakov, R. Mompo, J. Moody, M. T. Moreira, J. Mitchell, C. Mutin, P. Norreys, E. Öz, E. Ozturk, W. Pauw, A. Pardons, C. Pasquino, K. Pepitone, A. Petrenko, S. Pitman, G. Plyushchev, A. Pukhov, K. Rieger, H. Ruhl, J. Schmidt, I. A. Shalimova, E. Shaposhnikova, P. Sherwood, L. Silva, A. P. Sosedkin, R. Speroni, R. I. Spitsyn, K. Szczurek, J. Thomas, P. V. Tuev, M. Turner, V. Verzilov, J. Vieira, H. Vincke, C. P. Welsch, B. Williamson, M. Wing, G. Xia, and H. Zhang. AWAKE readiness for the study of the seeded self-modulation of a 400GeV proton bunch. *Plasma Phys. Control. Fusion*, 60, 2018.

[19] G. Plyushchev, R. Kersevan, A. Petrenko, and P. Muggli. A rubidium vapor source for a plasma source for AWAKE. *Journal of Physics D: Applied Physics*, 51(2), 2018. ISSN 13616463. doi: 10.1088/1361-6463/aa9dd7.

[20] M. Turner, E. Adli, A. Ahuja, O. Apsimon, R. Apsimon, A. M. Bachmann, M. Barros Marin, D. Barrientos,

F. Batsch, J. Batkiewicz, J. Bauche, V. K. Berglyd Olsen, M. Bernardini, B. Biskup, A. Boccardi, T. Bogey, T. Bohl, C. Bracco, F. Braunmüller, S. Burger, G. Burt, S. Bustamante, B. Buttenschön, A. Caldwell, M. Cascella, J. Chappell, E. Chevallay, M. Chung, D. Cooke, H. Damerau, L. Deacon, L. H. Deubner, A. Dexter, S. Doebert, J. Farmer, V. N. Fedosseev, G. Fior, R. Fiorito, R. A. Fonseca, F. Friebel, L. Garolfi, S. Gessner, I. Gorgisyan, A. A. Gorn, E. Granados, O. Grulke, E. Gschwendtner, A. Guerrero, J. Hansen, A. Helm, J. R. Henderson, C. Hessler, W. Hofle, M. Hüther, M. Ibison, L. Jensen, S. Jolly, F. Keeble, S. Y. Kim, F. Kraus, T. Lefevre, G. Legodec, Y. Li, S. Liu, N. Lopes, K. V. Lotov, L. Maricalva Brun, M. Martyanov, S. Mazzoni, D. Medina Godoy, V. A. Minakov, J. Mitchell, J. C. Molendijk, R. Mompo, J. T. Moody, M. Moreira, P. Muggli, E. Öz, E. Ozturk, C. Mutin, C. Pasquino, A. Pardons, F. Peña Asmus, K. Pepitone, A. Perera, A. Petrenko, S. Pitman, G. Plyushchev, A. Pukhov, S. Rey, K. Rieger, H. Ruhl, J. S. Schmidt, I. A. Shalimova, E. Shaposhnikova, P. Sherwood, L. O. Silva, L. Soby, A. P. Sosedkin, R. Speroni, R. I. Spitsyn, P. V. Tuev, F. Velotti, L. Verra, V. A. Verzilov, J. Vieira, H. Vincke, C. P. Welsch, B. Williamson, M. Wing, B. Woolley, and G. Xia. Experimental Observation of Plasma Wakefield Growth Driven by the Seeded Self-Modulation of a Proton Bunch. *Physical Review Letters*, 122(5):54801, 2019. ISSN 10797114. doi: 10.1103/PhysRevLett.122.054801.

[21] F. Braunmüller, T. Nechaeva, E. Adli, R. Agnello, M. Aladi, Y. Andrebe, O. Apsimon, R. Apsimon, A. M. Bachmann, M. A. Baistrukov, F. Batsch, M. Bergamaschi, P. Blanchard, P. N. Burrows, B. Buttenschön, A. Caldwell, J. Chappell, E. Chevallay, M. Chung, D. A. Cooke, H. Damerau, C. Davut, G. Demeter, L. H. Deubner, A. Dexter, G. P. Djotyan, S. Doebert, J. Farmer, A. Fasoli, V. N. Fedosseev, R. Fiorito, R. A. Fonseca, F. Friebel, I. Furno, L. Garolfi, S. Gessner, B. Goddard, I. Gorgisyan, A. A. Gorn, E. Granados, M. Granetzny, O. Grulke, E. Gschwendtner, V. Hafych, A. Hartin, A. Helm, J. R. Henderson, A. Howling, M. Hüther, R. Jacquier, S. Jolly, I. Y. Kargapolov, M. Kedves, F. Keeble, M. D. Kelisani, S. Y. Kim, F. Kraus, M. Krupa, T. Lefevre, Y. Li, L. Liang, S. Liu, N. Lopes, K. V. Lotov, M. Martyanov, S. Mazzoni, D. Medina Godoy, V. A. Minakov, J. T. Moody, P. I. Morales Guzmán, M. Moreira, P. Muggli, H. Panuganti, A. Pardons, F. Peña Asmus, A. Perera, A. Petrenko, J. Pucek, A. Pukhov, B. Ráczkevi, R. L. Ramjiawan, S. Rey, H. Ruhl, H. Saberi, O. Schmitz, E. Senes, P. Sherwood, L. O. Silva, R. I. Spitsyn, P. V. Tuev, M. Turner, F. Velotti, L. Verra, V. A. Verzilov, J. Vieira, C. P. Welsch, B. Williamson, M. Wing, J. Wolfenden, B. Woolley, G. Xia, M. Zepp, and G. Zevi Della Porta. Proton Bunch Self-Modulation in Plasma with Density Gradient. *Physical Review Letters*, 125(26):264801, 2020. ISSN 10797114. doi: 10.1103/PhysRevLett.125.264801.

[22] E. Gschwendtner, K. Lotov, P. Muggli, M. Wing, and AWAKE Collaboration. The AWAKE Run 2 programme and beyond. *Symmetry*, 2022.

[23] B. Buttenschön, N. Fahrenkamp, and O. Grulke. A high power, high density helicon discharge for the plasma wakefield accelerator experiment AWAKE. *Plasma Physics and Controlled Fusion*, 60, 2018. doi: 10.1088/1361-6587/aac13a.

[24] N. E. Torrado, N. C. Lopes, J. F. A. Silva, C. Amoedo, and A. Sublet. Double Pulse Generator for Unipolar Discharges in Long Plasma Tubes for the AWAKE Experiment. *IEEE Transactions on Plasma Science*, 51 (12):3619–3627, 2023. ISSN 19399375. doi: 10.1109/TPS.2023.3337314.

[25] F. F. Chen. Helicon discharges and sources: A review. *Plasma Sources Science and Technology*, 24(1), 2015. ISSN 13616595. doi: 10.1088/0963-0252/24/1/014001.

[26] Y. P. Raizer. *Gas discharge physics*. Number 173. Springer, 1991. ISBN 978-3-642-64760-4.

[27] G. G. Lister, J. E. Lawler, W. P. Lapatovich, and V. A. Godyak. The physics of discharge lamps. *Reviews of Modern Physics*, 76(2):541–598, 2004. ISSN 00346861. doi: 10.1103/RevModPhys.76.541.

[28] A. M. Valshin, S. V. Garnov, S. A. Belkov, and S. M. Pershin. High-Frequency (MHz) Ignition of Commercial Flash Lamps for Solid State Lasers. *Doklady Physics*, 67(1):32–37, 2022. ISSN 15626903. doi: 10.1134/S1028335822010062.

[29] W. T. Silfvast. *Laser Fundamentals*. Cambridge University Press, Cambridge, MA, 2008.

[30] M. Žumer, B. Zajec, R. Rozman, and V. Nemanič. Breakdown voltage reliability improvement in gas-discharge tube surge protectors employing graphite field emitters. *Journal of Applied Physics*, 111(8), 2012. ISSN 00218979. doi: 10.1063/1.4704699.

[31] M. A. Lieberman and A. Lichtenberg J. *Principles of Plasma Discharges and Materials Processing*. John Wiley & Sons, Inc., second edition, 2005. ISBN 9786468600.

[32] B. O. Aronsson, J. Lausmaa, and B. Kasemo. Glow discharge plasma treatment for surface cleaning and modification of metallic biomaterials. *Journal of Biomedical Materials Research*, 35(1):49–73, 1997. ISSN 00219304. doi: 10.1002/(SICI)1097-4636(199704)35:1⟨49::AID-JBM6⟩3.0.CO;2-M.

[33] T. von Woedtke, S. Reuter, K. Masur, and K. D. Weltmann. Plasmas for medicine. *Physics Reports*, 530(4): 291–320, 2013. ISSN 03701573. doi: 10.1016/j.physrep.2013.05.005.

[34] H. H. Kim, Y. Teramoto, A. Ogata, H. Takagi, and T. Nanba. Plasma Catalysis for Environmental Treatment and Energy Applications. *Plasma Chemistry and Plasma Processing*, 36(1):45–72, 2016. ISSN 02724324. doi: 10.1007/s11090-015-9652-7.

[35] N. C. Lopes, C. Russo, R. A. Bendoyro, M. Hilbert, J. Jiang, C. E. Clayton, and F. Fang. Plasma channels for multi-GeV laser-plasma accelerators using discharges in structured gas cells. *IEEE International Conference on Plasma Science*, 36(4):1728–1733, 2009. ISSN 07309244. doi: 10.1109/PLASMA.2009.5227317.

[36] A. J. Gonsalves, F. Liu, N. A. Bobrova, P. V. Sasorov, C. Pieronek, J. Daniels, S. Antipov, J. E. Butler, S. S. Bulanov, W. L. Waldron, D. E. Mittelberger, and W. P. Leemans. Demonstration of a high repetition rate capillary discharge waveguide. *Journal of Applied Physics*, 119(3), 2016. ISSN 10897550. doi: 10.1063/1.4940121.

[37] G. Loisch, J. Engel, M. Gross, M. Hochberg, H. Huck, G. Koss, O. Lishilin, A. Oppelt, S. Philipp, D. Richter, F. Stephan, and P. Weidemann. Jitter mitigation in low density discharge plasma cells for wakefield accelerators. *Journal of Applied Physics*, 125(6), 2019. ISSN 10897550. doi: 10.1063/1.5068753.

[38] F. Paschen. *Ueber die zum Funkenübergang in Luft, Wasserstoff und Kohlensäure bei verschiedenen Drucken erforderliche Potentialdifferenz*. J.A. Barth, Leipzig, Germany, 1889. doi: doi.org/10.1002/andp.18892730505.

[39] L. P. Babich. *High Energy Phenomena in Electric Discharges in Dense Gases*. Futurepast, Arlington, Virginia, 2003.

[40] M. Balmelli, R. Farber, L. Merotto, P. Soltic, D. Bleiner, C. M. Franck, and J. Biela. Experimental analysis of breakdown with nanosecond pulses for spark-ignition engines. *IEEE Access*, 9:100050–100062, 2021. ISSN 21693536. doi: 10.1109/ACCESS.2021.3095664.

[41] D. Levko, R. R. Arslanbekov, and V. I. Kolobov. Modified Paschen curves for pulsed breakdown. *Physics of Plasmas*, 26(6), 2019. ISSN 10897674. doi: 10.1063/1.5108732.

[42] C. Amoedo, N. C. Lopes, N. E. Torrado, P. Muggli, L. Verra, M. Turner, G. Zevi Della Porta, J. Pucek, M. Bergamaschi, A. Clairembaud, J. Mezger, F. Pannell, N. van Gills, E. Gschwendtner, M. Taborelli, A. Sublet, and AWAKE Collaboration. Demonstration of proton bunch self-modulation in a Discharge Plasma Source. *in preparation*, 2024.

[43] N. E. Torrado, C. Amoedo, A. Sublet, M. Taborelli, S. F. Pinto, J. F. Silva, and N. C. Lopes. Double pulse generator for AWAKE scalable discharge plasma source. *accepted by IOP Conference Series*, 2025.

[44] J. Mankowski and M. Kristiansen. A review of short pulse generator technology. *IEEE Transactions on Plasma Science*, 28(1):102–108, 2000. ISSN 00933813. doi: 10.1109/27.842875.

[45] S. N. Rukin. Pulsed power technology based on semiconductor opening switches: A review. *Review of Scientific Instruments*, 91(1), 2020. ISSN 10897623. doi: 10.1063/1.5128297.

[46] A. Elserougi, S. Ahmed, and A. Massoud. A boost converter-based ringing circuit with high-voltage gain for unipolar pulse generation. *IEEE Transactions on Dielectrics and Electrical Insulation*, 23(4):2088–2094, 2016. ISSN 10709878. doi: 10.1109/TDEI.2016.7556482.

[47] T. E. Salem, C. W. Tipton, and D. Porschet. Fabrication and practical considerations of a flyback transformer for use in high pulsed-power applications. *Proceedings of the Annual Southeastern Symposium on System Theory*, 2006:397–400, 2006. doi: 10.1109/ssst.2006.1619114.

[48] L. M. Redondo, E. Margato, and J. Fernando Silva. New method to build a high-voltage pulse supply using only semiconductor switches for plasma-immersion ion implantation. *Surface and Coatings Technology*, 136(1-3):51–54, 2001. ISSN 02578972. doi: 10.1016/S0257-8972(00)01010-0.

[49] L. M. Redondo and J. F. Silva. Flyback versus forward switching power supply topologies for unipolar pulsed-power applications. *IEEE Transactions on Plasma Science*, 37(1):171–178, 2009. ISSN 00933813. doi: 10.1109/TPS.2008.2006056.

[50] M. J. Edwards, P. K. Patel, J. D. Lindl, L. J. Atherton, S. H. Glenzer, S. W. Haan, J. D. Kilkenny, O. L. Landen, E. I. Moses, A. Nikroo, R. Petrasso, T. C. Sangster, P. T. Springer, S. Batha, R. Benedetti, L. Bernstein, R. Betti, D. L. Bleuel, T. R. Boehly, D. K. Bradley, J. A. Caggiano, D. A. Callahan, P. M. Celliers, C. J. Cerjan, K. C. Chen, D. S. Clark, G. W. Collins, E. L. Dewald, L. Divol, S. Dixit, T. Doeppner, D. H. Edgell, J. E. Fair, M. Farrell, R. J. Fortner, J. Frenje, M. G. Gatu Johnson, E. Giraldez, V. Y. Glebov, G. Grim, B. A. Hammel, A. V. Hamza, D. R. Harding, S. P. Hatchett, N. Hein, H. W. Herrmann, D. Hicks, D. E. Hinkel,

M. Hoppe, W. W. Hsing, N. Izumi, B. Jacoby, O. S. Jones, D. Kalantar, R. Kauffman, J. L. Kline, J. P. Knauer, J. A. Koch, B. J. Kozioziemski, G. Kyrala, K. N. Lafortune, S. L. Pape, R. J. Leeper, R. Lerche, T. Ma, B. J. Macgowan, A. J. Mackinnon, A. Macphee, E. R. Mapoles, M. M. Marinak, M. Mauldin, P. W. McKenty, M. Meezan, P. A. Michel, J. Milovich, J. D. Moody, M. Moran, D. H. Munro, C. L. Olson, K. Opachich, A. E. Pak, T. Parham, H. S. Park, J. E. Ralph, S. P. Regan, B. Remington, H. Rinderknecht, H. F. Robey, M. Rosen, S. Ross, J. D. Salmonson, J. Sater, D. H. Schneider, F. H. Séguin, S. M. Sepke, D. A. Shaughnessy, V. A. Smalyuk, B. K. Spears, C. Stoeckl, W. Stoeffl, L. Suter, C. A. Thomas, R. Tommasini, R. P. Town, S. V. Weber, P. J. Wegner, K. Widman, M. Wilke, D. C. Wilson, C. B. Yeamans, and A. Zylstra. Progress towards ignition on the National Ignition Facility. *Physics of Plasmas*, 20(7), 2013. ISSN 1070664X. doi: 10.1063/1.4816115.

[51] T. P. Yu, W. Yu, F. Q. Shao, S. X. Luan, D. B. Zou, Z. Y. Ge, G. B. Zhang, J. W. Wang, W. Q. Wang, X. H. Li, J. X. Liu, J. M. Ouyang, and A. Y. Wong. High-energy-density electron jet generation from an opening gold cone filled with near-critical-density plasma. *Journal of Applied Physics*, 117(2), 2015. ISSN 10897550. doi: 10.1063/1.4904420.

[52] G. A. Mesiats. *Pulsed Power*. Kluwer Academic/Plenum Publishers, Amsterdam, NL, 2005.

[53] M. E. Savage, L. F. Bennett, D. E. Bliss, W. T. Clark, R. S. Coats, J. M. Elizondo, K. R. LeChien, H. C. Harjes, J. M. Lehr, J. E. Maenchen, D. H. McDaniel, M. F. Pasik, T. D. Pointon, A. C. Owen, D. B. Seidel, D. L. Smith, B. S. Stoltzfus, K. W. Struve, W. A. Stygar, L. K. Warne, J. R. Woodworth, C. W. Mendel, K. R. Prestwich, R. W. Shoup, D. L. Johnson, J. P. Corley, K. C. Hodge, T. C. Wagoner, and P. E. Wakeland. An overview of pulse compression and power flow in the upgraded Z pulsed power driver. *PPPS-2007 - Pulsed Power Plasma Science 2007*, 2:979–984, 2007. doi: 10.1109/PPPS.2007.4652354.

[54] R. B. Spielman, C. Deeney, G. A. Chandler, M. R. Douglas, D. L. Fehl, M. K. Matzen, D. H. McDaniel, T. J. Nash, J. L. Porter, T. W. Sanford, J. F. Seamen, W. A. Stygar, K. W. Struve, S. P. Breeze, J. S. McGurn, J. A. Torres, D. M. Zagar, T. L. Gilliland, D. O. Jobe, J. L. McKenney, R. C. Mock, M. Vargas, T. Wagoner, and D. L. Peterson. Tungsten wire-array Z-pinch experiments at 200 TW and 2 MJ. *Physics of Plasmas*, 5 (5 PART 1):2105–2111, 1998. ISSN 1070664X. doi: 10.1063/1.872881.

[55] B. Cadilhon, L. Pécastaing, T. Reess, A. Silvestre De Ferron, P. Pignolet, S. Vauchamp, J. Andrieu, and M. Lalande. High pulsed power sources for broadband radiation. *IEEE Transactions on Plasma Science*, 38(10 PART 1):2593–2603, 2010. ISSN 00933813. doi: 10.1109/TPS.2010.2042732.

[56] M. Gundersen, P. T. Vernier, S. B. Cronin, and S. Kerketta. A Review of Diverse Academic Research in Nanosecond Pulsed Power and Plasma Science. *IEEE Transactions on Plasma Science*, 48(4):742–748, 2020. ISSN 19399375. doi: 10.1109/TPS.2020.2972934.

[57] K. Yatsui, W. Jiang, H. Suematsu, G. Imada, T. Suzuki, M. Hirai, and Xiaopeng Zhu. Industrial applications of pulsed particle beams and pulsed power technologies. *15th International Conference on High-Power Particle Beams - Proceedings, BEAMS-2004*, pages 613–617, 2004.

[58] A. M. Zungeru, H. Ezea, and J. Katende. Pulsed power system for wireless underground sensor networks. *2016 3rd International Conference on Electrical, Electronics, Computer Engineering and their Applications, EECEA 2016*, pages 126–132, 2016. doi: 10.1109/EECEA.2016.7470778.

[59] A. J. Varkey, M. D. Dlamini, and S. K. Mkhonta. Decontamination of Bacteria from Water with Moderate Electric and Magnetic Fields. *Life Sciences*, 2(11):1–5, 2017. doi: 10.20944/preprints201711.0202.v1.

[60] N. Ghasemi, F. Zare, and H. Hosano. A Review of Pulsed Power Systems for Degrading Water Pollutants Ranging from Microorganisms to Organic Compounds. *IEEE Access*, 7:150863–150891, 2019. ISSN 21693536. doi: 10.1109/ACCESS.2019.2947632.

[61] E. L. Neau. Environmental and Industrial Applications of Pulsed Power Systems. *IEEE Transactions on Plasma Science*, 22(1):2–10, 1994. ISSN 19399375. doi: 10.1109/27.281544.

[62] Z. Liu, A. J. Pemen, R. T. Van Hoppe, G. J. Winands, E. J. Van Heesch, and K. Yan. An efficient, repetitive nanosecond pulsed power generator with ten synchronized spark gap switches. *IEEE Transactions on Dielectrics and Electrical Insulation*, 16(4):918–925, 2009. ISSN 10709878. doi: 10.1109/TDEI.2009.5211834.

[63] M. A. Elgenedy, A. M. Massoud, S. Ahmed, and B. W. Williams. A High-Gain, High-Voltage Pulse Generator Using Sequentially Charged Modular Multilevel Converter Submodules, for Water Disinfection Applications. *IEEE Journal of Emerging and Selected Topics in Power Electronics*, 6(3):1394–1406, 2018. ISSN 21686785. doi: 10.1109/JESTPE.2017.2750244.

[64] L. Cheng, K. Mei, Z. Chen, W. Jia, Y. Wang, H. Wang, L. Xie, S. Shen, and W. Ding. High-Voltage Repetitive Nanosecond Pulse Generator Utilizing Power Synthesis of Modified Avalanche Transistorized Marx Circuits. *IEEE Transactions on Instrumentation and Measurement*, 71:1–16, 2022. ISSN 15579662. doi: 10.1109/TIM.2022.3167777.

[65] L. Pang, T. Long, K. He, Y. Huang, and Q. Zhang. A compact series-connected SiC MOSFETs module and its application in high voltage nanosecond pulse generator. *IEEE Transactions on Industrial Electronics*, 66 (12):9238–9247, 2019. ISSN 15579948. doi: 10.1109/TIE.2019.2891441.

[66] G. Duan, S. N. Vainshtein, and J. T. Kostamovaara. Modified High-Power Nanosecond Marx Generator Prevents Destructive Current Filamentation. *IEEE Transactions on Power Electronics*, 32(10):7845–7850, 2017. ISSN 08858993. doi: 10.1109/TPEL.2016.2632974.

[67] H. Niu and R. D. Lorenz. Evaluating different implementations of online junction temperature sensing for switching power semiconductors. *IEEE Transactions on Industry Applications*, 53(1):391–401, 2017. ISSN 00939994. doi: 10.1109/TIA.2016.2614773.

[68] H. Niu and R. D. Lorenz. Real-Time Junction Temperature Sensing for Silicon Carbide MOSFET with Different Gate Drive Topologies and Different Operating Conditions. *IEEE Transactions on Power Electronics*, 33(4):3424–3440, 2018. ISSN 08858993. doi: 10.1109/TPEL.2017.2704441.

[69] M. Rezanejad, A. Sheikholeslami, and J. Adabi. Modular switched capacitor voltage multiplier topology for pulsed power supply. *IEEE Transactions on Dielectrics and Electrical Insulation*, 21(2):635–643, 2014. ISSN 10709878. doi: 10.1109/TDEI.2013.004067.

[70] M. Hochberg, M. Sack, D. Herzog, A. Weisenburger, W. An, R. Fetzer, and G. Mueller. A fast modular semiconductor-based marx generator for driving dynamic loads. *IEEE Transactions on Plasma Science*, 47 (1):627–634, 2019. ISSN 00933813. doi: 10.1109/TPS.2018.2876503.

[71] M. N. Uddin, H. Allahyari, Y. H. Tabrizi, and H. Bahrami. A Solid-State Bipolar Pulse Power Generator for Dielectric Barrier Discharge Applications. *IEEE Transactions on Industry Applications*, 58(6):7942–7951, 2022. ISSN 19399367. doi: 10.1109/TIA.2022.3202156.

[72] E. O. Marx. *Erzeugung von verschiedenen Hochspannungsarten zu Versuchs-und Prüfzwecken*. 1925.

[73] J. Clementson, K. Rahbarnia, O. Grulke, and T. Klinger. Design of A, B, and C pulse forming networks using the VINPFN application. *IEEE Transactions on Power Electronics*, 29(11):5673–5679, 2014. ISSN 08858993. doi: 10.1109/TPEL.2013.2295245.

[74] F. Davanloo, C. B. Collins, and F. J. Agée. High-power, repetitive-stacked blumlein pulsers commutated by a single switching element. *IEEE Transactions on Plasma Science*, 26(5):1463–1475, 1998. ISSN 00933813. doi: 10.1109/27.736041.

[75] Y. Zhao, W. Xie, J. Jiang, L. Chen, S. Feng, M. Wang, and Z. Wang. Replacement of marx generator by tesla transformer for pulsed power system reliability improvement. *IEEE Transactions on Plasma Science*, 47(1):574–580, 2019. ISSN 00933813. doi: 10.1109/TPS.2018.2873078.

[76] A. Lodes, R. D. Curry, R. Narsetti, and L. M. Nichols. Pulsed electric fields inactivation of vegetative bacteria in drinking water utilizing magnetic pulse compressor technology. *Conference Record of the International Power Modulator Symposium and High Voltage Workshop*, 34(4):554–557, 2006. ISSN 10768467. doi: 10.1109/MODSYM.2006.365311.

[77] D. Zhang, Y. Zhou, J. Wang, and P. Yan. A compact, high repetition-rate, nanosecond pulse generator based on magnetic pulse compression system. *IEEE Transactions on Dielectrics and Electrical Insulation*, 18(4): 1151–1157, 2011. ISSN 10709878. doi: 10.1109/TDEI.2011.5976109.

[78] Y. Zhuge, J. Liang, M. Fu, T. Long, and H. Wang. Comprehensive Overview of Power Electronics Intensive Solutions for High-Voltage Pulse Generators. *IEEE Open Journal of Power Electronics*, 5(November): 21–40, 2024. ISSN 26441314. doi: 10.1109/OJPEL.2023.3340220.

[79] A. Elserougi, A. Massoud, and S. Ahmed. Multimodule Boost-Converter-Based Pulse Generators: Design and Operation. *IEEE Transactions on Plasma Science*, 48(1):219–227, 2020. ISSN 19399375. doi: 10. 1109/TPS.2019.2956126.

[80] A. Elserougi, A. M. Massoud, and S. Ahmed. A boost-inverter-based bipolar high-voltage pulse generator. *IEEE Transactions on Power Electronics*, 32(4):2846–2855, 2017. ISSN 08858993. doi: 10.1109/TPEL. 2016.2576562.

[81] S. Zabihi, F. Zare, G. Ledwich, A. Ghosh, and H. Akiyama. A new pulsed power supply topology based on positive buck-boost converters concept. *IEEE Transactions on Dielectrics and Electrical Insulation*, 17(6): 1901–1911, 2010. ISSN 10709878. doi: 10.1109/TDEI.2010.5658245.

[82] J. Ma, L. Yu, W. Sun, S. Dong, L. Gao, and C. Yao. Investigation and Evaluation of Solid-State Marx Pulse Generator Based on 3-D Busbar. *IEEE Transactions on Plasma Science*, 49(5):1597–1604, 2021. ISSN 19399375. doi: 10.1109/TPS.2021.3073489.

[83] J. F. Silva, L. M. Redondo, H. Canacsinh, and W. C. Dillard. Solid-state pulsed power modulators and capacitor charging applications. In *Power Electronics Handbook*, pages 621–685. Butterworth-Heinemann, fifth edition, 2024. doi: 10.1016/B978-0-323-99216-9.00040-8.

[84] W. Zeng, C. Yao, S. Dong, Y. Wang, J. Ma, Y. He, and L. Yu. Self-Triggering High-Frequency Nanosecond Pulse Generator. *IEEE Transactions on Power Electronics*, 35(8):8002–8012, 2020. ISSN 19410107. doi: 10.1109/TPEL.2020.2967183.

[85] M. Samizadeh Nikoo and S. M. A. Hashemi. High-Power Nanosecond Pulse Generator With High-Voltage SRD and GDT Switch. *IEEE Transactions on Plasma Science*, 43(9):3268–3276, 2015. ISSN 00933813. doi: 10.1109/TPS.2015.2411251.

[86] A. S. Kesar. A Compact, 10-kV, 2-ns Risetime Pulsed-Power Circuit Based on Off-the-Shelf Components. *IEEE Transactions on Plasma Science*, 46(3):594–597, 2018. ISSN 00933813. doi: 10.1109/TPS.2018.2803077.

[87] M. Samizadeh Nikoo, S. M. A. Hashemi, and F. Farzaneh. A Two-Stage DSRD-Based High-Power Nanosecond Pulse Generator. *IEEE Transactions on Plasma Science*, 46(2):427–433, 2018. ISSN 00933813. doi: 10.1109/TPS.2018.2792331.

[88] S. Korotkov, Y. Aristov, and A. Zhmodikov. Comparative Studies of High-Voltage Diode-Dynistor Generators of High-Power Nanosecond Pulses. *IEEE Transactions on Plasma Science*, 50(4):954–958, 2022. ISSN 19399375. doi: 10.1109/TPS.2022.3156386.

[89] I. V. Grekhov, V. M. Efanov, A. F. Kardo-Sysoev, and S. V. Shenderey. Power drift step recovery diodes (DSRD). *Solid State Electronics*, 28(6):597–599, 1985. ISSN 00381101. doi: 10.1016/0038-1101(85)90130-3.

[90] M. R. Degnon, A. Gusev, A. S. D. Ferron, G. Daulhac, A. Baranov, S. Boisne, M. R. Degnon, A. Gusev, A. S. D. Ferron, L. Pecastaing, L. Pecastaing, S. Member, and A. Baranov. Off-the-Shelf Diodes as High-Voltage Opening Switches To cite this version : Off-The-Shelf Diodes as High-Voltage Opening Switches. *IEEE Transactions on Plasma Science*, 50(10):3384–3392, 2022. doi: 10.1109/TPS.2022.3177702.

[91] A. Elserougi, A. M. Massoud, A. M. Ibrahim, and S. Ahmed. A high voltage pulse-generator based on DC-to-DC converters and capacitor-diode voltage multipliers for water treatment applications. *IEEE Transactions on Dielectrics and Electrical Insulation*, 22(6):3290–3298, 2015. ISSN 10709878. doi: 10.1109/TDEI.2015.005376.

[92] Z. Deng, Q. Yuan, S. Shen, J. Yan, Y. Wang, and W. Ding. High voltage nanosecond pulse generator based on avalanche transistor Marx bank circuit and linear transformer driver. *Review of Scientific Instruments*, 92 (3), 2021. ISSN 10897623. doi: 10.1063/5.0042523.

[93] Y. Feng, T. Sugai, and W. Jiang. Solid-state bipolar linear transformer driver using inductive energy storage. *IEEE Transactions on Plasma Science*, 49(9):2887–2892, 2021. ISSN 19399375. doi: 10.1109/TPS.2021.3103743.

[94] N. Ralbag, I. Felner, and D. Avnir. New reed switch design based on magnetic silver. *Materials Research Express*, 6(12), 2019. ISSN 20531591. doi: 10.1088/2053-1591/ab5141.

[95] J. F. Silva. *ELECTRÓNICA INDUSTRIAL : Semicondutores e Conversores de Potência*. Fundação Calouste Gulbenkian, 2011.

[96] M. H. Rashid. *Power Electronics Handbook*. Academic Press, 2001. ISBN 0125816502.

[97] W. Jiang, K. Yatsui, K. Takayama, M. Akemoto, E. Nakamura, N. Shimizu, A. Tokuchi, S. Rukin, V. Tarasenko, and A. Panchenko. Compact solid-state switched pulsed power and its applications. *Proceedings of the IEEE*, 92(7):1180–1195, 2004. ISSN 00189219. doi: 10.1109/JPROC.2004.829003.

[98] R. Hironaka, M. Watanabe, E. Hotta, A. Okino, M. Maeyama, K. C. Ko, and N. Shimizu. Performance of pulsed power generator using high-voltage static induction thyristor. *IEEE Transactions on Plasma Science*, 28(5):1520–1523, 2000. ISSN 00933813. doi: 10.1109/27.901225.

[99] K. Okamura, N. Nakajima, M. Souda, F. Endo, H. Matsuda, and E. Kaneko. Sub-Microsecond Pulse Switching Characteristics. *Conference Record of the Twenty-Third International Power Modulator Symposium - IEEE*, pages 123–126, 1998.

[100] S. R. Jang, H. J. Ryoo, G. Goussev, and G. H. Rim. Comparative study of MOSFET and IGBT for high repetitive pulsed power modulators. *IEEE Transactions on Plasma Science*, 40(10 PART 1):2561–2568, 2012. ISSN 00933813. doi: 10.1109/TPS.2012.2186592.

[101] M. Azizi, J. J. Van Oorschot, and T. Huiskamp. Ultrafast Switching of SiC MOSFETs for High-Voltage Pulsed-Power Circuits. *IEEE Transactions on Plasma Science*, 48(12):4262–4272, 2020. ISSN 19399375. doi: 10.1109/TPS.2020.3039372.

[102] J. H. Kim, B. D. Min, S. V. Shenderey, and G. H. Rim. High voltage pulsed power supply using IGBT stacks. *IEEE Transactions on Dielectrics and Electrical Insulation*, 14(4):921–926, 2007. ISSN 10709878. doi: 10.1109/TDEI.2007.4286526.

[103] B. N. Pushpakaran, M. Hinojosa, S. B. Bayne, V. Veliadis, D. Urciuoli, N. El-Hinnawy, P. Borodulin, S. Gupta, and C. Scozzie. Evaluation of SiC JFET performance during repetitive pulsed switching into an unclamped inductive load. *IEEE Transactions on Plasma Science*, 42(10):2968–2973, 2014. ISSN 00933813. doi: 10.1109/TPS.2014.2309273.

[104] J. Kołek and M. Hołub. Practical design of a high-voltage pulsed power supply implementing SiC technology for atmospheric pressure plasma reactors. *Applied Sciences (Switzerland)*, 9(7), 2019. ISSN 20763417. doi: 10.3390/app9071451.

[105] L. Collier, T. Kajiwara, J. Dickens, J. Mankowski, and A. Neuber. Fast SiC Switching Limits for Pulsed Power Applications. *IEEE Transactions on Plasma Science*, 47(12):5306–5313, 2019.

[106] L. Han, L. Liang, Y. Kang, and Y. Qiu. A Review of SiC IGBT: Models, Fabrications, Characteristics, and Applications. *IEEE Transactions on Power Electronics*, 36(2):2080–2093, 2021. ISSN 19410107. doi: 10.1109/TPEL.2020.3005940.

[107] K. Puschkarsky, T. Grasser, T. Aichinger, W. Gustin, and H. Reisinger. Review on SiC MOSFETs High-Voltage Device Reliability Focusing on Threshold Voltage Instability. *IEEE Transactions on Electron Devices*, 66(11):4604–4616, 2019. ISSN 15579646. doi: 10.1109/TED.2019.2938262.

[108] G. Lyu, Y. Wang, J. Wei, Z. Zheng, J. Sun, L. Zhang, and K. J. Chen. A Normally-off Copackaged SiC-JFET/GaN-HEMT Cascode Device for High-Voltage and High-Frequency Applications. *IEEE Transactions on Power Electronics*, 35(9):9671–9681, 2020. ISSN 19410107. doi: 10.1109/TPEL.2020.2971789.

[109] M. Xiao, Y. Ma, Z. Du, V. Pathirana, K. Cheng, A. Xie, E. Beam, Y. Cao, F. Udrea, H. Wang, and Y. Zhang. Multi-Channel Monolithic-Cascode HEMT (MC2-HEMT): A New GaN Power Switch up to 10 kV. *Technical Digest - International Electron Devices Meeting, IEDM*, 2021-Decem:5.5.1–5.5.4, 2021. ISSN 01631918. doi: 10.1109/IEDM19574.2021.9720714.

[110] E. R. da Silva and M. E. Elbuluk. *Fundamentals of Power Electronics*, volume 59. Springer, 2013. ISBN 9781447151036. doi: 10.1007/978-1-4471-5104-3_2.

[111] C. Burkhart, T. Beukers, M. Kemp, R. Larsen, K. Macken, M. Nguyen, J. Olsen, and T. Tang. ILC Marx modulator development program status. *PPC2009 - 17th IEEE International Pulsed Power Conference*, pages 807–810, 2009. doi: 10.1109/PPC.2009.5386365.

[112] E. G. Cook. Review of Solid-State Modulators. *arXiv*, pages 1–5, 2000.

[113] A. Welleman, J. Waldmeyer, and E. Ramezani. Solid state switches for pulse power modulators. *Proceedings of LINAC2002*, pages 707–709, 2002.

[114] D. Ma, W. Chen, and X. Ruan. A Review of Voltage/Current Sharing Techniques for Series-Parallel-Connected Modular Power Conversion Systems. *IEEE Transactions on Power Electronics*, 35(11):12383–12400, 2020. ISSN 19410107. doi: 10.1109/TPEL.2020.2984714.

[115] R. Pérez-Delgado, G. Velasco-Quesada, and M. Román-Lumbreras. Current sharing control strategy for IGBTs connected in parallel. *Journal of Power Electronics*, 16(2):769–777, 2016. ISSN 15982092. doi: 10.6113/JPE.2016.16.2.769.

[116] C. Liu, X. Xu, D. He, H. Liu, X. Tian, Y. Guo, G. Cai, C. Ma, and G. Mu. Magnetic-Coupling Current-Balancing Cells Based Input-Parallel Output-Parallel LLC Resonant Converter Modules for High-Frequency

Isolation of DC Distribution Systems. *IEEE Transactions on Power Electronics*, 31(10):6968–6979, 2016. ISSN 08858993. doi: 10.1109/TPEL.2015.2507172.

[117] M. Sasaki, H. Nishio, and W. T. Ng. Dynamic gate resistance control for current balancing in parallel connected IGBTs. *Conference Proceedings - IEEE Applied Power Electronics Conference and Exposition - APEC*, pages 244–249, 2013. doi: 10.1109/APEC.2013.6520216.

[118] W. Hartmann, R. Fleck, R. Graba, and M. Hergt. Characterization of commercial IGBT modules for pulsed power applications. *Digest of Technical Papers-IEEE International Pulsed Power Conference*, pages 1–4, 2013. doi: 10.1109/PPC.2013.6627625.

[119] J. P. Miranda, L. A. Barros, and J. G. Pinto. A Review on Power Electronic Converters for Modular BMS with Active Balancing. *Energies*, 16(7), 2023. ISSN 19961073. doi: 10.3390/en16073255.

[120] V. Petrushyn, V. Horoshko, J. Plotkin, N. Almuratova, and Z. Toigozhinova. Power balance and power factors of distorted electrical systems and variable speed asynchronous electric drives. *Electronics (Switzerland)*, 10(14), 2021. ISSN 20799292. doi: 10.3390/electronics10141676.

[121] O. García, P. Zumel, A. Castro de, P. Alou, and J. A. Cobos. Current Self-Balance Mechanism in Multiphase Buck Converter. *IEEE Transactions on Power Electronics*, 24(6):1600–1606, 2009. ISSN 19410107. doi: 10.1109/TPEL.2009.2013859.

[122] Q. Wu, M. Wang, W. Zhou, and X. Wang. Current Balancing of Paralleled SiC mosfets for a Resonant Pulsed Power Converter. *IEEE Transactions on Power Electronics*, 35(6):5557–5561, 2020. ISSN 19410107. doi: 10.1109/TPEL.2019.2952326.

[123] Q. Zhang, X. Zhuang, Y. Liu, C. Wang, and H. Guo. A novel autonomous current-sharing control strategy for multiple paralleled DC–DC converters in islanded DC microgrid. *Energies*, 12(20), 2019. ISSN 19961073. doi: 10.3390/en12203951.

[124] M. Ricco, J. Meng, T. Gherman, G. Grandi, and R. Teodorescu. Smart battery pack for electric vehicles based on active balancing with wireless communication feedback. *Energies*, 12(20), 2019. ISSN 19961073. doi: 10.3390/en12203862.

[125] T. Duraisamy and D. Kaliyaperumal. Machine Learning-Based Optimal Cell Balancing Mechanism for Electric Vehicle Battery Management System. *IEEE Access*, 9:132846–132861, 2021. ISSN 21693536. doi: 10.1109/ACCESS.2021.3115255.

[126] T. Sen, J. Baek, and M. Chen. Current Balancing of Paralleled Switches in Resonant Converters with Multiphase Coupled Inductor. *2021 IEEE 22nd Workshop on Control and Modelling of Power Electronics, COMPEL 2021*, pages 1–8, 2021. doi: 10.1109/COMPEL52922.2021.9646034.

[127] M. Noah, S. Endo, H. Ishibashi, K. Nanamori, J. Imaoka, K. Umetani, and M. Yamamoto. A Current Sharing Method Utilizing Single Balancing Transformer for a Multiphase LLC Resonant Converter with Integrated Magnetics. *IEEE Journal of Emerging and Selected Topics in Power Electronics*, 6(2):977–992, 2018. ISSN 21686785. doi: 10.1109/JESTPE.2017.2777508.

[128] R. A. Fonseca, L. O. Silva, F. S. Tsung, V. K. Decyk, W. Lu, C. Ren, W. B. Mori, S. Deng, S. Lee, T. Katsouleas, and J. C. Adam. OSIRIS: A three-dimensional, fully relativistic particle in cell code for modeling plasma based accelerators. *Lecture Notes in Computer Science (including subseries Lecture Notes in Artificial Intelligence and Lecture Notes in Bioinformatics)*, 2331 LNCS(PART 3):342–351, 2002. ISSN 16113349. doi: 10.1007/3-540-47789-6_36.

[129] T. G. Engel, A. L. Donaldson, and M. Kristiansen. The Pulsed Discharge Arc Resistance and its Functional Behavior. *IEEE Transactions on Plasma Science*, 17(2):323–329, 1989. ISSN 19399375. doi: 10.1109/27.24643.

[130] L. Yuan, L. Sun, and H. Wu. Simulation of Fault Arc Using Conventional Arc Models. *Energy and Power Engineering*, 05(04):833–837, 2013. ISSN 1949-243X. doi: 10.4236/epe.2013.54b160.

[131] C. Birdsall and A. Langdon. *Plasma Physics Via Computer Simulation*, volume 7. Taylor & Francis Group, Florida, 2004.

[132] M. Moreira, P. Muggli, and J. Vieira. Mitigation of the Onset of Hosing in the Linear Regime through Plasma Frequency Detuning. *Physical Review Letters*, 130(11):115001, 2023.

[133] F. Cruz, T. Grismayer, R. Torres, A. Chen, A. Spitkovsky, R. Fonseca, and L. Silva. Particle-in-cell simulations of pulsar magnetospheres: Transition between electrosphere and force-free regimes. *Astronomy & Astrophysics*, 229, 2024. ISSN 0004-6361. doi: 10.1051/0004-6361/202347926.

[134] S. I. Barannik, S. Vasserman, and A. Lukin. Resistance and inductance of a gas arc. *Soviet Physics ' Technical Physics*, 19:1449'1453, 1975.

[135] M. M. Popovic. Investigation of the beginning of high current discharges in pulsed arcs. *Proceedings of the International Conference Gaseous Discharges*, pages 32–36, 1974.

[136] A. E. Vlastós. The resistance of sparks.pdf. *Journal of Applied Physics*, 72, 1972.

[137] I. V. Demenik. Resistance of a xenon plasma in a large flash lamp. *Soviet Physics -Technical Physics*, 13:829–832, 1968.

[138] G. M. Goncharenko and I. N. Romanenko. Discharge channel in helium at 100 atm and in air.pdf. *Soviet Physics -Technical Physics*, 15:1990–1995, 1971.

[139] M. J. Kushner, W. D. Kimura, and S. R. Byron. Arc resistance of laser triggered spark gaps. *Journal of Applied Physics*, 58:1744–1751, 1985.

[140] A. M. Cassie. Theorie Nouvelle des Arcs de Rupture et de la Rigidité des Circuits. *Cigre*, 102:588–608, 1939.

[141] O. Mayr. Beitrage zur Theorie des Statischen und des Dynamischen Lichthogens. *Archiv für Elektrotechnik*, 37(12):588–608, 1943.

[142] P. R. Gajare, A. P. Chaudhari, and G. K. Mahajan. Analysis and Modilization of Electric Arc Model for High Voltage Circuit Breaker Based on Matlab/Simulink. *Resincap Journal of Science & Engineering*, 1 (8):202–207, 2017.

[143] P. W. Smith. *Transient Electronics: Pulsed Circuit Technology*. Wiley, Hoboken, NJ, 2011. ISBN 978-0-470-85258-3.

[144] R. A. Torres and T. M. Jahns. Design of High-Performance Toroidal DC-link Inductor for Current-Source Inverters. *2019 IEEE Applied Power Electronics Conference and Exposition (APEC)*, pages 2694–2701, 2019.

[145] J. Mezger, M. Bergamaschi, L. Ranc, A. Sublet, J. Pucek, M. Turner, A. Clairembaud, and P. Muggli. Implementation of Light Diagnostics for Wakefields at AWAKE. *submitted to Elsevier*, 2024.

[146] L. Verra, C. Amoedo, N. Torrado, A. Clairembaud, J. Mezger, F. Pannell, J. Pucek, N. Van Gils, M. Bergamaschi, G. Zevi Della Porta, N. Lopes, A. Sublet, M. Turner, E. Gschwendtner, P. Muggli, R. Agnello, C. C. Ahdida, Y. Andrebe, O. Apsimon, R. Apsimon, J. M. Arnesano, V. Bencini, P. Blanchard, P. N. Burrows, B. Buttenschön, A. Caldwell, M. Chung, D. A. Cooke, C. Davut, G. Demeter, A. C. Dexter, S. Doebert, J. Farmer, A. Fasoli, R. Fonseca, I. Furno, E. Granados, M. Granetzny, T. Graubner, O. Grulke, E. Guran, J. Henderson, M. Kedves, F. Kraus, M. Krupa, T. Lefevre, L. Liang, S. Liu, K. Lotov, M. Martinez Calderon, S. Mazzoni, K. Moon, P. I. Morales Guzmán, M. Moreira, T. Nechaeva, N. Okhotnikov, C. Pakuza, A. Pardons, K. Pepitone, E. Poimendidou, A. Pukhov, R. L. Ramjiawan, L. Ranc, S. Rey, R. Rossel, H. Saberi, O. Schmitz, E. Senes, F. Silva, L. Silva, B. Spear, C. Stollberg, C. Swain, A. Topaloudis, P. Tuev, F. Velotti, V. Verzilov, J. Vieira, E. Walter, C. Welsch, M. Wendt, M. Wing, J. Wolfenden, B. Woolley, G. Xia, V. Yarygova, and M. Zepp. Filamentation of a relativistic proton bunch in plasma. *Physical Review E*, 109(5):1–8, 2024. ISSN 24700053. doi: 10.1103/PhysRevE.109.055203.

[147] M. Turner, E. Walter, C. Amoedo, N. Torrado, N. Lopes, A. Sublet, M. Bergamaschi, J. Pucek, J. Mezger, N. van Gils, L. Verra, G. Z. Della Porta, J. Farmer, A. Clairembaud, F. Pannell, E. Gschwendtner, P. Muggli, and AWAKE Collaboration. Experimental Observation of Motion of Ions in a Resonantly Driven Plasma Wakefield Accelerator. *submitted to Physical Review Letters*, 2024.

[148] A. Clairembaud, M. Turner, and P. Muggli. Development of self-modulation as a function of plasma length. *submitted to Elsevier*, 2024.

[149] J. P. Farmer, A. Caldwell, and A. Pukhov. Preliminary Investigation of a Higgs Factory based on Proton-Driven Plasma Wakefield Acceleration. *New Journal of Physics*, 26:113011, 2024. ISSN 13672630. doi: 10.1088/1367-2630/ad8fc5.